creative commons
COMMONS DEED

저작자표시-비영리-변경금지 2.0 대한민국

이용자는 아래의 조건을 따르는 경우에 한하여 자유롭게

- 이 저작물을 복제, 배포, 전송, 전시, 공연 및 방송할 수 있습니다.

다음과 같은 조건을 따라야 합니다:

저작자표시. 귀하는 원저작자를 표시하여야 합니다.

비영리. 귀하는 이 저작물을 영리 목적으로 이용할 수 없습니다.

변경금지. 귀하는 이 저작물을 개작, 변형 또는 가공할 수 없습니다.

- 귀하는, 이 저작물의 재이용이나 배포의 경우, 이 저작물에 적용된 이용허락조건을 명확하게 나타내어야 합니다.
- 저작권자로부터 별도의 허가를 받으면 이러한 조건들은 적용되지 않습니다.

저작권법에 따른 이용자의 권리는 위의 내용에 의하여 영향을 받지 않습니다.

이것은 이용허락규약(Legal Code)을 이해하기 쉽게 요약한 것입니다.

Disclaimer

dCollection

공학박사 학위논문

Seismic System Reliability Analysis Considering Uncertainties and Correlations of Engineering Demand Parameters

구조물 지진응답의 불확실성과 상관관계를 고려한 지진 시스템 신뢰성 해석

2022년 8월

서울대학교 대학원

건설환경공학부

강 철 영

Seismic System Reliability Analysis Considering Uncertainties and Correlations of Engineering Demand Parameters

구조물 지진응답의 불확실성과 상관관계를 고려한
지진 시스템 신뢰성 해석

지도교수 송 준 호
공동논문지도교수 권 오 성

이 논문을 공학박사 학위논문으로 제출함
2022년 8월

서울대학교 대학원
건설환경공학부
강 철 영

강철영의 공학박사 학위논문을 인준함
2022년 8월

위 원 장 김 호 경 (인)

부 위 원 장 송 준 호 (인)

위 원 권 오 성 (인)

위 원 채 윤 병 (인)

위 원 전 종 수 (인)

Abstract

As urban communities get sophisticated and complex, it is becoming increasingly important to assure the resilience of infrastructure systems against earthquakes, which may cause many casualties and critical socioeconomic losses. To this end, seismic system reliability analysis, such as regional loss assessment and network reliability analysis, needs to be performed with various uncertainties in seismic motions and structural responses properly considered. Thus, it is essential to incorporate the uncertainties and correlations of engineering demand parameters (EDP) of structures for accurate seismic system reliability analysis. The conditional mean of EDP given IM is often predicted by a regression function of the selected IM while its variability is represented by the residual termed "EDP residual." Therefore, the correlation between the EDPs should be determined based on those between IMs ("IM correlation") and EDP residuals ("EDP residual correlation"). However, the incorporation of both types of correlations and accurate estimation of EDP residual correlation remain a challenging task with significant difficulties. To tackle the challenges, this dissertation not only proposes a theoretical framework to evaluate the correlation between EDPs of different structures in a system, but also develops various methods for estimating the EDP residuals of structures based on structural analyses, regression models, and deep neural network (DNNs) models.

First, in order to consider the EDP correlation in the seismic system reliability analysis, the correlation between safety factors of two different structures is formulated in terms of IM and EDP residual correlations. Based on these formulas, the probability of structure joint failure is computed, and the contribution of each

correlation to the EDP correlation is investigated. In addition, a method for estimating the variances and correlation coefficients of EDP residuals using Incremental Dynamic Analysis (IDA) is developed. The variances and correlations of EDPs are evaluated by incorporating ground motion prediction equation (GMPE) and statistical analysis of EDP residuals from IDA curves. A numerical example of regional seismic loss assessment demonstrates that the proposed theoretical framework and IDA-based method can further improve the prediction accuracy of total loss exceedance probability of a region. To facilitate applications of the proposed method, this dissertation also proposes a regression model and guidelines to predict the variances and correlations of EDP residuals without performing IDA.

Second, an IM-invariant method is proposed to estimate the EDP residuals of building structures as an alternative to the IDA-based method that provides high accuracy but requires huge computational cost. Taking advantage of the significantly reduced calculation time, a more general expression for the EDP residuals and their correlations is obtained. In addition, a comprehensive investigation is also performed using many ground motions to find primary structural characteristics affecting the uncertainties and correlations of EDPs. Numerical examples of urban areas with various types of archetype buildings are introduced to demonstrate the effects of the structural characteristics on the EDP residual and total regional losses.

To further facilitate the applications of EDP residual correlation to practical regional seismic loss assessment, nonlinear regression models are developed to predict the standard deviations and correlation coefficients of EDP residuals of buildings structures using easy-to-obtain predictors describing the primary structural characteristics. The accuracy of the developed regression models is verified by the

examples of regional loss assessment using the EDP residual regression models without additional structural analysis.

Although the regression models can efficiently consider the EDP residual in regional seismic loss assessment, the accuracy and applicability of the predicted EDP residual are remaining challenges. In order to improve the prediction accuracy and extend its applicability, two frameworks for regional seismic loss assessment based on deep neural networks (DNNs) are proposed. The first framework estimates the EDP residuals of buildings by combining the EDP residuals of various single-degree-of-freedom (SDOF) systems through the modal combination rules. In this framework, three DNN models are constructed to predict the EDP residuals of SDOF systems. On the other hand, the second framework directly predicts the EDP residuals of specific types of buildings using two DNN models. A large number of building structures having various first and second modal periods and damping ratios are employed in this regard. The applicability and effectiveness of the frameworks are verified by numerical examples of regional seismic loss assessment, for which time history-based "exact" solutions exist. The numerical examples demonstrate that the proposed theoretical framework and methods for estimating the EDP residuals can correct the significant bias in seismic system reliability analysis.

Keyword: Earthquake engineering, Engineering demand parameters, Correlation, Seismic reliability analysis, Regional seismic loss assessment, Nonlinear regression, Deep neural network, Fragility analysis, Uncertainty quantification, Modal analysis, Time history analysis

Student Number: 2016-22796

Table of Contents

List of Figures

List of Tables

Chapter 1. Introduction

1.1 Motivation

Earthquake is one of the most catastrophic natural disasters subject to large uncertainties. Strong earthquake events can severely damage structures and infrastructure systems, resulting in injuries and socioeconomic losses. With the rapid increase in urban concentration and connectivity, the socioeconomic loss from an earthquake event can be huge. Thus, many recent studies focused on evaluating the resilience, i.e., the holistic capability to minimize the loss through reliability, redundancy and recovery against such catastrophic events (Lim et al., 2022). Naturally, such efforts require assessing the regional loss with proper consideration of uncertainties in earthquake hazards, seismic responses of structures, structural damages, and socioeconomic losses.

In particular, complex urban systems such as large building inventories or lifeline networks of gas, water, electricity, and sewer are subject to various types of uncertainties. Moreover, the seismic responses of structures, e.g. buildings in an inventory, bridges in a network, may have significant correlation between each other because the structures are subjected to the uncertain ground motion intensities showing spatial correlation, and seismic responses of the structures given a ground motion intensity generally show significant correlations. Therefore, system-level seismic reliability analysis regarding regional loss, network connectivity, or network flow should incorporate the correlation between the seismic responses accurately. By investigating seismic performances of networks with and without the correlations,

many studies showed that post-hazard vulnerability can be underestimated if the correlations are ignored (Goda and Hong, 2008a; Song and Ok, 2010; Sokolov and Wenzel, 2011; Wang et al., 2019; Kim et al., 2020a).

The limit state of each structure is often described in terms of an engineering demand parameter (EDP), a structural response quantity that can be used to estimate damage to components and systems. The conditional mean of EDP is often predicted by a regression function of the selected intensity measure (IM) of ground motions while its variability is represented by the residual (Baker and Cornell, 2008; Bradley, 2013). The EDP residual is a random variable adopted to describe the variance of EDP for a given IM. Therefore, the EDP correlation is affected by the correlation between the IMs, and that between the residuals. In this dissertation, for simplicity, these correlations are termed as "IM correlation" and "EDP residual correlation," respectively. The IM correlation is a correlation between selected seismic intensities reaching different structures in a region by a given earthquake scenario. This correlation is relevant to the residuals of empirical seismic attenuation relation, termed ground motion prediction equation (GMPE) (Boore and Atkinson, 2008; Campbell and Bozorgnia, 2008; Abrahamson et al., 2016). On the other hand, the EDP residual correlation is related to the uncertainty in the structural response that cannot be explained by the selected IM alone.

The IM correlation is described by spatial correlation models as the correlation between the intensities at two different sites for a given earthquake scenario (Boore et al., 2003; Wang and Takada, 2005; Baker and Cornell, 2006; Goda and Hong, 2008b; Jayaram and Baker, 2009; Sokolov et al., 2010; Loth and Baker, 2013). The spatial correlation models have been adopted in various seismic system reliability

analyses, such as lifeline networks of transportation, gas, water, and electricity (Adachi and Ellingwood, 2009; Lim and Song, 2012; Kurtz et al., 2016; Dong and Frangopol, 2017; Stern et al., 2017; De Risi et al., 2018; Wang et al., 2019). In particular, Goda and Hong (2008a) and Kim et al. (2020a) evaluated regional seismic loss of spatially distributed buildings in a virtual city located in the Vancouver area. These studies showed that a proper consideration of IM correlation improves the accuracy of the seismic system reliability analysis.

On the other hand, research efforts on EDP residual correlation and its effects on system reliability have been relatively limited, while some studies (Lee and Kiremidjian, 2007; Baker and Cornell, 2008; Bradley and Lee, 2010) attempted to consider the EDP residual correlation within a single structure. But they did not quantitatively estimate the correlation between the EDP residuals of different structures. Considering these efforts and limitations in the literature, it is desirable to develop a theoretical framework that can incorporate both types of correlations for the seismic system reliability analysis and methods for estimating the correlation between EDP residuals of structures in a system.

1.2 Objectives and scopes

In order to evaluate the uncertainties and correlations of EDPs of structures in a system, the dissertation aims to achieve the following objectives: (1) incorporating the effects of both IM and EDP residual correlations on the seismic system reliability analysis, (2) developing methods to accurately estimate the variances and correlations of EDP residuals of structures, (3) facilitating the consideration of EDP residual correlation in seismic system reliability analyses using regression models

and deep neural networks (DNN), and (4) demonstrating the proposed theoretical framework and methods for estimating the EDP residuals of building structures by their applications to regional seismic loss assessment.

First, this dissertation focuses on developing a framework that can incorporate the EDP correlation into seismic system reliability analysis. To this end, the correlation between the safety factors of two different structures is formulated in terms of the IM correlation and EDP residual correlation. Based on the formula, the contribution of each correlation to the safety factor correlation is quantified.

Second, a method for accurately estimating the EDP residuals of structures using incremental dynamic analysis (IDA) (Vamvatsikos and Cornell, 2002) is developed to consider the EDP residual correlation. This IDA-based method estimates the variances and correlations of EDP residuals using structural responses to the selected ground motion set. Although the IDA-based method provides accurate estimation results, there is a limitation in that the estimation results may vary depending on the selected ground motions and require high computational costs. To address this, the dissertation additionally proposed an IM-invariant method, a non-IDA-based method for estimating the EDP residuals of structures based on the behavior in the elastic range. Taking advantage of the IM-invariant method, a more general expression of the EDP residuals of building structures with various structural characteristics can be obtained by employing many ground motions for the estimation. In addition, primary structural characteristics affecting the uncertainties and correlations of EDP residuals of building structures are identified through a comprehensive investigation using the EDP residuals estimated by the IM-invariant method.

Third, to facilitate applications of the proposed framework to regional seismic loss analyses, alternative methods are introduced to predict the EDP residuals of building structures without additional structural analysis based on regression models and deep neural networks (DNNs). The developed regression models approximate the standard deviations and correlation coefficients of EDP residuals using easy-to-obtain predictors describing the primary structural characteristics. In order to further improve the accuracy and applicability of the predicted EDP residual, two DNN-based frameworks are proposed. The first framework combines the EDP residuals of single degree of freedom (SDOF) systems through the modal combination to estimate the EDP residuals of building structures, i.e., multi degree of freedom (MDOF) system. To this end, three DNN models that respectively predict the means, standard deviations, and correlation coefficients of EDP residuals are proposed with appropriate means of summing the EDP residual of SDOF systems. On the other hand, the second framework presents two DNN models that directly predict the EDP residuals of specific types of building structures. A large number of MDOF systems having various first and second modal periods and damping ratios are employed in this regard.

Regional seismic loss assessment is one of the representative seismic system reliability analyses that can intuitively show the effect of EDP correlation on a system. Therefore, numerical examples in this dissertation focus on evaluating the seismic losses of urban areas. The developed framework for incorporating the IM and EDP residual correlations and two estimation methods are tested and demonstrated through regional loss assessment of a virtual city located in California. The accuracy and applicability of the regression models and two DNN-based

frameworks are verified by repeating the regional loss assessments and comparing the results.

1.3 Organization

The organization of the dissertation is illustrated in Figure 1.1. Chapter 2 develops a framework that incorporates the IM and EDP residual correlations for seismic system reliability analysis. Chapter 3 proposes an IDA-based method for estimating the EDP residuals of structures and demonstrates the effect of considering the EDP residual correlation on regional seismic loss assessment. A method to estimate the variances and correlations of EDP residuals of steel building structures is also developed. In Chapter 4, an IM-invariant method is proposed as an alternative to the IDA-based method to obtain a more general expression of EDP residuals. Furthermore, regression models for predicting the EDP residuals of building structures are developed to facilitate the consideration of EDP residual correlation. The IM-invariant method and the developed regression models are tested and verified through numerical examples of virtual urban areas. Chapter 5 proposes two DNN-based frameworks for estimating the EDP residuals of building structures with superior accuracy and applicability. Then, regional seismic loss assessments are carried out using the DNN-based frameworks and the results are compared with those obtained by the IM-invariant method and the developed regression models. Finally, Chapter 6 provides a summary of the developments and major findings. The dissertation concludes with discussions and recommendations for further studies.

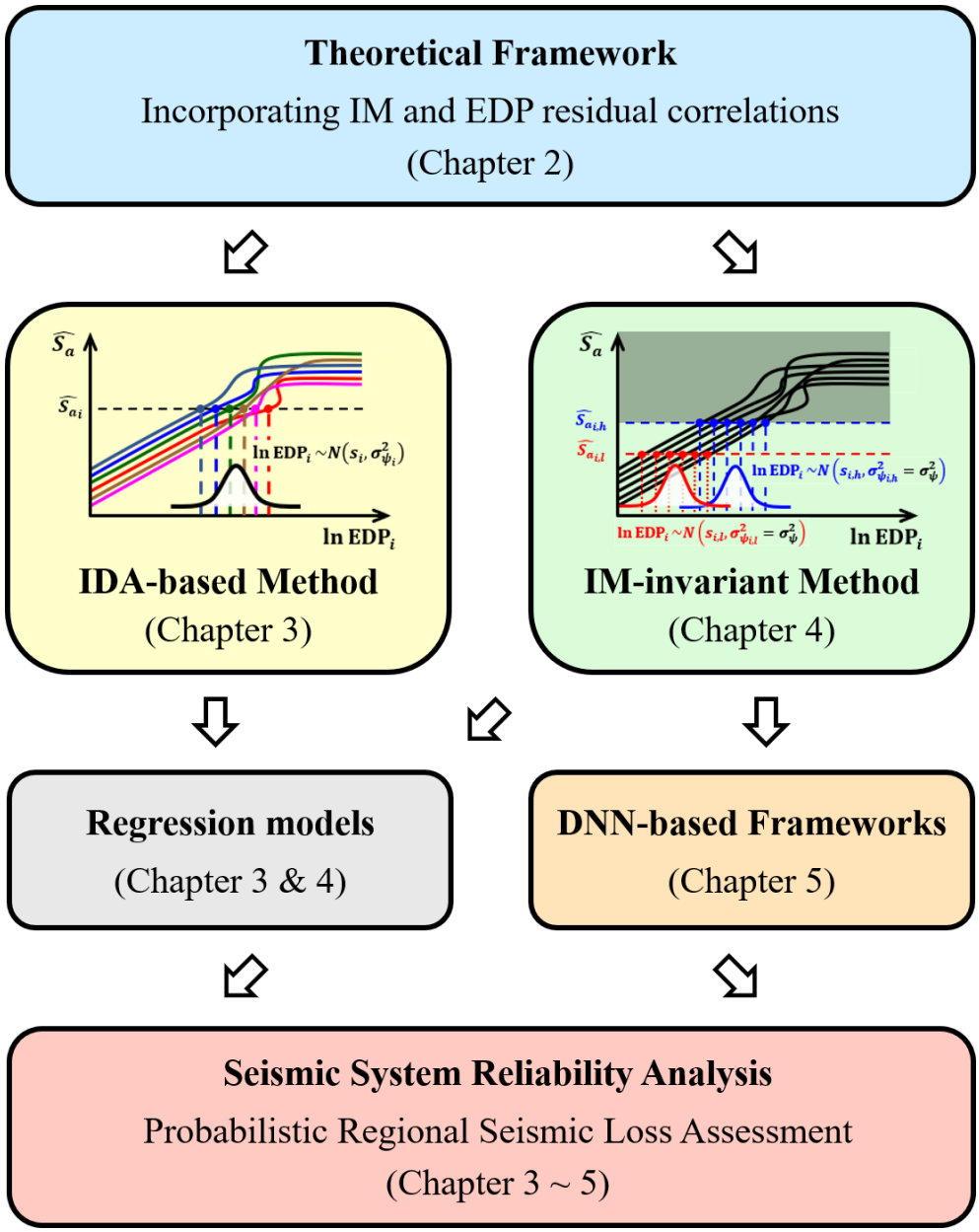

Figure 1.1 Organization of the dissertation

Chapter 2. Theoretical Framework to Evaluate Uncertainties and Correlations of Engineering Demand Parameters

2.1 Introduction

Structural failures bring about fundamental concerns which should be resolved for accurate regional seismic loss assessment. In particular, structures in urban areas show correlated failures due to their adjacent locations and similar structural characteristics. To consider the correlated failures between the structures in a region, it is necessary to adequately quantify the uncertainties and correlations of the structures' engineering demand parameters (EDP). Many previous studies (Baker and Cornell, 2008; Bradley, 2013) described the EDP of a structure as the sum of a regression function on the selected intensity measure (IM) and a residual termed "EDP residual." Therfore, the correlation coefficient between the EDPs is determined by the correlations of IM and EDP residual, termed "IM correlation" and "EDP residual correlation," respectively. For accurate seismic system reliability analysis, both types of uncertainties and correlations should be incorporated into the correlation between EDPs.

The uncertainties and correlations of EDPs are related to the IMs applied to the structures and the EDP residuals for given IMs. As shown in Figure 2.1, since the seismic intensity reaching a structure by an earthquake event depends on various conditions, empirical seismic attenuation relations termed ground motion prediction equations (GMPE) (Boore and Atkinson, 2008; Campbell and Bozorgnia, 2008; Abrahamson et al., 2016) have been developed to predict the IM and its uncertainties

in consideration of these conditions. The IM correlation is described by spatial correlation models (Boore et al., 2003; Wang and Takada, 2005; Baker and Cornell, 2006; Goda and Hong, 2008b; Jayaram and Baker, 2009; Sokolov et al., 2010; Loth and Baker, 2013) as the correlation between the intensities at two different sites for a given earthquake scenario.

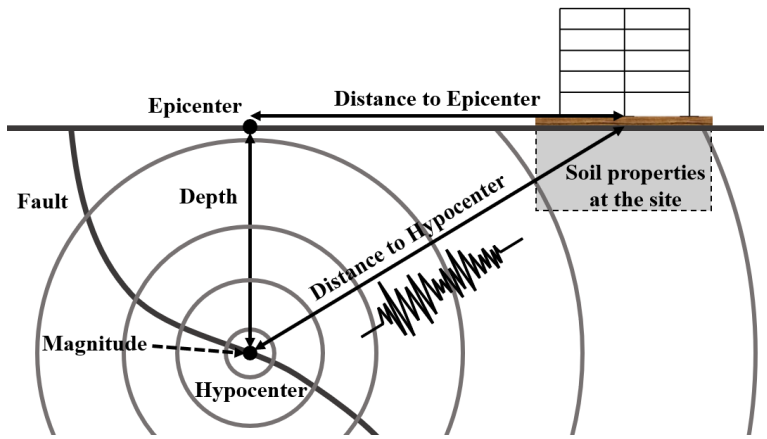

Figure 2.1 Propagation of seismic wave induced by earthquake event

On the other hand, the uncertainties and correlations of EDP residuals of structures originate from the uncertainties in frequency content, duration, and energy that cannot be totally captured by the selected IM alone. As shown in Figure 2.2, even if the same value of seismic intensity is applied, the seismic responses of the structure may vary. For this reason, it was necessary to quantify the uncertainties and correlations of EDP residuals, but research efforts on the EDP residual have not been sufficient. Lee and Kiremidjian (2007) introduced a residual error term consisting of three parts: independent, partially correlated, and highly correlated, but each part was assumed to be a specific percentage of the total residual. Baker and Cornell (2008) handled the EDP residual separately from the EDP predicted for a given

intensity measure and stated that EDP residual correlation could be determined through structural analysis. Bradley et al. (2010) computed the EDP residual correlation between different response parameters of a structure, such as maximum interstory drift ratios and peak floor accelerations in a 10-story building by performing multiple time history analyses. They provided guidelines for estimating EDP residual correlations of structural elements within a structure, but not for those between different structures.

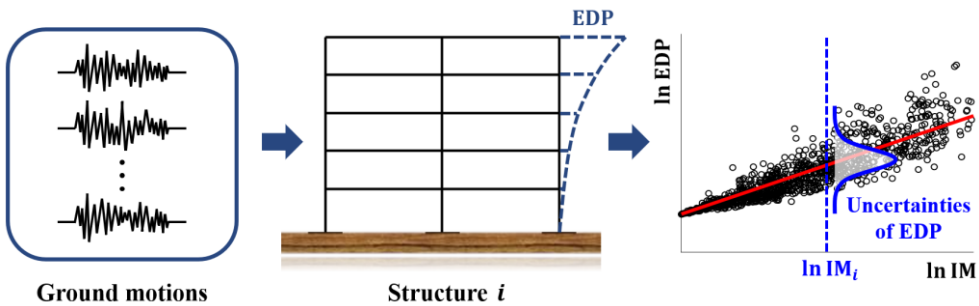

Figure 2.2 Uncertainties of EDP of a structure for given ground motions

Therefore, this chapter develops a theoretical framework for incorporating the EDP correlation into seismic system reliability analysis. In order to consider the IM and EDP residual correlations, this study first quantifies the uncertainties of the IM at the site and that of the EDP residual of the structure corresponding to the given IM. Next, the correlation between the safety factors is formulated in terms of the IM correlation and EDP residual correlation. Based on this formula, the probability of structure joint failure is computed using the formulated correlation coefficient between the safety factors. In addition, the contribution of each correlation to the safety factor correlation is identified (Kang et al., 2021).

2.2 Uncertainties in engineering demand parameters (EDPs)

A GMPE is often used to predict the IM of sites in a civil infrastructure system given an earthquake scenario. For a scenario characterized by earthquake magnitude M, epicentral distance R_i, and a set of other explanatory variables λ_i, the GMPE predicts the intensity measure at the site of the ith structure as

$$\ln Y_i = f(M, R_i, \lambda_i) + \eta + \varepsilon_i \tag{2.1}$$

where $\ln Y_i$ denotes the natural logarithm of the selected IM such as spectral acceleration (S_a), peak ground acceleration (PGA) and peak ground velocity (PGV); $f(M, R_i, \lambda_i)$ represents the attenuation relation; and η and ε_i respectively denote the inter-event residual representing the earthquake-to-earthquake variability and intra-event residual describing site-to-site variability (Abrahamson and Youngs 1992). In this dissertation, without losing generality, the spectral acceleration at the natural period T_n is selected as an IM. Using a GMPE, the natural logarithms of the spectral accelerations at the ith and jth structures, i.e., $\widehat{S_{a_i}}$ and $\widehat{S_{a_j}}$, are predicted as

$$\widehat{S_{a_i}} = f\left(M, R_i, \lambda_i, T_n^i\right) + \eta\left(T_n^i\right) + \varepsilon_i\left(T_n^i\right) \tag{2.2}$$

$$\widehat{S_{a_j}} = f\left(M, R_j, \lambda_j, T_n^j\right) + \eta\left(T_n^j\right) + \varepsilon_j\left(T_n^j\right) \tag{2.3}$$

where the residuals, defined for a given period T_n, are assumed to be zero-mean Gaussian random variables. It is also assumed that $\eta(T_n)$ and $\varepsilon(T_n)$ are statistically independent of each other while $\varepsilon_i(T_n)$ and $\varepsilon_j(T_n)$ are subject to the spatial correlation. $f(M, R_i, \lambda_i, T_n)$ is the mean of $\widehat{S_{a_i}}$, and thus the same as the natural logarithm of the median spectral acceleration.

Let us now consider D_i, an EDP of a structure, e.g., roof displacement, maximum interstory drift ratio (IDR). The mean EDP of a structure is predicted by a regression function of the selected IM, while its uncertainty can be expressed by the residual term, "EDP residual," i.e.,

$$\widehat{D}_i = s_i\left(\widehat{S_{a_i}}\right) + \psi_i\left(\widehat{S_{a_i}}\right) \tag{2.4}$$

where $s_i(\cdot)$ denotes the regression function of $\widehat{D}_i$ on $\widehat{S_{a_i}}$; and $\psi_i\left(\widehat{S_{a_i}}\right)$ is the residual of $\widehat{D}_i$ given $\widehat{S_{a_i}}$, called EDP residual. If $\psi_i\left(\widehat{S_{a_i}}\right)$ is assumed to follow a zero-mean Gaussian distribution, $\widehat{D}_i$ follows a Gaussian distribution $\widehat{D}_i \sim N\left(s_i\left(\widehat{S_{a_i}}\right), \sigma^2_{\psi_i\left(\widehat{S_{a_i}}\right)}\right)$. When the power-law (Cornell et al., 2002) is introduced to describe the relationship between EDP and IM, Eq. (2.1) can be expressed as

$$\widehat{D}_i = \ln a_i + b_i \widehat{S_{a_i}} + \psi_i\left(\widehat{S_{a_i}}\right) \tag{2.5}$$

where a_i and b_i are the parameters of the power-law model $D_i = a_i \cdot \left(S_{a_i}\right)^{b_i}$, identified by structural analyses.

2.3 Correlation between EDPs of structures

2.3.1 Correlation coefficient between safety factors

Seismic fragility is defined as the conditional probability that the selected EDP D_i exceeds a specified limit state d_i given a value of IM. When assuming the EDP follows a Lognormal distribution, the safety factor $F_i = \ln d_i - \ln D_i = \hat{d}_i - \widehat{D}_i$ follows a Gaussian distribution. Substituting Eq. (2.5) into $\widehat{D}_i$ in the safety factor, the (marginal) fragility of the ith structure given $\widehat{S_{a_i}} = x$ is computed as

$$P\left(F_i \le 0 \middle| \widehat{S_{a_i}} = x\right) = P\left(\psi_i(x) \ge \hat{d}_i - s_i(x)\right) = 1 - \Phi\left(\frac{\hat{d}_i - s_i(x)}{\sigma_{\psi_i(x)}}\right) \tag{2.6}$$

where $\Phi(\cdot)$ denotes the cumulative distribution function (CDF) of the standard Gaussian distribution. From the total probability theorem, the failure probability by a given earthquake scenario can be computed as

$$P_{f_i} = \int_{-\infty}^{\infty} P\left(F_i \le 0 \middle| \widehat{S_{a_i}} = x\right) f_{\widehat{S_{a_i}}}(x)dx = \int_{-\infty}^{\infty} \left[1 - \Phi\left(\frac{\hat{d}_i - s_i(x)}{\sigma_{\psi_i(x)}}\right)\right] f_{\widehat{S_{a_i}}}(x)dx \tag{2.7}$$

where $f_{\widehat{S_{a_i}}}(\cdot)$ denotes the probability density function (PDF) of $\widehat{S_{a_i}}$ for a given earthquake scenario, which is assumed to follow the Gaussian distribution in Eq. (2.2).

Next, the joint failure probability of the ith and jth structures given an earthquake scenario – critical information for system reliability analysis – can be described as follows by extending Eq. (2.7):

$$P_{f_{ij}} = \int_{-\infty}^{\infty}\int_{-\infty}^{\infty} P\left(F_i \le 0 \cap F_j \le 0 \middle| \widehat{S_{a_i}} = x_i, \widehat{S_{a_j}} = x_j\right) \times f_{\widehat{S_{a_i}}\widehat{S_{a_j}}}(x_i, x_j)dx_i dx_j \tag{2.8}$$

where $f_{\widehat{S_{a_i}}\widehat{S_{a_j}}}$ denotes the joint PDF of $\widehat{S_{a_i}}$ and $\widehat{S_{a_j}}$. Assuming the safety factors follow a bivariate Gaussian distribution, the joint failure probability in Eq. (2.8) can be efficiently computed by a single-fold integration (Ditlevsen and Madsen, 1996) as

$$P_{f_{ij}} = P_{f_i}P_{f_j} + \int_0^{\rho_{F_iF_j}} \varphi_2(-\beta_i, -\beta_j; \rho)d\rho \tag{2.9}$$

where $\beta_i = -\Phi^{-1}(P_{f_i})$ denotes the generalized reliability index of the ith structure; $\rho_{F_iF_j}$ is the correlation coefficient between the safety factors F_i and F_j; and $\varphi_2(\cdot,\cdot;\rho)$ denotes the bi-variate standard Gaussian PDF with correlation coefficient ρ.

Eq. (2.9) indicates that the joint failure probability can be computed efficiently by a single-fold integration if the component failure probabilities in Eq. (2.7) and the correlation coefficient $\rho_{F_iF_j}$ are available. To facilitate the joint failure probability calculations using Eq. (2.9), the correlation coefficient $\rho_{F_iF_j}$ is derived in this study as follows under the assumption that the spectral acceleration and EDP residual are uncorrelated to each other (see Appendix A for details of the derivation):

$$\begin{aligned}\rho_{F_iF_j} &= \frac{b_i b_j \sigma_{\widehat{S_{a_i}}} \sigma_{\widehat{S_{a_j}}}}{\sqrt{b_i^2 \sigma_{\widehat{S_{a_i}}}^2 + \sigma_{\psi_i}^2}\sqrt{b_j^2 \sigma_{\widehat{S_{a_j}}}^2 + \sigma_{\psi_j}^2}} \rho_{\widehat{S_{a_i}}\widehat{S_{a_j}}} \\ &\quad + \frac{\sigma_{\psi_i}\sigma_{\psi_j}}{\sqrt{b_i^2 \sigma_{\widehat{S_{a_i}}}^2 + \sigma_{\psi_i}^2}\sqrt{b_j^2 \sigma_{\widehat{S_{a_j}}}^2 + \sigma_{\psi_j}^2}} \rho_{\psi_i\psi_j} \\ &= A_S \rho_{\widehat{S_{a_i}}\widehat{S_{a_j}}} + A_\psi \rho_{\psi_i\psi_j}\end{aligned} \tag{2.10}$$

where $\sigma_{\widehat{S_{a_i}}}$, $\sigma_{\widehat{S_{a_j}}}$, σ_{ψ_i}, and σ_{ψ_j} denote the standard deviations of $\widehat{S_{a_i}}$, $\widehat{S_{a_j}}$, ψ_i, and ψ_j, respectively; b_i and b_j are the power-law model parameters of the structures; $\rho_{\widehat{S_{a_i}}\widehat{S_{a_j}}}$ is the correlation coefficient between $\widehat{S_{a_i}}$ and $\widehat{S_{a_j}}$ reaching the ith and jth structures by a given earthquake scenario, termed "IM correlation"; and $\rho_{\psi_i\psi_j}$ is the correlation coefficient between ψ_i and ψ_j, termed "EDP residual correlation." These correlations are illustrated in Figure 2.3. A_S and A_ψ in Eq. (2.10) quantifies the contributions of the IM correlation $\rho_{\widehat{S_{a_i}}\widehat{S_{a_j}}}$ and the EDP residual correlation $\rho_{\psi_i\psi_j}$ to the correlation coefficient between safety factors.

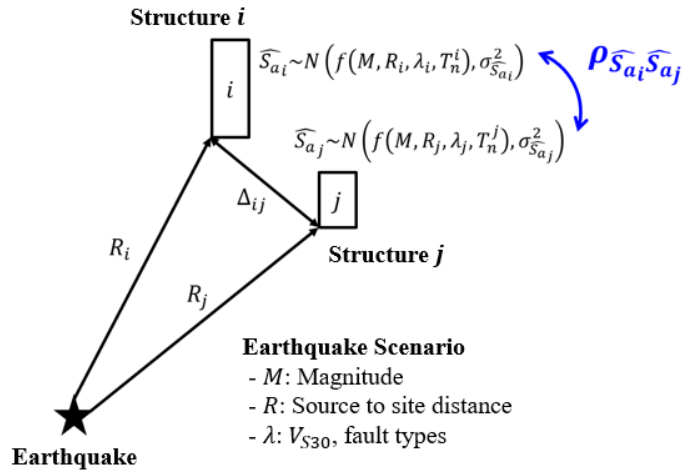

(a)

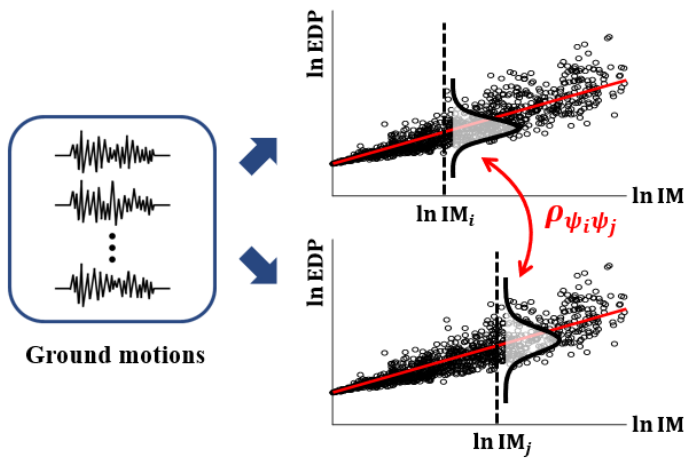

(b)

Figure 2.3 Two types of correlations in seismic system reliability analysis: (a) IM correlation, and (b) EDP residual correlation

Earlier studies that considered only IM correlation $\rho_{\widehat{S_{a_i}}\widehat{S_{a_j}}}$ employed $\sigma_{\widehat{S_{a_i}}}$ and $\rho_{\widehat{S_{a_i}}\widehat{S_{a_j}}}$ which were derived from existing GMPE studies (Boore et al., 2003; Wang and Takada, 2005; Baker and Cornell, 2006; Boore and Atkinson, 2008; Campbell and Bozorgnia, 2008; Goda and Hong, 2008b; Jayaram and Baker, 2009; Sokolov et al., 2010; Loth and Baker, 2013; Abrahamson et al., 2016) as

$$\sigma_{\widehat{S_{a_i}}} = \sqrt{\left[\sigma_\eta\left(T_n^i\right)\right]^2 + \left[\sigma_\varepsilon\left(T_n^i\right)\right]^2} \tag{2.11}$$

$$\begin{aligned}\rho_{\widehat{S_{a_i}}\widehat{S_{a_j}}} = \rho_{\eta\eta}\left(T_n^i, T_n^j\right)\frac{\sigma_\eta\left(T_n^i\right)\sigma_\eta\left(T_n^j\right)}{\sigma_{\widehat{S_a}}\left(T_n^i\right)\sigma_{\widehat{S_a}}\left(T_n^j\right)} \\ + \rho_{\varepsilon_i\varepsilon_j}\left(\Delta_{ij}, T_n^i, T_n^j\right)\frac{\sigma_{\varepsilon_i}\left(T_n^i\right)\sigma_{\varepsilon_j}\left(T_n^j\right)}{\sigma_{\widehat{S_a}}\left(T_n^i\right)\sigma_{\widehat{S_a}}\left(T_n^j\right)}\end{aligned} \tag{2.12}$$

where $\sigma_\eta(T_n)$ and $\sigma_\varepsilon(T_n)$ respectively denote the standard deviations of the inter- and intra-event residuals; $\rho_{\eta\eta}\left(T_n^i, T_n^j\right)$ is the correlation coefficient between the inter-event residuals at two different periods T_n^i and T_n^j; and $\rho_{\varepsilon_i\varepsilon_j}\left(\Delta_{ij}, T_n^i, T_n^j\right)$ denotes the spatial correlation coefficient between the intra-event residuals at two sites i and j with distance Δ_{ij} (km). Without losing generality, the examples in this study employ the correlation coefficient between intra-event residuals proposed by Goda and Hong (2008b), i.e.,

$$\begin{aligned}\rho_{\varepsilon_i\varepsilon_j}\left(\Delta_{ij}, T_n^i, T_n^j\right) &= \rho_{\varepsilon_i\varepsilon_j}\left(\Delta_{ij}, T_{\max}\right) \\ &= \exp\left[-(0.68 - 0.16\ln T_{\max})\Delta_{ij}^{0.44}\right]\end{aligned} \tag{2.13}$$

where $T_{\max} = \max\left[T_n^i, T_n^j\right]$ represents the maximum value among T_n^i and T_n^j (sec). The correlation coefficient between inter-event residuals, $\rho_{\eta\eta}\left(T_n^i, T_n^j\right)$ is calculated by the model proposed by Baker and Cornell (2006),

$$\begin{aligned}\rho_{\eta\eta}\left(T_n^i, T_n^j\right) = 1 - \cos\left[\frac{\pi}{2} - 0.359\ln\frac{T_{\max}}{T_{\min}}\right. \\ \left. -0.163 I_{(T_{\min}<0.189)}\ln\frac{T_{\min}}{0.189}\ln\frac{T_{\max}}{T_{\min}}\right]\end{aligned} \tag{2.14}$$

where $T_{\min} = \min\left[T_n^i, T_n^j\right]$ denotes the minimum value among T_n^i and T_n^j (sec); and $I_{(T_{\min}<0.189)}$ is an indicator function which gives 1 if $T_{\min}$ is less than 0.189 sec and 0 otherwise.

2.3.2 Contributions of IM and EDP residual correlations

The derivations of the joint failure probability (Eq. (2.9)) and the correlation coefficient (Eq. (2.10)) are demonstrated and verified by the following numerical example. The results by three methods, i.e., Monte-Carlo simulation (MCS) with 10^6 samples, double-fold integration in Eq. (2.8), and the proposed single-fold integration by Eqs. (2.9) and (2.10), are compared. The example employs the following parameter values that are typical for steel moment frames under strong earthquake scenarios:

$$\text{Limit state: } d = \begin{bmatrix} d_i \\ d_j \end{bmatrix} = \begin{bmatrix} 0.02 \\ 0.03 \end{bmatrix}$$

$$\text{Power-law model parameters: } a = \begin{bmatrix} a_i \\ a_j \end{bmatrix} = \begin{bmatrix} 0.05 \\ 0.07 \end{bmatrix}$$

$$b = \begin{bmatrix} b_i \\ b_j \end{bmatrix} = \begin{bmatrix} 0.8 \\ 0.9 \end{bmatrix}$$

$$\text{Spectral acceleration: } \mu_{\widehat{S_a}} = \begin{bmatrix} \widehat{S_{a\,i}} \\ \widehat{S_{a\,j}} \end{bmatrix} = \begin{bmatrix} \ln 0.2 \\ \ln 0.4 \end{bmatrix} \tag{2.15}$$

$$\Sigma_{\widehat{S_a}\widehat{S_a}} = \begin{bmatrix} 0.5 & 0.2 \\ 0.2 & 0.3 \end{bmatrix}$$

$$\text{EDP residual: } \mu_{\psi} = \begin{bmatrix} \psi_i \\ \psi_j \end{bmatrix} = \begin{bmatrix} 0 \\ 0 \end{bmatrix}$$

$$\Sigma_{\psi\psi} = \begin{bmatrix} 0.1 & 0.1 \\ 0.1 & 0.2 \end{bmatrix}$$

where $\mu_{\widehat{S_a}}$ and $\Sigma_{\widehat{S_a}\widehat{S_a}}$ respectively denote the mean vector and the covariance matrix of $\widehat{S_{a\,i}}$ and $\widehat{S_{a\,j}}$; and μ_{ψ} and $\Sigma_{\psi\psi}$ are the mean vector and the covariance matrix of ψ_i and ψ_j, respectively.

Table 2.1 summarizes the results by the three methods. MCS can estimate all probabilistic measures but requires a large number of samples when failure probabilities are low. The joint failure probability of the ith and jth structures is

calculated accurately through a double-fold integration in Eq. (2.8), but this approach cannot identify the relative contributions of the different types of correlations via A_S and A_ψ. The proposed method estimates the correlation coefficient by Eq. (2.10) and substitutes it into Eq. (2.9) to compute the joint failure probability. The results confirm that the proposed method can compute the joint failure probability and the correlation coefficient between the safety factors efficiently without compromising accuracy.

Table 2.1 Comparison between the joint failure probability and the correlation coefficient computed by three methods

Method	P_{f_i}	P_{f_j}	$P_{f_{ij}}$	A_S	A_ψ	$\rho_{F_iF_j}$
MCS	0.283	0.513	0.225	0.647	0.329	0.567
Eq. (2.8)	0.283	0.514	0.224	-	-	-
Eq. (2.9)	0.283	0.514	0.224	0.647*	0.328*	0.566*

* calculated by Eq. (2.10).

The derivation in Eq. (2.10) shows that A_S, A_ψ and $\rho_{F_iF_j}$ depend on the power-law model parameters (b_i, b_j) and the standard deviations of IM and EDP residuals ($\widehat{S_{a_i}}$, $\widehat{S_{a_j}}$, ψ_i, and ψ_j). To investigate the effects of these parameters and standard deviations on the contribution of IM and EDP residual correlations (A_S, A_ψ) and the correlation coefficient between the safety factors $\rho_{F_iF_j}$, let us consider the case in which $b_i = b_j = b$, $\sigma_{\widehat{S_{a_i}}} = \sigma_{\widehat{S_{a_j}}} = \sigma_{\widehat{S_a}}$, and $\sigma_{\psi_i} = \sigma_{\psi_j} = \sigma_\psi$. Then, it can be shown that $A_S = r^2/(r^2+1)$, and $A_\psi = 1/(r^2+1)$ where $r = b \cdot \sigma_{\widehat{S_a}}/\sigma_\psi$ as plotted in Figure 2.4. Figure 2.5 shows $\rho_{F_iF_j}$ for three combinations of $\rho_{\widehat{S_{a_i}}\widehat{S_{a_j}}}$ and $\rho_{\psi_i\psi_j}$. In both figures, as r increases, the contribution of IM correlation

becomes larger while that of EDP residual correlation gets smaller. The term $\sigma_{\widehat{S_a}}/\sigma_\psi$ in the ratio r quantifies the relative dominance of the uncertainty of IM compared to that of the EDP residual. On the other hand, the term b in r represents the sensitivity of EDP with respect to IM, identified by the regression model. If a system includes pairs of structures with small values of r, ignoring the EDP residual correlation may significantly underestimate the total EDP correlations in seismic system reliability analysis.

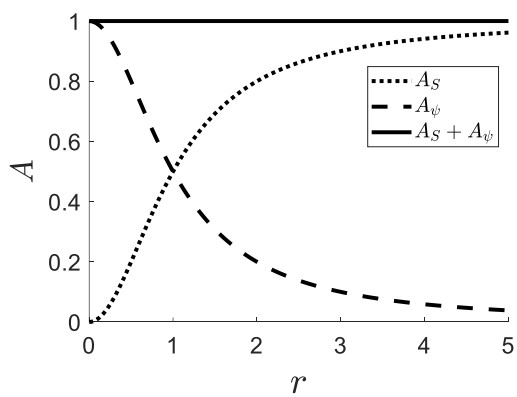

Figure 2.4 Contributions of IM and EDP residual correlations to the safety factor correlation when $b_i = b_j = b$, $\sigma_{\widehat{S_{a_i}}} = \sigma_{\widehat{S_{a_j}}} = \sigma_{\widehat{S_a}}$, and $\sigma_{\psi_i} = \sigma_{\psi_j} = \sigma_\psi$

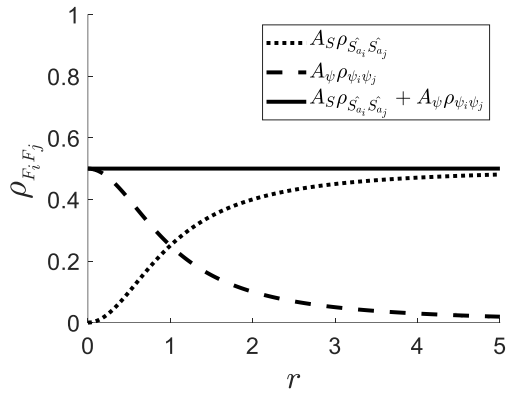

(a)

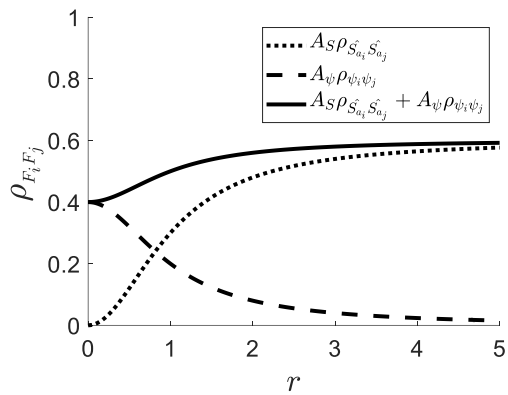

(b)

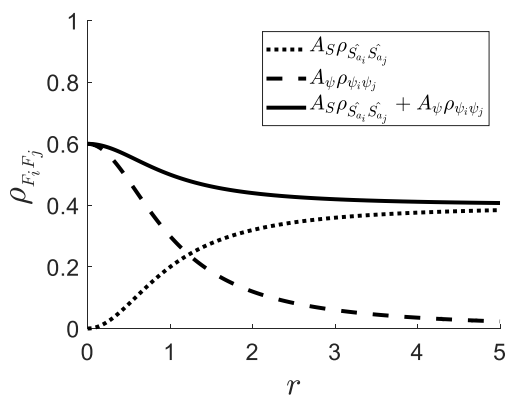

(c)

Figure 2.5 The correlation coefficient between safety factors when $b_i = b_j = b$, $\sigma_{\widehat{S_{a_i}}} = \sigma_{\widehat{S_{a_j}}} = \sigma_{\widehat{S_a}}$, and $\sigma_{\psi_i} = \sigma_{\psi_j} = \sigma_\psi$: (a) $\rho_{\widehat{S_{a_i}}\widehat{S_{a_j}}} = \rho_{\psi_i\psi_j} = 0.5$, (b) $\rho_{\widehat{S_{a_i}}\widehat{S_{a_j}}} = 0.6$, $\rho_{\psi_i\psi_j} = 0.4$, and (c) $\rho_{\widehat{S_{a_i}}\widehat{S_{a_j}}} = 0.4$, $\rho_{\psi_i\psi_j} = 0.6$

2.4 Summary

A theoretical framework was proposed in this study to accurately consider the effects of the correlations between engineering demand parameters (EDP) of structures on seismic system reliability analysis. To this end, the correlation between the safety factors of two different structures is newly derived in terms of the correlation between intensity measures (IM) and that between the EDP residuals. Furthermore, by quantifying the contribution of each correlation according to the power-law model parameter and the standard deviations of IM and EDP residual, the effect of considering the EDP residual correlation was demonstrated.

Chapter 3. Incremental Dynamic Analysis-based Method for Considering EDP Correlation

3.1 Introduction

To evaluate the seismic fragility and failure probabilities discussed in Section 2.3.1, it is essential to first determine the relationship between IM and EDP, which is described through the power-law model as in Eq. (2.5). To this end, pushover analysis and nonlinear time history analysis are most widely used. Pushover analysis is a static analysis procedure to determine the relationship between base shear and global deformation. Many prior studies (Shinozuka et al., 2000; Rossetto et al., 2016) used pushover analysis for quick evaluation of the fragility although the method tends to underestimate interstory drift of a structure. On the other hand, time history analysis is considered the most accurate method to cover a wide range of IM-EDP relationships in various situations. Furthermore, the nonlinear time history analysis makes it possible to obtain structural responses subject to the uncertainties in frequency content, duration, and energy that cannot be totally captured by the selected IM alone. Therefore, this study introduces a method to accurately evaluate the relationship between IM and EDP of a structure and the variances and correlations of EDPs of structures through nonlinear time history analysis. The proposed method performs Incremental Dynamic Analysis (IDA) (Vamvatsikos and Cornell, 2002) for a pair of structures with the same suite of ground motion time histories to evaluate the EDP residual correlation. These EDP residual correlations and the IM correlation are substituted into a new formula derived in this dissertation, i.e., Eq. (2.10) to evaluate the correlation coefficients between EDPs of structures in

the target system.

Regional seismic loss assessment is performed to demonstrate the effect of consideration of EDP correlation on seismic system reliability analysis. An accurate evaluation of regional seismic loss is essential for establishing an emergency response plan in the event of an earthquake, which can reduce casualties and socioeconomic losses in an urban community. To evaluate the loss in a region with spatially distributed buildings, the spectral acceleration is selected as IM and maximum interstory drift ratio (IDR) is selected as EDP. This chapter presents a method to assess the regional seismic loss using the theoretical framework proposed in Chapter 2. The contribution of the EDP residual correlation is confirmed by comparing the total loss exceedance probability of an urban area according to the type of correlation considered.

It is noted that the nonlinear structural analysis repeated for IDA would require high computational costs and structural modeling efforts. To facilitate applications of the proposed theoretical framework to large-size systems, this study proposes a method to approximate the EDP residual correlation between steel building structures using a nonlinear regression model along with a detailed guideline. The proposed regression model and guideline are verified through an example of a regional loss assessment (Kang et al., 2021).

3.2 Development of IDA-based method

3.2.1 IDA-based method for estimating variances and correlation coefficients of EDP residuals of structures

This study adopts, without loss of general applicability, Incremental Dynamic

Analysis (IDA) (Vamvatsikos and Cornell, 2002) for evaluating the variability in the seismic demand of structures through nonlinear time history analysis. The overall procedure is illustrated in Figure 3.1. In IDA, selected ground motion time histories are repeatedly scaled to perform a series of nonlinear time history analysis. As a result, for each of the selected ground motions, an IDA curve – the relationship between IM of the scaled ground motion and the corresponding EDP – is obtained. Using these IDA curves representing the seismic behavior of the structure, the structural fragility function can be derived (Ellingwood et al., 2007). The followings are details of the IDA-based procedure proposed for evaluating the variances and correlations of EDP residuals required for Eqs. (2.9) and (2.10):

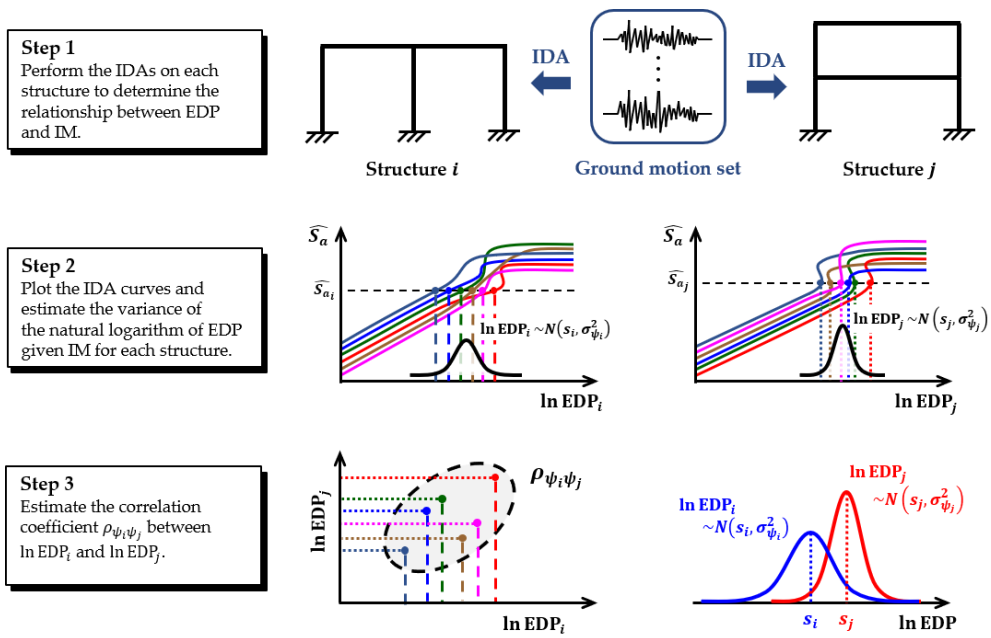

Figure 3.1 Overall procedure for estimating the variances and correlations of the natural logarithms of EDP residuals

(Step 1) Perform IDA for each structure to determine the relationship between the natural logarithms of EDP and IM

Suppose the ith and jth structures in a system are of interest, and the spectral acceleration (S_a) at the first mode period of each structure is selected as IM. First, the IDA is performed for each structure using the common set of ground motions, i.e., the spectral acceleration of each ground motion is incrementally scaled until the structures become dynamically unstable.

(Step 2) Plot the IDA curves and estimate the variance of the natural logarithm of EDP given IM for each structure

Depending on the choice of IM and EDP, the corresponding IDA curves may show various shapes. In the examples of this study, without losing general applicability, the spectral acceleration (S_{a_i}) and the maximum IDR are selected as IM and EDP, respectively. From the IDA curves, the conditional variance of the natural logarithm of EDP ($\widehat{S_{a_i}}$) given IM is estimated by using x-coordinates of the intersections of IDA curves with the horizontal line at $\widehat{S_{a_i}}$. If IDA curves are flattened before reaching the given IM, one cannot find the corresponding intersection points and the corresponding EDP values, as illustrated in Figure 3.2.

Let us consider the case in which some of the curves flatten before reaching $\widehat{S_{a_i}}$, as shown in Figure 3.2. Since this means that the structure has reached collapse state, the regression model i.e., $s_i = \ln a_i + b_i \widehat{S_{a_i}}$ cannot describe the relationship between IM and EDP. To overcome this issue, the proposed IDA-based method defines alternative EDP values for the flattened curves, using an alternative estimation method (Jalayer and Cornell, 2009). The proposed framework first finds

the maximum IM value at which all IDA curves do not flatten, i.e., $\widehat{S_{a_i}}$ when the structure is in the "near-collapse" level. Next, x-coordinates of the intersections of IDA curves at $\widehat{S_{a_i}}$, i.e., black and red dots in Figure 3.2, are identified. Then the variance of the natural logarithm of EDP can be estimated by all of EDP values. Since the EDP residual is estimated by the mean of a given intensity predicted by the attenuation relation in Eq. (2.1), the structural collapse rarely occurs. Therefore, the use of an alternative estimation method does not significantly affect the results. As mentioned earlier, the regression model can describe the IM-EDP relationship in structural performance level before the structure collapses. In order to properly account for collapse state of structures, it is necessary to estimate the parameters of regression model through probability-based seismic assessment method (Jalayer and Cornell, 2009).

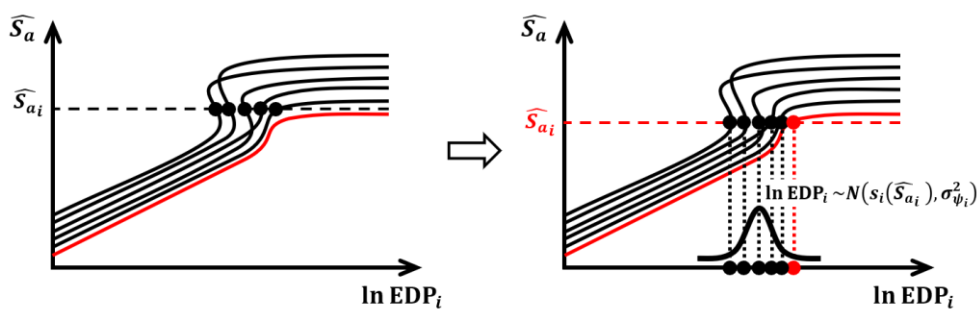

Figure 3.2 Procedure for estimating the variance of the natural logarithm of EDP when some of IDA curves flatten before reaching a given IM

(Step 3) Estimate EDP residual correlation between structures i and j

The relationship between EDPs of two structures obtained by IDA using the common set of ground motions can be represented by a scatter plot, as illustrated in Figure 3.1. From this, the correlation coefficient between the EDP residuals, i.e., $\rho_{\psi_i\psi_j}$ in

Eq. (2.10), can be estimated by as many points as the number of ground motions used in the IDA.

3.2.2 Ground motion selection for IDA-based method

It is widely recognized that the results of IDA are significantly affected by the selected ground motion set. This was reported in many other previous studies using IDA to estimate the fragility of individual structures (Miano et al., 2017; Deniz et al., 2018). The same issue occurs in the estimation of EDP residual correlation presented in this study. Therefore, this study adopts the far-field ground motion selection criteria of the PEER NGA database (PEER 2013) to reduce the subjectivity of selecting the ground motion set. Among diverse ground motions satisfying the adopted criteria, in particular, the far-field ground motion set in FEMA P695 (FEMA 2009) is used for the IDA-based method. This ground motion set has been used to evaluate the collapse of archetypes designed for Seismic Design Category (SDC) B, C, or D criteria. This set includes 22 pairs of horizontal ground motions in two orthogonal directions (i.e., total 44 ground motion records), recorded from sites located more than 10 km apart from the fault rupture (See Appendix B for details of the selected ground motions). The ground motion set was utilized in various studies (Elkady and Lignos, 2015; Elkady, 2016; Kohrangi et al., 2017; Bakalis and Vamvatsikos, 2018).

3.3 Evaluation of regional seismic losses considering correlation between EDPs of structures

3.3.1 Probabilistic regional seismic loss assessment

Regional seismic losses can be predicted by evaluating the structural damage for a given earthquake event (Steelman et al., 2007; FEMA, 2012a; Gardoni et al., 2018). As mentioned earlier, ignoring the correlation between EDPs of structures in the same region may underestimate the uncertainty in the estimated loss. In the following, the main formulation of probabilistic regional loss assessment is first introduced with consideration of EDP correlations and applied to an example to investigate the effect of EDP correlation on the regional seismic loss. It is noted that, the probabilistic regional seismic loss assessment is applicable to the cases in which the damage of each structure is assessed at the global level in terms of a single type of EDP.

To accurately evaluate the seismic risk of an urban area, it is necessary to estimate the mean and standard deviation of the total economic loss. When m damage states are used to describe the damage of each building, the mean and variance of the loss of the ith building, and the correlation coefficient between the losses of the ith and jth buildings are respectively derived as

$$\mu_{L_i} = \sum_{k=1}^{m} l_i^{DS_k} P_{f_i}^{DS_k} \tag{3.1}$$

$$\sigma_{L_i}^2 = E\left[L_i^2\right] - \mu_{L_i}^2 = \sum_{k=1}^{m} \left(l_i^{DS_k}\right)^2 P_{f_i}^{DS_k} - \mu_{L_i}^2 \tag{3.2}$$

$$\rho_{L_iL_j} = \frac{E[L_iL_j] - \mu_{L_i}\mu_{L_j}}{\sigma_{L_i}\sigma_{L_j}} = \frac{\sum_{k=1}^{m}\sum_{l=1}^{m} l_i^{DS_k} l_j^{DS_l} P(L_i = l_i^{DS_k} \cap L_j = l_j^{DS_l}) - \mu_{L_i}\mu_{L_j}}{\sigma_{L_i}\sigma_{L_j}} \quad (3.3)$$

where L_i is the economic loss of the ith building; μ_{L_i} and σ_{L_i} respectively denote the mean and standard deviation of L_i; $l_i^{DS_k}$ and $P_{f_i}^{DS_k}$ respectively represent the loss and probability of the ith building in damage state k; and $\rho_{L_iL_j}$ is the correlation coefficient between L_i and L_j. The probability $P(L_i = l_i^{DS_k} \cap L_j = l_j^{DS_l})$ in Eq. (3.3) is equal to the joint failure probability of the buildings with respect to the *k*th and *l*th damage state, which can be calculated by substituting the correlation coefficient between EDPs calculated using Eq. (2.10) into Eq. (2.9).

Suppose the total loss of N buildings in the region is estimated in terms of the replacement cost of individual buildings as $L = \sum_{i=1}^{N} \alpha_i L_i$ where α_i is the ratio of the replacement cost to the actual loss of the ith building. Then, the mean and variance of the total regional loss are respectively derived as

$$\mu_L = \sum_{i=1}^{N} \alpha_i \mu_{L_i} \quad (3.4)$$

$$\sigma_L^2 = \sum_{i=1}^{N} \alpha_i^2 \sigma_{L_i}^2 + 2\sum_{i=1}^{N-1}\sum_{j=i+1}^{N} \alpha_i\alpha_j\sigma_{L_i}\sigma_{L_j}\rho_{L_iL_j} \quad (3.5)$$

In the following examples, the ratios $\alpha_i,\ i = 1, \dots, N,$ are assumed to be 1 for simplicity. It is noted that the mean of the total loss, μ_L is not affected by the correlation between the losses of different structures, which comes from that between EDPs. On the other hand, the EDP correlation affects the variance of the total loss σ_L. Therefore, as the correlation between safety factors increases, the probability that

the total loss exceeds a certain loss L' increases, as shown by the shaded region in Figure 3.3.

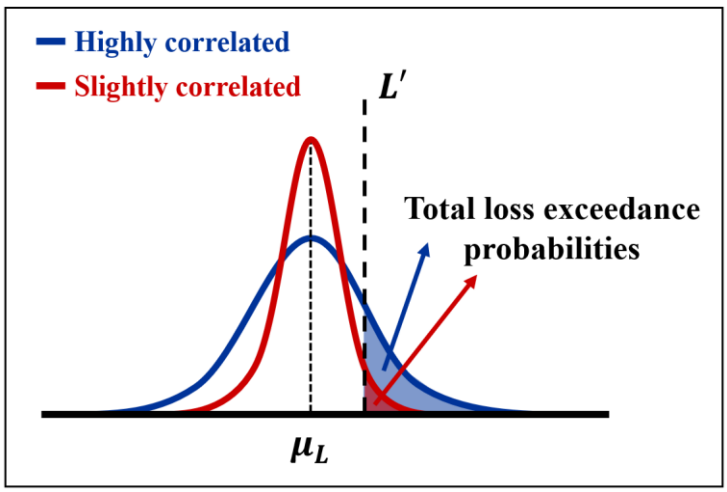

Figure 3.3 Effects of safety factor correlation on the probability that the total loss exceeds a certain loss L'

Assuming that the total loss L follows a Lognormal distribution (Goda and Ren, 2010) with the mean and standard deviation derived in Eqs. (3.4) and (3.5), the probability that the loss exceeds a threshold l_0 is computed as

$$P(L > l_0) = 1 - P(L \leq l_0) = 1 - \Phi\left(\frac{\ln l_0 - \lambda_L}{\zeta_L}\right) \tag{3.6}$$

where λ_L and ζ_L respectively denote the mean and standard deviation of the natural logarithm of L, obtained by $\lambda_L = \ln \mu_L - 0.5 \ln(1 + \delta_L^2)$ and $\zeta_L = \sqrt{\ln(1 + \delta_L^2)}$ in which $\delta_L = \sigma_L / \mu_L$.

3.3.2 Structural modeling of reference buildings

For the example of regional seismic loss assessment with EDP correlations considered, this study adopts fifteen archetype steel moment frame (SMF) buildings with five different heights (2, 4, 8, 12, and 20 stories) and three strong-column weak-beam (SCWB) ratios (SCWB > 1.0, > 1.5, and > 2.0). The modulus of elasticity (E) and the yield stress (F_y) of the beams and columns are assumed to be 200 GPa (29,000 ksi), and 379 MPa (55 ksi), respectively. The adopted SMF buildings (Elkady and Lignos, 2015; Elkady, 2016) were designed according to ANSI/AISC 341-10 (AISC, 2010a), ANSI/AISC 358-10 (AISC, 2010b), and ASCE/SEI 7-10 (ASCE, 2010). These buildings adopt a rectangular plan view with perimeter three-bay SMFs in each loading direction, as shown in Figure 3.4. As a result, SMFs in basic seismic force-resisting systems are assumed to have the response modification coefficient of $R = 8$, and system overstrength factor of $\Omega_0 = 3$.

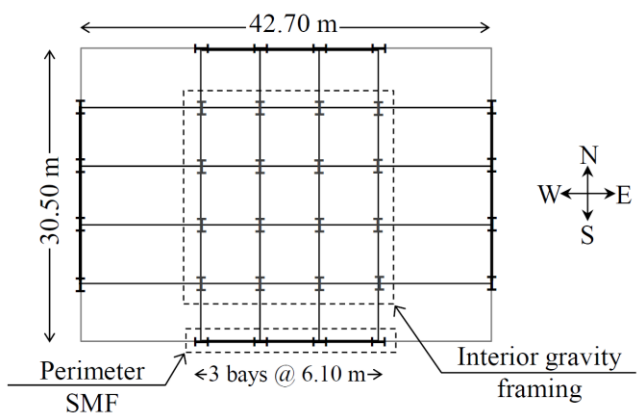

Figure 3.4 Plan view of fifteen archetype buildings (Elkady, 2016)

Two-dimensional nonlinear structural models of fifteen archetype buildings are modeled and analyzed in OpenSees software (Mazzoni et al., 2006). All of the members are modeled as elastic elements with rotational flexural springs. In particular, the rotational flexural springs of the beams and columns are represented by the modified Ibarra-Medina-Krawinkler (IMK) deterioration model (Ibarra et al., 2005; Lignos and Krawinkler, 2011) while the panel zone is modeled using the parallelogram model proposed by Gupta and Krawinkler (1999). The gravity loads of internal gravity frames are also considered using a leaning column, which is connected to the SMFs via axial rigid links. To consider the P-Delta effects in the structural analysis, the corotational transformation in OpenSees is used. The details of fifteen SMF buildings such as the member sizes and the coefficients of beam-to-column panel zone can be found in Elkady (2016).

For the building models introduced above, IDAs are performed by OpenSees using 44 ground motions in the far-field ground motion set which is described in Appendix B. From the analysis results, 44 IDA curves are obtained for each building, and the parameters of the power-law model, i.e., a, and b are determined through a regression analysis. In this study, the modeling uncertainties of buildings are not considered and it is assumed that the seismic responses obtained by structural analyses were reliable. The characteristics of the fifteen building models and the parameters of the power-law regression models are summarized in Table 3.1. For example, the IDA curves and the corresponding regression model obtained for Building No. 8 are shown in Figure 3.5.

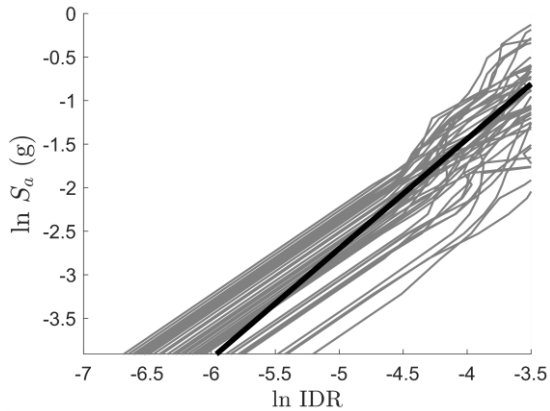

Figure 3.5 IDA curves (gray) and power-law regression model (black) of Building No. 8 (8 stories and SCWB > 1.5)

Table 3.1 Characteristics of fifteen archetype buildings and parameters of power law regression models

Building No.	No. of stories	First mode period (sec)	SCWB ratio	Parameters of power-law model	
				a	b
1	2	0.877	> 1.0	0.0342	0.915
2	2	0.832	> 1.5	0.0292	0.898
3	2	0.805	> 2.0	0.0262	0.898
4	4	1.520	> 1.0	0.0478	0.814
5	4	1.488	> 1.5	0.0513	0.820
6	4	1.453	> 2.0	0.0484	0.832
7	8	2.037	> 1.0	0.0585	0.799
8	8	1.978	> 1.5	0.0574	0.794
9	8	1.957	> 2.0	0.0556	0.783
10	12	2.722	> 1.0	0.0757	0.806
11	12	2.665	> 1.5	0.0715	0.796
12	12	2.508	> 2.0	0.0666	0.789
13	20	3.600	> 1.0	0.0813	0.738
14	20	3.484	> 1.5	0.0733	0.717
15	20	3.394	> 2.0	0.0874	0.728

3.3.3 Numerical example of regional seismic loss assessment

To demonstrate the proposed evaluation method and investigate the effects of EDP correlations on regional seismic losses, we consider a virtual city in California. The locations of 1,000 virtual buildings modeled by the fifteen archetypes are randomly generated over a rectangular region (4.0 km $\times$ 2.5 km) with uniform soil conditions, as shown in Figure 3.6. The random generation of the buildings is uniform in terms of the building archetypes and the locations in the area.

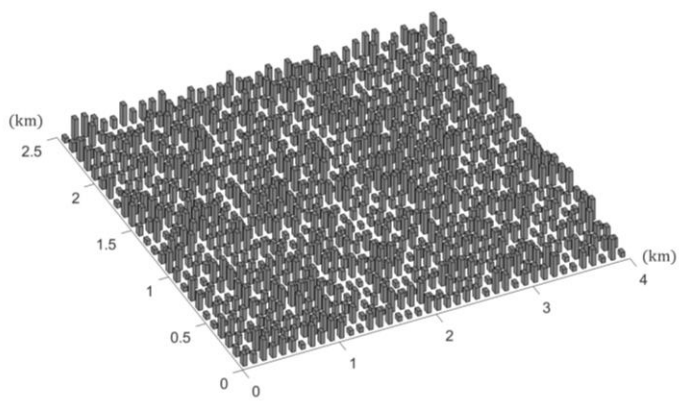

Figure 3.6 A virtual city consisting of 1,000 randomly generated buildings

In HAZUS (FEMA, 2012a), structural damage to a building is described by one of the five damage states: none, slight, moderate, extensive, and complete. Table 3.2 summarizes the limit states of the buildings defined in terms of the selected EDP, i.e., maximum IDR (FEMA, 2000; FEMA, 2012b). From the four limit states in Table 3.2, five damage states are derived as described in Table 3.3. For example, the criteria for the damage state "DS1", i.e., $d_{LS1} \leq D < d_{LS2}$ means that the maximum IDR is between the first and second limit states in Table 3.2. Table 3.3 also shows how the damage state probabilities, i.e., failure probabilities, can be

computed from the probability of exceeding the limit states, and the losses assumed for each damage state. For simplicity, in this example, all the buildings are assumed to have the same values of total loss, and normalized to 1. Therefore, the maximum loss of the building, i.e., collapse, is defined as 1. For example, if a building is in the 'Extensive' state in a given earthquake scenario, the loss of the building is calculated as $1 \times 0.5 = 0.5$.

Table 3.2 Limit states of fifteen archetype buildings

Limit State	$LS1$	$LS2$	$LS3$	$LS4$
Limit of IDR (d_{LS})	0.5%	1%	2%	4%

Table 3.3 Damage states and corresponding economic losses of fifteen archetype buildings

Damage State	Definition	l^{DS}
None	$EDP < d_{LS1}$	0%
Slight	$d_{LS1} \leq EDP < d_{LS2}$	5%
Moderate	$d_{LS2} \leq EDP < d_{LS3}$	25%
Extensive	$d_{LS3} \leq EDP < d_{LS4}$	50%
Complete	$d_{LS4} \leq EDP$	100%

An earthquake scenario with a moment magnitude of $M = 7$, an epicentral distance of 66.2 km, and the shear wave velocity of $V_{S30} = 760$ m/s is created in accordance with the GMPE guideline for selecting predictor variables within the range of $M = 5{\sim}8$, $R_{jb} < 200$ km, and $V_{S30} = 180{\sim}1300$ m/s. To predict the ground motion intensities of the buildings, the GMPE by Boore and Atkinson (2008) is employed in this example. The regional loss exceedance probability in Eq. (3.6) is

computed by the proposed method, as shown in Figure 3.7 and Table 3.4. The loss is evaluated for the four different assumptions: (1) 'Statistically Independent' ($\rho_{\widehat{S_{a_i}}\widehat{S_{a_j}}} = \rho_{\psi_i\psi_j} = 0$), (2) 'EDP Residual Correlated' ($\rho_{\widehat{S_{a_i}}\widehat{S_{a_j}}} = 0, \rho_{\psi_i\psi_j} \neq 0$), (3) 'IM Correlated' ($\rho_{\widehat{S_{a_i}}\widehat{S_{a_j}}} \neq 0, \rho_{\psi_i\psi_j} = 0$), and (4) 'Both Correlated' ($\rho_{\widehat{S_{a_i}}\widehat{S_{a_j}}} \neq 0, \rho_{\psi_i\psi_j} \neq 0$).

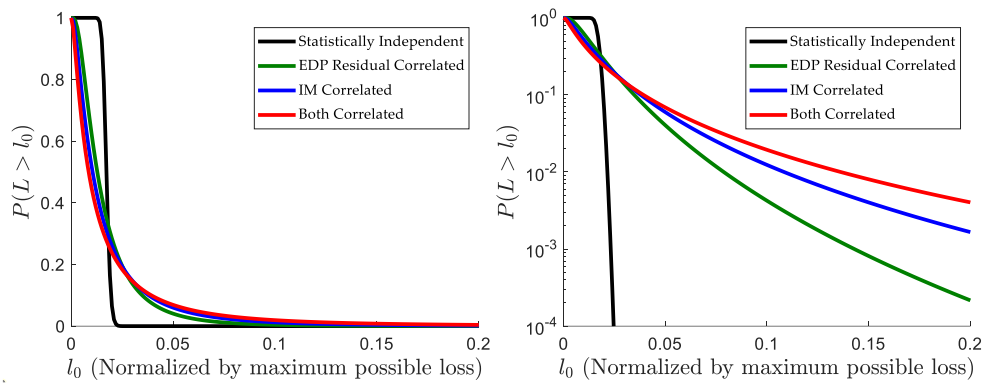

Figure 3.7 Loss exceedance probability computed by the proposed method: (a) linear scale, and (b) linear-log scale

Table 3.4 Comparison between loss exceedance probabilities under four different assumptions on correlations

l_0	Loss exceedance probability $P(L > l_0)$			
	Statistically Independent	EDP Residual Correlated	IM Correlated	Both Correlated
5%	$< 10^{-10}$	0.0406	0.0600	0.0690
10%	$< 10^{-10}$	0.0042	0.0124	0.0194
15%	$< 10^{-10}$	0.0008	0.0040	0.0080
20%	$< 10^{-10}$	0.0002	0.0017	0.0040

The results indicate that, if the correlation is not taken into account, i.e., EDPs of different structures are assumed to be statistically independent of each other, the probability that the loss ratio is less than 0.017 is close to 1, while the probability of getting loss ratio greater than 0.017 is close to zero. When only the IM correlation is considered in evaluating the EDP correlation, the exceedance probability is underestimated as 43 to 87% of the probability computed considering both correlations. In this example, the ratio of A_S to A_ψ is approximately 7 to 3, which makes the impact of IM correlation more significant than that of the EDP residual correlation. It should be noted that the ratio can vary depending on the characteristic of the region, density and types of buildings in the region, and similarity to adjacent buildings.

3.4 Regression-based estimation of EDP residuals of steel buildings

The example in Section 3.3 demonstrates the needs for considering EDP correlations in the probabilistic evaluation of the regional loss. To estimate the EDP residual correlation, IDA was performed for individual structures in the region. However, in practice, one may not afford to perform IDA for each structure in a region to evaluate the variances and correlations of EDP residuals in Eqs. (2.9) and (2.10) due to the high computational cost and complexity of structural modeling. Therefore, to facilitate applications of the proposed method to large-size systems, this section introduces an efficient regression-based method for estimating the variances and correlations of EDP residuals.

3.4.1 Regression model for estimating correlation coefficient between EDP residuals of steel building structures

For a rapid estimation of the EDP residual correlation, a nonlinear regression model is developed in terms of parameters influencing the EDP residual correlation in general. Because the EDP residual correlation has values between 0 and 1, this study adopts a logistic regression model

$$\rho_{\psi_i\psi_j}(\boldsymbol{x}) = \frac{\exp(\beta_0 + \beta_1 x_1 + \beta_2 x_2 + \cdots + \beta_n x_n)}{1 + \exp(\beta_0 + \beta_1 x_1 + \beta_2 x_2 + \cdots + \beta_n x_n)} \tag{3.7}$$

where $\beta_0, \beta_1, \ldots, \beta_n$ denote the regression coefficients which are estimated based on training data; and $x_1, \ldots, x_n$ denote predictors of EDP residual correlation. The model parameters are determined by the least squares approach, which finds the values of the coefficients that minimize the residual sum of squares (RSS)

$$\begin{aligned} \text{RSS} &= \sum_{i=1}^{N} \left[y_i - \rho_{\psi_i\psi_j}(\boldsymbol{x}_i) \right]^2 \\ &= \sum_{i=1}^{N} \left[y_i - \frac{\exp(\beta_0 + \beta_1 x_{i1} + \beta_2 x_{i2} + \cdots + \beta_n x_{in})}{1 + \exp(\beta_0 + \beta_1 x_{i1} + \beta_2 x_{i2} + \cdots + \beta_n x_{in})} \right]^2 \end{aligned} \tag{3.8}$$

where N denotes the number of training data; and y_i means the EDP residual correlation of the ith pair of EDPs in the training set.

After careful consideration for accurate estimation without overfitting, two predictors are selected for the regression model to consider the effects of the first mode period of structure and SCWB ratio, both of which strongly affect the seismic response of the structures. Initially, several well-known structural properties were considered as candidates, but the two predictors were finally selected through statistical investigation on the correlation between the predictors and their effect on the response. During the process, the predictors that are hard to obtain in practice

were excluded to obtain a useful regression model in practice. In detail, the selected dimensionless predictors are $x_1 = \min(T_n^i, T_n^j) / \max(T_n^i, T_n^j)$, and $x_2 = \min(\mathrm{SCWB}_i, \mathrm{SCWB}_j) / \max(\mathrm{SCWB}_i, \mathrm{SCWB}_j)$. For simplicity, it is assumed that the joint distribution of EDP residuals is invariant to $\widehat{S_a}$. Therefore, the EDP residual correlations that were calculated for each $\widehat{S_a}$ in Section 3.2 are averaged over $\widehat{S_a}$ to obtain training data of the regression in this study. As shown in Figure 3.8, the yield strengths of structures affect the EDP residual correlation. The overall correlation coefficient slightly increases as the yield strength increases. Therefore, additional nonlinear structural analysis is conducted for the cases where the yield strength of the member (F_y) is 310 MPa (45 ksi) and 448 MPa (65 ksi) in addition to 379 MPa (55 ksi) investigated in Section 3.2.

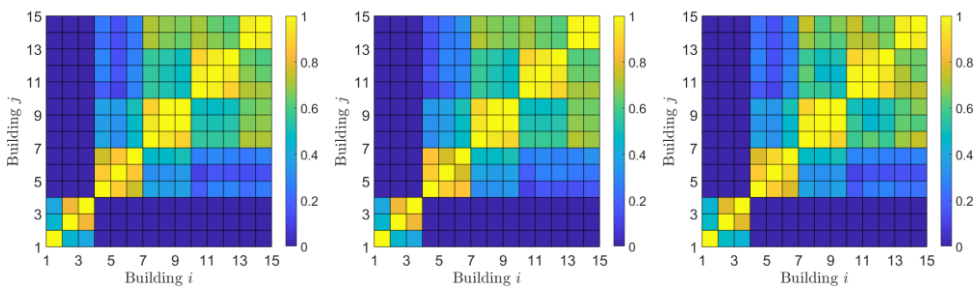

(a) (b) (c)

Figure 3.8 Effects of yield strengths (a) $F_y = 310$ MPa, (b) $F_y = 379$ MPa, and (c) $F_y = 448$ MPa on the EDP residual correlations

In total, 360 non-redundant data points representing combinations of 3 yield strength values and 120 correlation coefficients (15 pairs of identical buildings and $15 \times (15-1)/2 = 105$ pairs of different buildings) were originally used as training data set to develop the regression model on EDP residual correlation. It was observed that a significant portion of the training data with near-zero EDP residual correlation

coefficients, such as EDP residual correlation between a low-rise and a high-rise building, made the regression inaccurate for large correlation cases. This led to underestimating the correlation coefficient between safety factors and subsequent underestimation of the regional loss. To prevent the underestimation of regional total loss, the regression was performed using a subset, i.e., a total of 201 data with a correlation coefficient larger than 0.3. As a result, this study obtains the regression model for a pair of buildings with a different number of stories

$$\rho_{\psi_i\psi_j}(\boldsymbol{x}) = \frac{\exp(-2.375 + 3.530x_1 + 0.565x_2)}{1 + \exp(-2.375 + 3.530x_1 + 0.565x_2)} \tag{3.9}$$

If the buildings have the same number of stories, the EDP residual correlation is predicted as 1. Table 3.5 shows the standard error, *t*-statistic, and *p*-value of the regression model parameters in Eq. (3.9). It is shown that the ratio of the first mode period has the most significant effect on the EDP residual correlation. Although the coefficient of β_2 is small, the effect of the SCWB ratio should not be ignored because its *p*-value is still low. Figure 3.9 compares the EDP residual correlations in Section 3.3.3 with those by the regression model in Eq. (3.9). The regression model predicts relatively high correlation coefficients of EDP residuals for conservative regional loss assessment. Nevertheless, it is confirmed that the regression model can represent the overall trend of the EDP residual correlation.

Table 3.5 The results for the logistic regression model on EDP residual correlation

Parameter	Coefficient	Standard error	*t*-statistic	*p*-value
β_0	-2.375	0.307	-7.734	1.3×10^{-13}
β_1	3.530	0.320	11.025	2.0×10^{-16}
β_2	0.565	0.236	2.398	0.017

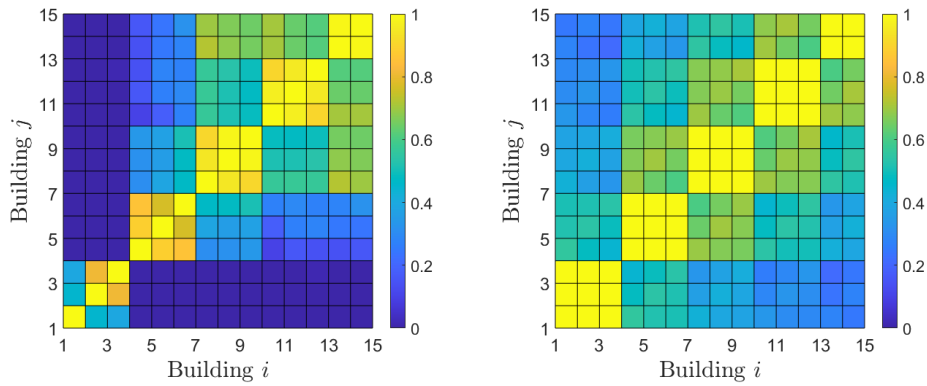

(a) (b)

Figure 3.9 EDP residual correlations: (a) evaluation by IDA, and (b) estimation by regression equation in Eq. (3.9)

3.4.2 Guideline on estimating variance of EDP residual

Eq. (2.10) shows that an overestimation of the variances of the EDP residual, $\sigma_{\psi_i}^2$ and $\sigma_{\psi_j}^2$ would lead to overestimating the relative contribution of the EDP residual correlation $\rho_{\psi_i\psi_j}$ to $\rho_{F_iF_j}$ (quantified by A_ψ), and underestimating that of the IM correlation $\rho_{\widehat{S_{a_i}}\widehat{S_{a_j}}}$ (quantified by A_S). Since the IM correlation is usually larger than the EDP residual correlation, an overestimation of $\sigma_{\psi_i}^2$ and $\sigma_{\psi_j}^2$ therefore results in an underestimation of $\rho_{F_iF_j}$ and the loss exceedance probability $P(L > l_0)$. To avoid this issue, we investigated the variances of EDP residuals estimated for 1,000 hypothetical buildings of the example in Section 3.3.3. Although the earthquake scenario depicted a sufficiently strong earthquake, it is confirmed that, in most structures, the range of the corresponding $\widehat{S_a}$ made all the IDA curves exhibit elastic behavior. This means that the variability of EDP residual is mostly caused by the higher mode effects. It was also observed that the variability of EDP

residual is almost invariant to $\widehat{S_a}$ in the range where all of the IDA curves are linear. For this reason, it is recommended to estimate the variance of EDP residual by that of the residual ε in the power-law regression model, i.e., $\widehat{D}_i = s_i(\widehat{S_{a_i}}) + \varepsilon_i = \ln a_i + b_i\widehat{S_{a_i}} + \varepsilon_i$ (See Figure 3.10). It was confirmed that, by following this guideline, one can avoid underestimating the correlation between safety factors, and the loss exceedance probability, which can be caused by overestimating $\sigma_{\psi_i}^2$.

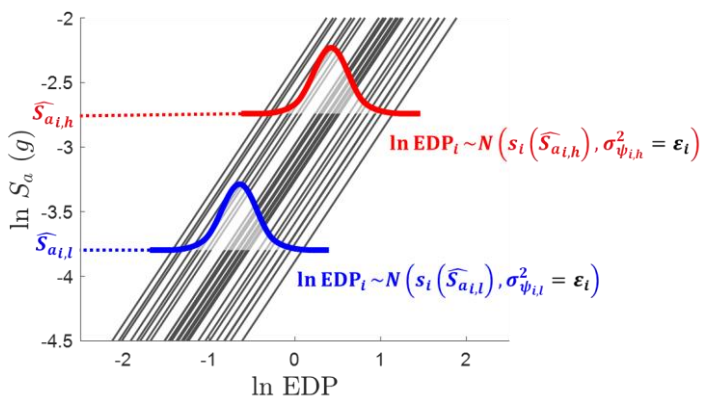

Figure 3.10 Estimating variance of EDP residual when the corresponding $\widehat{S_a}$ is in an elastic range for all IDA curves

3.4.3 Verification of regression-based estimation of EDP residuals of variances and correlations of SMF buildings

To verify the proposed regression-based estimation of the variances and correlations of EDP residuals in regional loss assessment, the probabilistic regional loss assessment in Section 3.3 is repeated using the regression-based estimation in Section 3.4 instead of performing full IDAs. As shown in Figure 3.11 and Table 3.6, the loss exceedance probabilities obtained by the approximate method introduced in Section 3.4.1 and 3.4.2 match those presented in Section 3.3.3. This result

demonstrates that the variances and correlation coefficients estimated by the proposed method provides enough accuracy in predicting the uncertainties in EDPs and regional loss. The relative contribution of IM correlation is slightly underestimated due to the overestimation of the variance of EDP residual. However, this overestimation of the contribution of EDP residual correlation cancels the error, and thus the overall evaluation is not significantly affected. The regression-based prediction introduces overestimates in the exceedance probability, particularly in "Both Correlated" case, but the difference is negligible. Although this particular regression model cannot cover the EDP residuals of general structural systems, the proposed regression-based approach can be adopted for efficient estimation of EDP residual correlations.

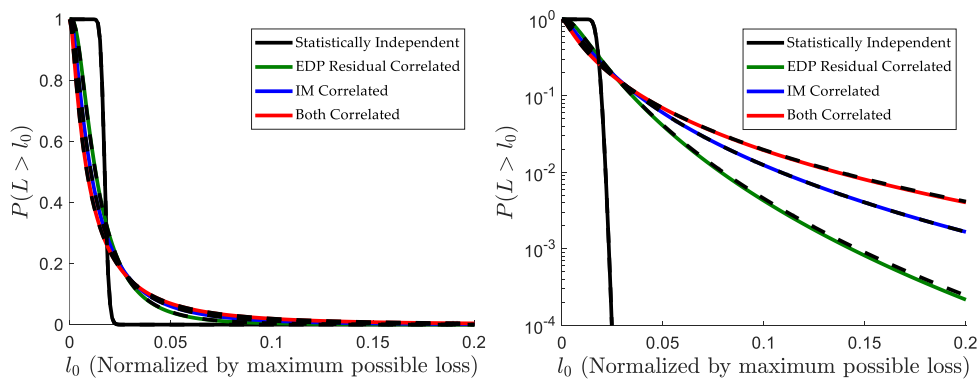

Figure 3.11 Comparison of loss exceedance probability using original EDP residual correlation (solid lines) and regression-based estimates of EDP residual correlation (black dashed lines): (a) linear scale, and (b) linear-log scale

Table 3.6 Comparison between the results of total loss assessment under three different assumptions on correlations

l_0	Loss exceedance probability $P(L > l_0)$					
	EDP Residual Correlated		IM Correlated		Both Correlated	
	Original	Regression	Original	Regression	Original	Regression
5%	0.0406	0.0416	0.0600	0.0598	0.0690	0.0692
10%	0.0042	0.0045	0.0124	0.0123	0.0194	0.0197
15%	0.0008	0.0009	0.0040	0.0040	0.0080	0.0082
20%	0.0002	0.0002	0.0017	0.0017	0.0040	0.0041

3.5 Summary

This chapter developed a method for estimating the variances and correlations of EDP residuals of structures by Incremental Dynamic Analysis (IDA). Taking advantage of IDA, the proposed method can describe the IM-EDP relationship and quantify the uncertainties and correlations of EDPs in structure performance level. To reduce the subjectivity of the ground motion selection, 44 ground motions satisfying the selection criteria of the PEER NGA database were adopted. The applications to the fifteen archetype SMF buildings with different heights and SCWB ratios tested the accuracy and applicability of the proposed method.

To demonstrate the effect of EDP correlation on the seismic system reliability analysis, a probabilistic regional loss assessment was performed for a virtual region and an earthquake scenario. The total loss exceedance probabilities are evaluated for the four different assumptions. The comparison of the results demonstrates the importance of considering the correlation between EDPs of structures. In particular, the results confirmed that proper consideration of the correlation between EDPs of

structures can significantly increase the prediction accuracy of loss exceedance probability of a region.

Furthermore, to facilitate applications of the proposed framework of EDP correlation assessment, an approximate method was also proposed to estimate the correlation coefficients of EDP residual through nonlinear regression, along with a guideline to quantify the variance of EDP residual. By applying the approximate method to the same regional loss assessment example as before, it was confirmed that the regression-based approximation of correlation coefficient and variance of EDP residuals can provide sufficiently accurate results, even without performing full IDAs for individual structures in the region.

Chapter 4. IM-invariant Method for Quantifying EDP Residuals of Building Structures

4.1 Introduction

To estimate the EDP residuals of structures, the IDA-based method was developed and applied to regional seismic loss assessment in Chapter 3 (Kang et al., 2021). However, the IDA-based method has a limitation in that the estimation results may vary depending on the selected ground motions and requires high computational costs. Therefore, in order to obtain a more general expression for the EDP residuals and their correlation, this study proposes an alternative method termed "IM-invariant method" that can utilize many ground motions by reducing the computation time. The IM-invariant method estimates the EDP residuals using the elastic-range-responses of structures, which can significantly reduce the analysis time and use much more ground motions compared to the IDA-based method.

It should also be noted that the EDP residual is affected by uncertainties in frequency content, duration, and energy, which cannot be predicted by the selected IM alone (Baker and Cornell, 2008). For example, the uncertainties in the frequency content are manifested as higher mode effects even if the structure exhibits elastic behavior (Maniatakis et al., 2013). To further elucidate the effects of such uncertainties on the variances and correlations of EDPs, this study investigates primary structural characteristics that affect EDP residuals. To this end, the EDP residuals of various buildings are estimated using the IM-invariant method proposed in this study to identify contributions of the structural characteristics to the EDP residuals and provide a guideline. The IM-invariant method can significantly reduce

the computational cost but requires complex structural modeling (Jalayer and Cornell, 2009; Vamvatsikos and Fragiadakis, 2010). To reduce such computational costs, this study also develops nonlinear regression models to approximate the variances and correlation coefficients of EDP residuals using easy-to-obtain predictors describing the primary structural characteristics.

Four virtual urban areas are introduced to demonstrate the proposed IM-invariant method. By adopting buildings with various heights and materials, the effects of structural characteristics on the EDP residual and the total regional loss are investigated. The contribution of the EDP residual correlation to the total regional loss estimation and the effects of the spatial distribution of buildings are studied. This study also provides guidelines on whether the EDP residual correlation needs to be considered. The accuracy of the developed regression models is confirmed by the regional loss assessment using the EDP residual regression models without additional structural analysis. (Kang et al., 2022)

4.2 Elastic-range-based estimation of EDP residuals

4.2.1 Development of IM-invariant method

The IDA-based method illustrated in Figure 3.1 can accurately estimate the EDP residuals considering the nonlinearities of structural systems but inevitably entails enormous computational costs. To alleviate the cost, a guideline was proposed to estimate the variances of EDP residuals of structures by those of the power-law regression residuals in Section 3.4.2. Based on the guideline, this chapter proposes an IM-invariant, i.e., non-IDA-based method for estimating EDP residuals of structures using the elastic-range responses as shown in Figure 4.1.

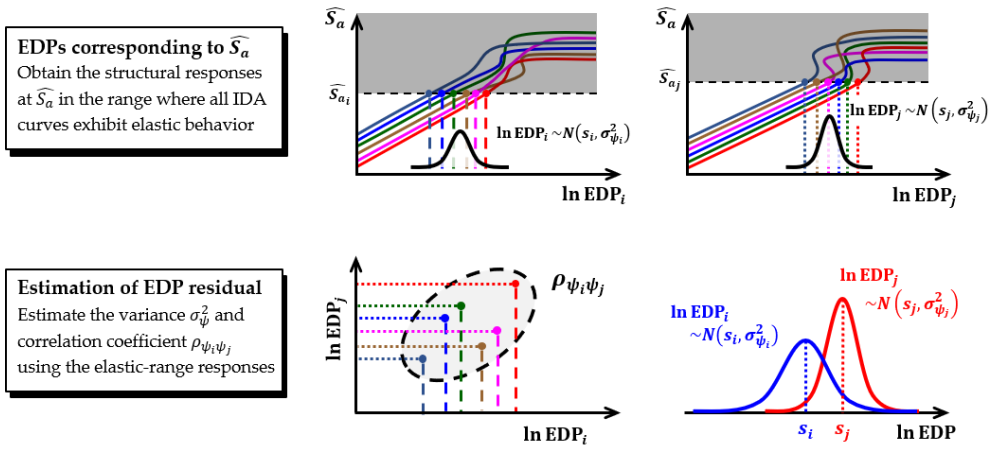

Figure 4.1 IM-invariant method for estimating variances and correlation coefficients of EDP residuals using elastic-range-responses in IDA curves

Of course, the inelastic behavior leads to a significant increase in the standard deviations of the EDP residuals, σ_{ψ_i} and σ_{ψ_j}, which eventually affects both correlations in Eq. (2.10). It is noted that if a structure exhibits inelastic behavior, the variance of the EDP residual should increase significantly. Nevertheless, the IM-invariant method is proposed based on the following reasoning:

- **Increase in the contribution of IM correlation to safety factor correlation**

  Compared to the IDA-based method, the standard deviation of EDP residual, σ_{ψ} estimated by the IM-invariant method is relatively small. Therefore, the contribution of EDP residual correlation decreases while the contribution of the IM correlation increases. Since $\rho_{\widehat{S_{a_i}}\widehat{S_{a_j}}}$ is generally larger than $\rho_{\psi_i\psi_j}$ in regional seismic loss assessment, it is found that increase of σ_{ψ} leads to the decrease of $\rho_{F_iF_j}$ as shown in Figure 2.4(c). In addition, the nonlinear behaviors of structures further reduce the correlation coefficient between the

EDP residuals. Therefore, when estimating the probability that the total loss in a region exceeds a large threshold l_0 in Eq. (3.6), the correlation coefficients between the safety factors can be estimated conservatively by applying the IM-invariant method. On the other hand, in the case of a small threshold l_0, the loss exceedance probability can be underestimated, but this study focuses on the case where sufficient seismic loss has occurred in the region.

- **Similarity between the result of the IDA-based method and that of the IM-invariant method**

  In the IDA-based method, the alternative method is applied if some of the curves flatten before reaching a target $\widehat{S_a}$. This method finds the maximum IM value at which all IDA curves do not flatten and adopts responses of structures in the near-collapse level. As more ground motions are used in the IDA-based method, the maximum IM can be lowered as shown in Figure 4.2. Therefore, if a sufficient number of ground motions are used, the results of the IDA-based method and the IM-invariant method can be similar.

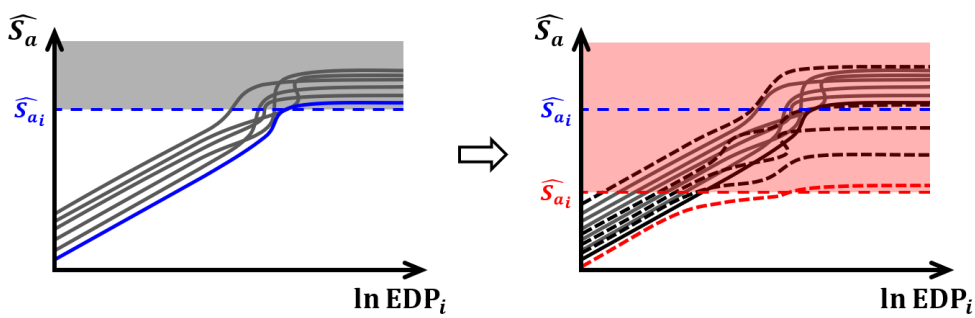

Figure 4.2 Changes in maximum IM in structural performance level with increasing number of ground motions used in IDA-based method

- **Range of corresponding IM for a given earthquake scenario**

  According to the evaluation of regional seismic losses by various earthquake scenarios, even in a strong earthquake scenario, the corresponding $\widehat{S_a}$ is usually located in the range where all IDA curves exhibit elastic behavior.

Therefore, this study also employs an IM-invariant method that estimates the variances and correlation coefficients of EDP residuals of building structures based on the elastic range for more efficient estimation. In particular, this IM-invariant method assumes the mean EDP is determined by S_a but the variance $\sigma_{\psi_i}^2$ is not affected by S_a within the elastic range, as illustrated in Figure 4.3. In addition, the correlation coefficient $\rho_{\psi_i\psi_j}$ is also estimated as a single value regardless of the scale of the intersection points. Because the natural logarithms of IM and EDP have a linear relationship, the correlation coefficient is not affected by the scale factor applied to the ground motions.

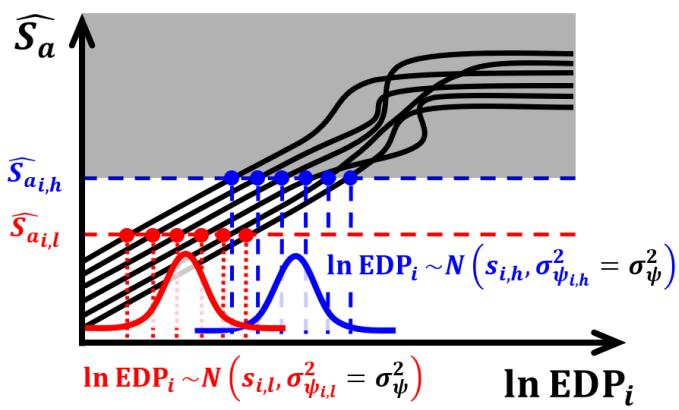

Figure 4.3 Variance of EDP residual of structure estimated as a single value by IM-invariant method

4.2.2 Ground motion selection for IM-invariant method

As reported in many previous studies (Kiani and Khanmohammadi, 2015; Jalayer et al., 2017; Kim et al., 2021), the results of analysis methods based on multiple ground motions such as IDA are strongly influenced by the selected ground motion set. Therefore, the proposed IM-invariant method is expected to provide different estimates of the variances and correlations of EDP residuals depending on the selected ground motion set. To reduce such differences, several specific ground motion sets, such as the far-field and near-field ground motion sets in FEMA P695 (FEMA, 2009), were utilized to estimate the response of structures in various studies (Billah et al., 2013; Deniz et al., 2018; Kang et al., 2021). However, more ground motions with various characteristics are required to handle the EDP residuals of general building structures. To this end, a set of 1,499 ground motions in the NGA database (Power et al., 2008) is used in this study. Even though many ground motions are used, the proposed IM-invariant method dramatically reduces computational cost compared to the IDA-based approach in Section 3.2 because analyses at a single spectral acceleration in the elastic range provide the variance and correlation of EDP.

4.3 Quantification of EDP residuals using structural characteristics of building structures

4.3.1 Effects of damping and higher modes on EDP residual

The uncertainties in EDP residuals originate from those in the frequency content, duration, and energy of ground motions that cannot be entirely captured by the selected IM alone. The uncertainty in the frequency content leads to higher mode effects, while the other two uncertainties emerge through the nonlinear structural

behavior. Because a significant level of EDP residual is observed even when a building is in the elastic range, it is inferred that the higher mode effects significantly contribute to the uncertainties of the EDP residual.

To demonstrate the uncertainties caused by higher mode effects, let us consider an example building with the first, second, and third mode periods of 1.0 sec, 0.3 sec, and 0.15 sec respectively, damping of 5%, and the base shear coefficient at yielding of $0.3\,g$ from the first mode pushover analysis. For the estimation of the EDP residual in the elastic range, all ground motions are scaled such that the spectral acceleration with 5% damping at 1 sec is $0.2\,g$, which is smaller than the base shear coefficient at yielding. The natural logarithm of spectral accelerations ($\ln S_a$) and displacements ($\ln S_d$) are shown in Figure 4.4. In the first mode period T_1, all ground motions show the identical value of IM, i.e., $\ln S_a$ and $\ln S_d$ because of the scaling. In the second and third modes, however, large dispersions in $\ln S_a$ and $\ln S_d$ are observed. These uncertainties are propagated to those in the EDP of a multi-degree-of-freedom (MDOF) system and tend to amplify as the number of considered modes increases.

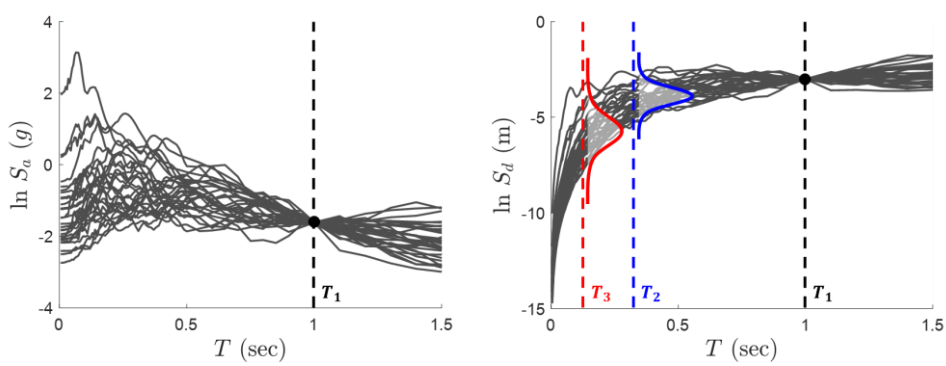

(a) (b)

Figure 4.4 Response spectra scaled at the first mode period of building with 5% damping: (a) spectral acceleration, and (b) spectral displacement

On the other hand, damping of the building also contributes to the observed EDP residual of an MDOF system. In general, selecting an appropriate IM is critical for the fragility analysis of a building structure. Among various IMs describing seismic intensity, the 5% damped spectral acceleration at the first mode period of a building, $S_a(T_1, 5\%)$ is known as one of the best options (Kazantzi and Vamvatsikos, 2015). However, if the damping coefficient of the building is not equal to 5%, different spectral displacement S_d can occur for a given $S_a(T_1, 5\%)$. This effect is demonstrated by the IDA curves of a bilinear single degree of freedom (SDOF) system. Figure 4.5 compares the IDA results for a structure with 2% damping to those of the same structure but with 5% damping. The results confirm that additional uncertainties arise in the EDP when the actual damping differs from the one assumed in the IM selection. Moreover, the uncertainty further amplifies in the nonlinear range. It is noted that the EDP residual could be observed even when higher mode effects are negligible.

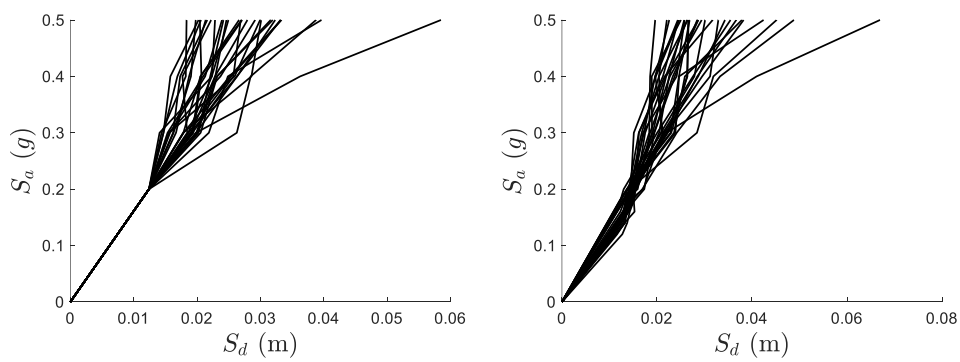

Figure 4.5 IDA curves of a bilinear SDOF system with different damping: (a) 5% damping, and (b) 2% damping

Let us now consider the MDOF system in Figure 4.4, but with 2% damping. Figure 4.6 shows $\ln S_a$ and $\ln S_d$ obtained by scaling all ground motions to $S_a = 0.2\ g$ at the first mode of the structure. In this case, the variability of S_a is observed even at the first mode because $S_a(T_1, 5\%)$ is selected as IM. More significant variabilities are observed at the second and third modes than in Figure 4.6. Table 4.1 compares the means and standard deviations of $\ln S_d$ with different damping ratios at each mode. It is seen that damping is a critical characteristic of a building structure that affects the uncertainties of EDPs.

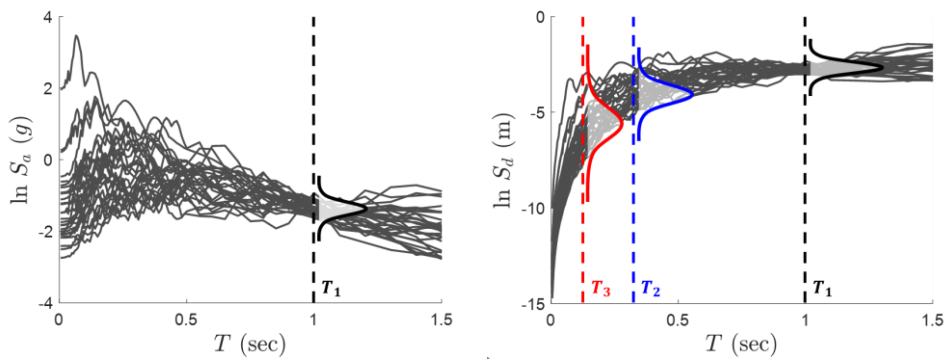

(a) (b)

Figure 4.6 Response spectra scaled at the first mode period of building with 2% damping: (a) spectral acceleration, and (b) spectral displacement

Table 4.1 Mean and standard deviation of spectral displacement for each mode when $S_a(T_1, 5\%)$ is used as IM

Parameters	5% damping (matched)			2% damping (mismatched)		
	1st mode	2nd mode	3rd mode	1st mode	2nd mode	3rd mode
$\mu_{\ln S_d}$	-3.006	-4.396	-5.791	-2.755	-4.162	-5.508
$\sigma_{\ln S_d}$	0	0.735	1.045	0.177	0.740	1.081

4.3.2 Investigation of contributions of damping and higher mode effects to EDP residual of building

This study now compares the contributions of damping and higher mode effects to the EDP residuals of 90 archetype buildings with six different heights (3, 5, 7, 10, 15, and 20 stories) and 15 damping ratios (1, 2, …, 15% damped buildings). The modulus of elasticity (E) and the yield stress (F_y) of the beams and columns are assumed to be 200 GPa $(29{,}000$ ksi$)$, and 414 MPa $(60$ ksi$)$, respectively. Two-dimensional moment-resisting frame models representing 90 archetype buildings are analyzed using OpenSees (Mazzoni et al., 2006). The parameters of Rayleigh damping (Hall, 2006) are determined based on the damping ratios at the first and third modes.

Time history analyses were performed for the buildings using 1,499 ground motions scaled to a specific value of $S_a(T_1, 5\%)$. Through the analysis results, the standard deviations of the residuals of two types of EDPs, roof displacement and maximum inter-story drift ratio (IDR), were estimated, as shown in Figure 4.7. By comparing the results of different MDOF systems and damping levels, the contribution of the damping and higher mode effects can be investigated. Figure 4.7 shows that the standard deviation of EDP residual increases as the damping ratio deviates from 5%. Especially, σ_ψ increases sharply as the damping ratio decreases from 5%. However, as the height of a building increases, the relative contribution of damping becomes relatively small compared to the higher mode effects. It is also seen that the higher mode effects stand out more if maximum IDR is selected as the EDP. This is because maximum IDR is more sensitively influenced by the higher modes than the roof displacement. From the perspective of the first mode periods of

the buildings, for both EDPs, the effects of damping decrease when the first mode period increases. In particular, in the case of maximum IDR, the difference due to damping almost disappears when the first mode period is longer than 1.5 sec.

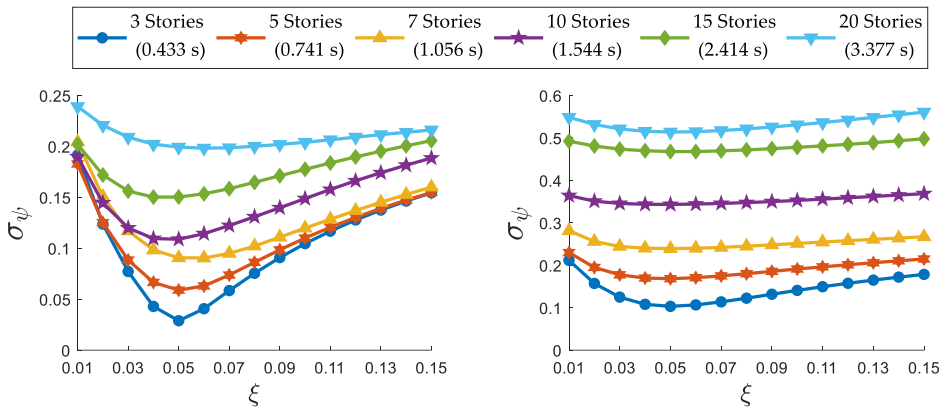

Figure 4.7 Standard deviations of residuals of two EDPs for reference buildings according to damping: (a) roof displacement, and (b) maximum IDR

The correlation coefficient of the EDP residual between the ith and jth buildings is also affected by damping and higher mode effects. A negative correlation can occur if one of the buildings has less than 5% damping while the other has more than 5% damping. For example, Figure 4.8 shows the process of estimating the correlation coefficient when the damping ratios of the ith and jth buildings are 2% and 10%, respectively. When the spectral displacements of the building are expressed according to damping, as shown in Figure 4.8(a), a ground motion inducing a relatively lower EDP at $\xi < 5\%$ produces larger EDP at $\xi > 5\%$. Therefore, a negative correlation should be observed between the EDPs of the two buildings. Such results are confirmed by the scatter plot of the EDPs in Figure 4.8(b).

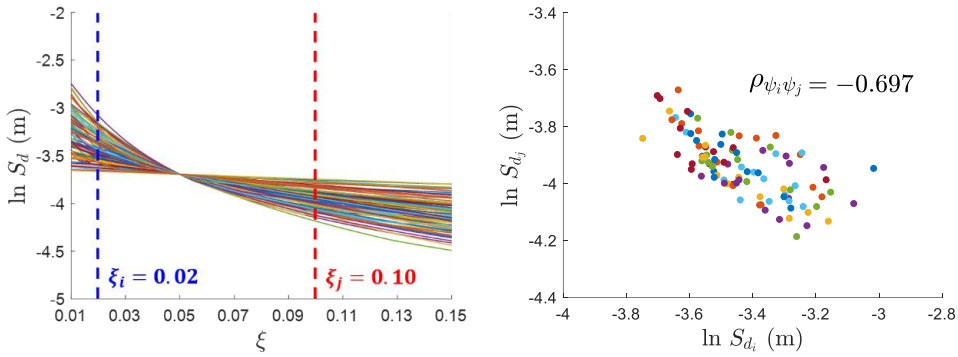

(a) (b)

Figure 4.8 Case of negative correlation between EDP residual: (a) spectral displacement scaled at the first mode period of the building, and (b) scatter plot of EDP residuals of the two buildings and correlation

Figure 4.9 shows the correlation coefficients between the EDP residuals of the ith and jth buildings while varying their damping coefficients. It is seen that the estimated EDP residual correlation increases as the height of the building increases. Figure 4.9(a) shows that significant negative correlations can be estimated between low-rise buildings. On the other hand, such cases diminish as the buildings' heights increase, as shown in Figures 4.9(b) and (c). The negative correlation is no longer observed between high-rise buildings because the higher mode effects make a more dominant contribution than damping. A negative correlation between the EDPs reduces the standard deviation of the loss and the exceedance probability.

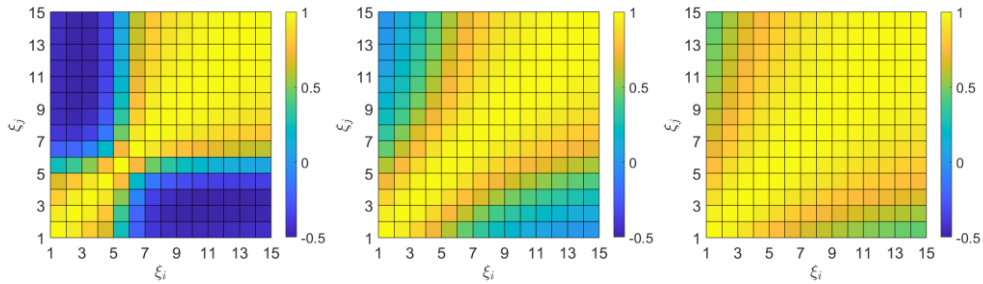

(a) (b) (c)

Figure 4.9 EDP residual correlation estimated according to the damping of the ith and jth buildings: (a) 3-story, (b) 7-story, and (c) 10-story buildings

4.4 Regression-based estimation of variances and correlations of EDP residuals of building structures

The IM-invariant method in Section 4.2 significantly reduces the required number of structural analyses of individual buildings but still requires modeling and analysis of each building structure in the region. To facilitate consideration of variances and correlations of EDP residuals in regional seismic loss assessment, this study develops regression models for estimating the variances and correlations of EDP residuals using predictors identified in Section 4.3.

4.4.1 Regression model of standard deviation of EDP residual

According to Section 4.3, the variance of an EDP residual is strongly influenced by the first mode period (T_n) and damping ratio (ξ) of the building. Thus, nonlinear regression models are developed using these structural characteristics as predictors. As shown in Figure 4.7, when the first mode period of the building exceeds around 1.5 sec, the effect of damping on the variance becomes relatively insignificant. Therefore, segmented regression is introduced to describe the difference in damping effects according to the first mode period. Consequently, the regression model of the

standard deviation of EDP residual, i.e., the square root of the variance, is developed as

$$\sigma_{\psi}(\boldsymbol{x}) = \beta_0 + \beta_1 x_1 + \beta_{11} x_1^2 + \beta_2 x_2 + \beta_{22} x_2^2 + (\beta_2^* x_2 + \beta_{22}^* x_2^2) I_{(x_1 > 1.5)} \quad (4.1)$$

where $\beta_0, \beta_1, \beta_{11}, \beta_2$ and β_{22} are the regression model parameters; x_1 and x_2 are predictors of the regression model representing T_n and ξ, respectively; β_2^* and β_{22}^* are the additional regression parameters for the segmented regression; and $I_{(x_1>1.5)}$ is an indicator function which is one if x_1 exceeds 1.5 sec and 0 otherwise. The parameters are determined by minimizing the residual sum of squares (RSS)

$$\text{RSS} = \sum_{i=1}^{N} \left[y_i - \sigma_{\psi}(\boldsymbol{x}_i) \right]^2 \quad (4.2)$$

where $\boldsymbol{x}_i = (x_1, x_2)_i,\ i = 1, \ldots, N,$ is the predictor values of the ith building in the training data set; and y_i and $\sigma_{\psi}(\boldsymbol{x}_i)$ respectively denote the sample variance of the corresponding building and the prediction by the regression model in Eq. (4.1).

For a regression model covering a practical range of the building characteristics, additional structural analyses are performed for the number of stories and damping ratios, which were not covered in Section 4.3. As a result, 95 data representing the combination of 5 damping ratios (2, 5, 7, 10, and 15 percent) and 19 stories (from 2 to 20 stories) are used as training data set. Regression models are developed for the variances of roof displacement and maximum IDR, i.e., primary EDPs regarding damage to building structures.

First, for the roof displacement, through a careful model selection process, the predictor x_1^2 was excluded from the regression model in Eq. (4.1). As a result, the regression model for the roof displacement (unit: inch) is obtained as

$$\sigma_{\psi}(\boldsymbol{x}) = 0.114 + 0.032x_1 - 1.652x_2 + 12.198x_2^2 + (0.689x_2 - 5.146x_2^2)I_{(x_1>1.5)} \quad (4.3)$$

On the other hand, the regression model for the maximum IDR includes the predictor x_1^2, that is,

$$\sigma_{\psi}(\boldsymbol{x}) = 0.064 + 0.240x_1 - 0.029x_1^2 - 1.080x_2 + 7.440x_2^2 + (0.727x_2 - 4.121x_2^2)I_{(x_1>1.5)} \quad (4.4)$$

Tables 4.2 and 4.3 provide the standard error, *t*-statistic, and *p*-value of the regression model parameters in Eqs. (4.3) and (4.4). These results confirm that all predictors in the models significantly affect the variance of EDP residual. It is also seen that β_2^* and β_{22}^* have the opposite signs of β_2 and β_{22} respectively, reducing damping effects when the first mode period is longer than 1.5 sec. The relationship between the standard deviation of EDP residual and the predictors is visualized in Figure 4.10. Figure 4.11 compares the standard deviations of EDP residual estimated by the method in Section 4.2 and those by the regression models in Eqs. (4.3) and (4.4). The results confirm that the regression models can predict the overall trend of EDP uncertainty.

Table 4.2 Statistics of the regression model parameters for the standard deviation of roof displacement residual

Parameter	Coefficient	Standard error	*t*-statistic	*p*-value
β_0	0.114	0.008	15.011	2.0×10^{-16}
β_1	0.032	0.003	11.196	2.0×10^{-16}
β_2	-1.652	0.181	-9.104	2.3×10^{-14}
β_2^*	0.689	0.169	4.082	9.7×10^{-5}
β_{22}	12.198	1.085	11.240	2.0×10^{-16}
β_{22}^*	-5.146	1.142	-4.505	2.0×10^{-5}

Table 4.3 Statistics of the regression model parameters for the standard deviation of maximum IDR residual

Parameter	Coefficient	Standard error	*t*-statistic	*p*-value
β_0	0.064	0.007	8.835	9.0×10^{-14}
β_1	0.240	0.007	36.821	2.0×10^{-16}
β_{11}	−0.029	0.002	−19.349	2.0×10^{-16}
β_2	−1.080	0.130	−8.316	1.0×10^{-12}
β_2^*	0.727	0.126	5.775	1.1×10^{-7}
β_{22}	7.440	0.773	9.621	2.2×10^{-15}
β_{22}^*	−4.121	0.830	−4.960	3.4×10^{-6}

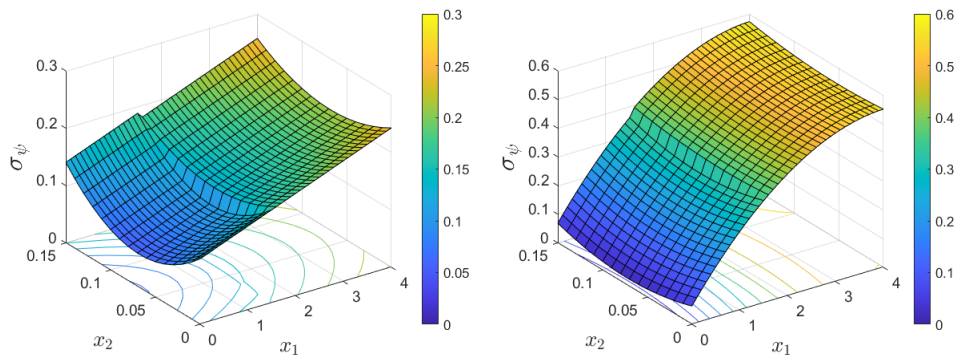

(a) (b)

Figure 4.10 Standard deviation of EDP residual predicted by regression models: (a) roof displacement, and (b) maximum IDR

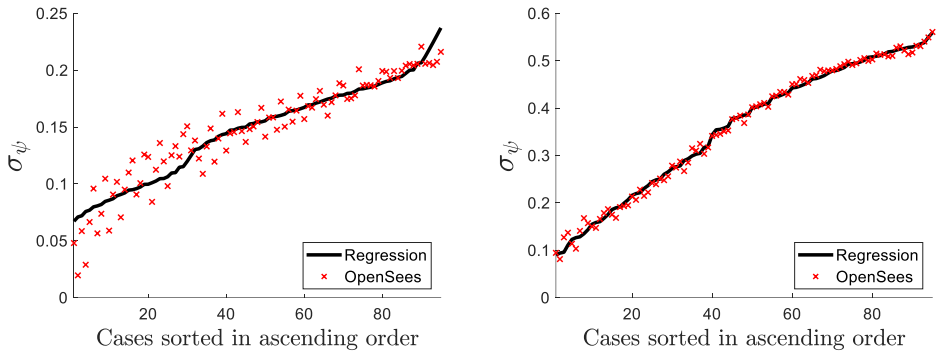

(a) (b)

Figure 4.11 Comparison between the standard deviations by the IM-invariant method and the predictions by regression models: (a) roof displacement, and (b) maximum IDR

4.4.2 Regression model of correlation coefficient between EDP residuals

Nonlinear regression models are developed to predict the correlation coefficient between EDP residuals. Since the EDPs of buildings in the same region usually show positive correlations, this study adopts a logistic regression model whose output is between 0 and 1. After a careful model selection process, the following second-order multivariate polynomial regression model is adopted:

$$\rho_{\psi_i\psi_j}(\boldsymbol{x}) = \frac{\exp(\beta_0 + \beta_1 x_1 + \beta_{11} x_1^2 + \cdots + \beta_n x_n + \beta_{nn} x_n^2)}{1 + \exp(\beta_0 + \beta_1 x_1 + \beta_{11} x_1^2 + \cdots + \beta_n x_n + \beta_{nn} x_n^2)} \tag{4.5}$$

where $\beta_0, \beta_1, \beta_{11}, \ldots, \beta_n, \beta_{nn}$ are the regression parameters; and $x_1, \ldots, x_n$ denote predictors of the regression model. The optimal parameters are determined by the least-squares approach. To consider the higher mode effects discussed in Section 4.3, the first three mode periods were initially considered as predictors. Eventually, the second and third were excluded to avoid overfitting. As a result, the two dimensionless predictors selected for the regression models are $x_1 = \min(T_n^i, T_n^j)$ /

$\max(T_n^i, T_n^j)$, and $x_2 = \min(\xi_i, \xi_j) / \max(\xi_i, \xi_j)$. The regression model for a pair of building structures with different structural characteristics is

$$\rho_{\psi_i\psi_j}(\boldsymbol{x}) = \frac{\exp(-9.14 + 8.73x_1 + 5.40x_2 - 3.14x_2^2)}{1 + \exp(-9.14 + 8.73x_1 + 5.40x_2 - 3.14x_2^2)} \tag{4.6}$$

On the other hand, when maximum IDR is selected as EDP, the square of the term related to the first mode period of the structure is added for more accurate prediction. Using 3,457 cases in which the correlation coefficients exceed 0.3, the regression model is developed as

$$\rho_{\psi_i\psi_j}(\boldsymbol{x}) = \frac{\exp(-1.66 + 2.67x_1 + 1.28x_1^2 + 1.03x_2 - 0.66x_2^2)}{1 + \exp(-1.66 + 2.67x_1 + 1.28x_1^2 + 1.03x_2 - 0.66x_2^2)} \tag{4.7}$$

If the buildings have the same structural characteristics, the correlation coefficient between EDP residuals is predicted as 1. Tables 4.4 and 4.5 present the standard error, *t*-statistic, and *p*-value of the regression model parameters in Eqs. (4.6) and (4.7). The results confirm that both predictors affect the EDP residual correlation while the ratio of the first mode periods contributes slightly more. Figures 4.12 and 4.13 compare the EDP residual correlations estimated by the IM-invariant method in Section 4.2.1 against those by the regression models in Eqs. (4.6) and (4.7). It is seen that the developed regression models adequately describe the EDP residual correlations.

Table 4.4 Statistics of the regression model parameters for the correlation between roof displacement residuals

Parameter	Coefficient	Standard error	*t*-statistic	*p*-value
β_0	-9.140	0.183	-50.010	2.0×10^{-16}
β_1	8.728	0.167	52.130	2.0×10^{-16}
β_2	5.397	0.275	19.660	2.0×10^{-16}
β_{22}	-3.140	0.210	-14.980	2.0×10^{-16}

Table 4.5 Statistics of the regression model parameters for the correlation between maximum IDR residuals

Parameter	Coefficient	Standard error	*t*-statistic	*p*-value
β_0	-1.662	0.087	-19.038	2.0×10^{-16}
β_1	2.673	0.282	9.490	2.0×10^{-16}
β_{11}	1.284	0.244	5.263	1.5×10^{-7}
β_2	1.032	0.142	7.272	4.4×10^{-13}
β_{22}	-0.663	0.116	-5.695	1.3×10^{-8}

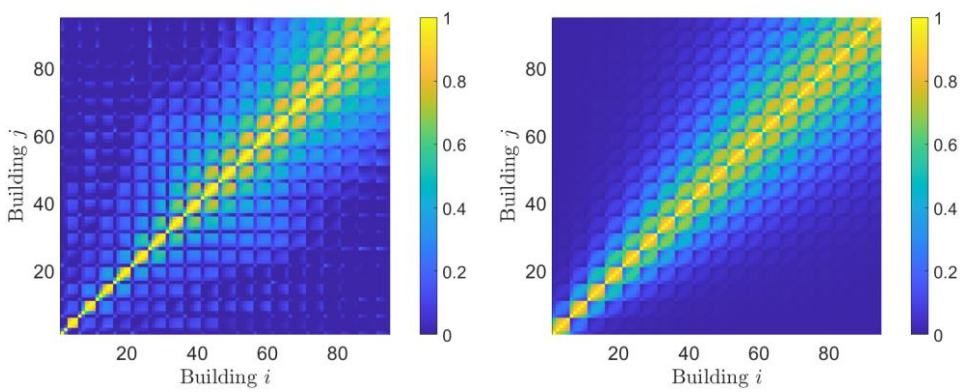

Figure 4.12 Correlation coefficients between roof displacement residuals: (a) evaluation by structural analysis, and (b) prediction by regression equation

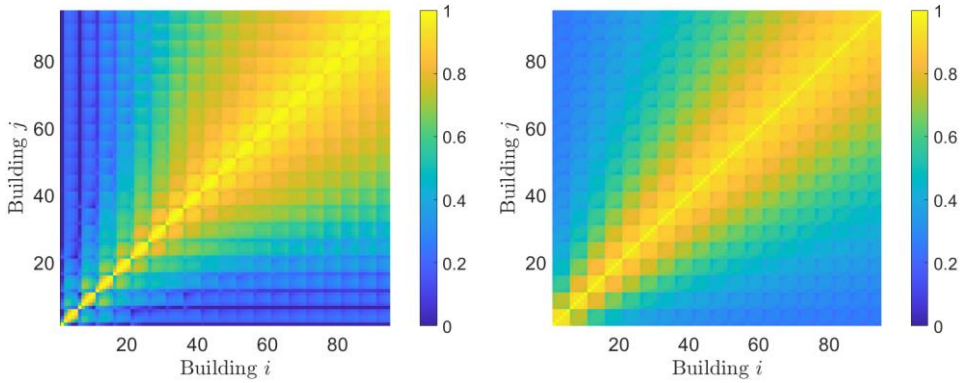

(a) (b)

Figure 4.13 Correlation coefficients between maximum IDR residuals: (a) evaluation by structural analysis, and (b) prediction by regression equation

4.5 Numerical examples of regional loss assessment

4.5.1 Regional loss assessment of four virtual cities

To demonstrate the IM-invariant method proposed in Section 4.2 and examine the effects of the EDP correlation on the regional loss assessment, this study considers four virtual cities in California created using 44 different archetype buildings of HAZUS (FEMA, 2012a) listed in Table 4.6. In order to identify the effects of damping and higher modes on EDP residuals, these archetype buildings are modeled with a focus on the first mode period and damping ratio rather than the detailed structural design. Table 4.7 presents the proportion of each archetype building distributed in City A (steel and wood buildings), City B (concrete and masonry buildings), City C (high-rise buildings, ≥ 8 stories), and City D (low-rise buildings, < 8 stories). In each virtual city, 500 virtual building models are randomly generated and distributed over a $2.5\ \text{km} \times 2.5\ \text{km}$ square region with uniform soil conditions, as shown in Figure 4.14.

Table 4.6 Characteristics of 44 archetype buildings

Building No.	Building types	No. of stories	First mode period (sec)	Damping ratio
1 to 2	S1L[a]	2 to 3	0.285 to 0.433	0.02
3 to 6	S1M[a]	4 to 7	0.586 to 1.056	0.02
7 to 19	S1H[a]	8 to 20	1.216 to 3.377	0.02
20 to 21	C1L[b]	2 to 3	0.285 to 0.433	0.07
22 to 25	C1M[b]	4 to 7	0.586 to 1.056	0.07
26 to 38	C1H[b]	8 to 20	1.216 to 3.377	0.07
39	URML[c]	2	0.285	0.10
40 to 41	URMM[c]	3 to 4	0.433 to 0.586	0.10
42	W1[d]	2	0.285	0.15
43 to 44	W2[d]	3 to 4	0.433 to 0.586	0.15

[a] S1L, S1M, and S1H are steel moment frames with low-, mid-, and high-rise, respectively.
[b] C1L, C1M, and C1H are concrete moment frames with low-, mid-, and high-rise, respectively.
[c] URML and URMM are unreinforced masonry bearing walls with low- and mid-rise, respectively.
[d] W1 and W2 are wood frames with a floor area of less than and more than 5,000 square feet, respectively.

Table 4.7 Archetype building portfolios of four virtual cities

Building types	Number of archetype buildings			
	City A	City B	City C	City D
S1L	46	-	-	56
S1M	92	-	-	111
S1H	294	-	250	-
C1L	-	46	-	55
C1M	-	91	-	111
C1H	-	295	250	-
URML	-	23	-	28
URMM	-	45	-	56
W1	22	-	-	27
W2	46	-	-	56

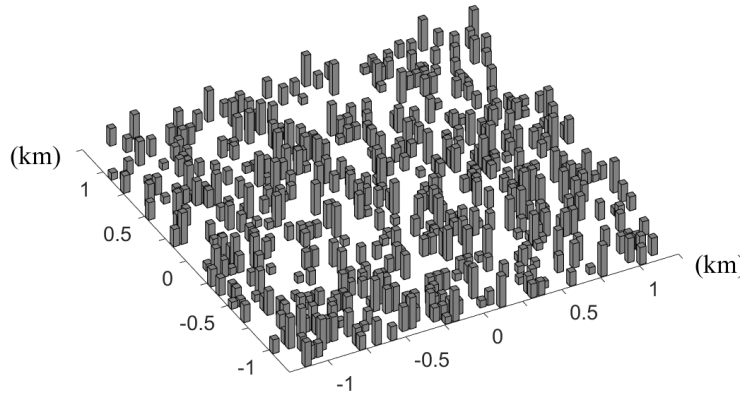

Figure 4.14 A virtual city consisting of 500 randomly generated buildings

As before, the seismic damage of a building is described by five damage states: none, slight, moderate, extensive, and complete. Each damage state is assumed to occur when the EDP exceeds the corresponding threshold defined for each archetype building and seismic design level. Table 4.8 shows the limit states of the 44 archetype buildings defined for the maximum IDR. These limit states were introduced based on the Low-Code seismic design levels in HAZUS (FEMA, 2012a). It is noted that these damage states can be assessed at the global level in terms of a single type of EDP. Table 4.9 summarizes the five damage states based on HAZUS (FEMA, 2012a) and the corresponding assumed economic losses of 44 archetypes buildings. For simplicity, the replacement cost in Eqs. (3.2) and (3.3) and the total loss of all buildings are assumed to be 1.

Table 4.8 Limit states of 44 archetype buildings defined in terms of maximum IDR

Building types	d_{LS1}	d_{LS2}	d_{LS3}	d_{LS4}
S1L	0.0060	0.0096	0.0203	0.0500
S1M	0.0040	0.0064	0.0135	0.0333
S1H	0.0030	0.0048	0.0101	0.0250
C1L	0.0050	0.0080	0.0200	0.0500
C1M	0.0033	0.0053	0.0133	0.0333
C1H	0.0025	0.0040	0.0100	0.0250
URML	0.0030	0.0060	0.0150	0.0350
URMM	0.0020	0.0040	0.0100	0.0233
W1	0.0040	0.0099	0.0306	0.0750
W2	0.0040	0.0099	0.0306	0.0750

Table 4.9 Damage states and corresponding economic losses of 44 archetype buildings

Damage State	Definition	l^{DS}
None	$EDP < d_{LS1}$	0%
Slight	$d_{LS1} \leq EDP < d_{LS2}$	5%
Moderate	$d_{LS2} \leq EDP < d_{LS3}$	25%
Extensive	$d_{LS3} \leq EDP < d_{LS4}$	50%
Complete	$d_{LS4} \leq EDP$	100%

In this example, it is assumed that an earthquake scenario with a moment magnitude of $M = 7.5$ and an epicentral distance of 35.4 km occurs. The shear wave velocity of the site is assumed to be $V_{S30} = 760$ m/s throughout the region. For predictions of the ground motion intensities of the buildings with the IM correlations considered, this example uses the GMPE by Boore and Atkinson (2008) along with the inter and intra-event correlation models developed by Baker and Cornell (2006) and Goda and Hong (2008b). The EDP correlations are estimated based on the linear relationship between the natural logarithms of EDP and IM using

the IM-invariant method presented in Section 4.2. Therefore, the parameter b in Eq. (2.5) is always 1.0, while the parameter a can be estimated through structural analysis using 1,499 ground motions. The EDPs of the buildings for a given earthquake scenario are estimated using these parameters. The regional loss assessment is carried out under each of the following assumptions: (1) 'Statistically Independent' ($\rho_{\widehat{S_{a_i}}\widehat{S_{a_j}}} = \rho_{\psi_i\psi_j} = 0$), (2) 'EDP Residual Correlated' ($\rho_{\widehat{S_{a_i}}\widehat{S_{a_j}}} = 0, \rho_{\psi_i\psi_j} \neq 0$), (3) 'IM Correlated' ($\rho_{\widehat{S_{a_i}}\widehat{S_{a_j}}} \neq 0, \rho_{\psi_i\psi_j} = 0$), and (4) 'Both Correlated' ($\rho_{\widehat{S_{a_i}}\widehat{S_{a_j}}} \neq 0, \rho_{\psi_i\psi_j} \neq 0$). The probabilities that the total regional loss exceeds the normalized threshold l_0 are shown in Figure 4.15.

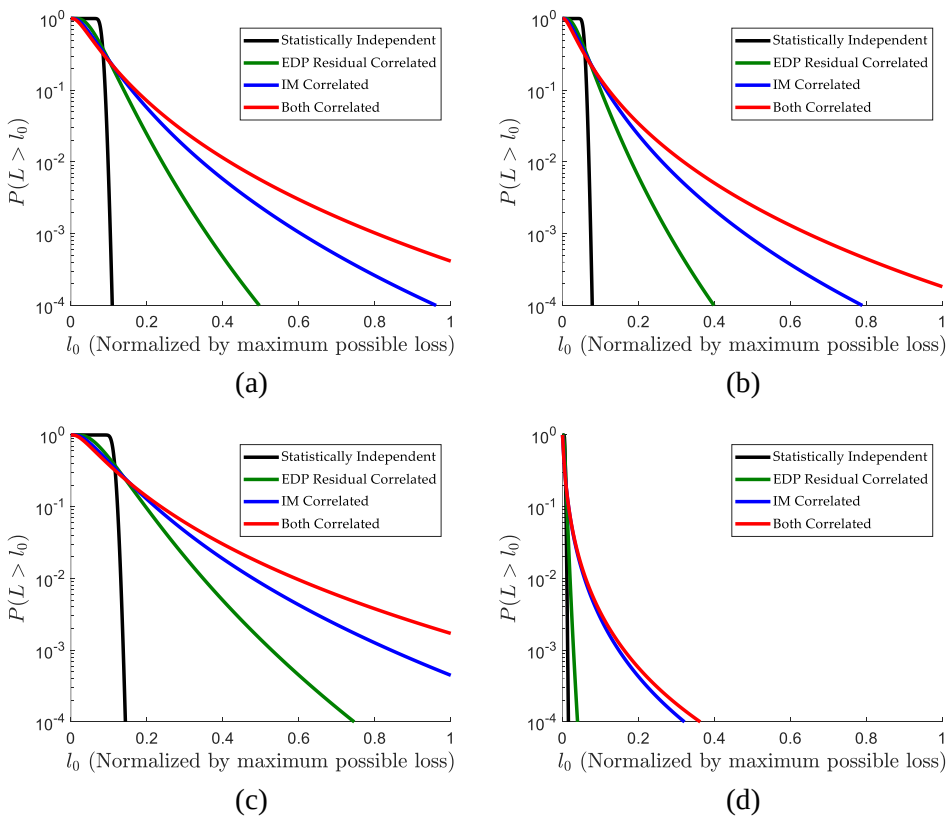

Figure 4.15 Loss exceedance probability under four assumptions on correlations: (a) City A, (b) City B, (c) City C, and (d) City D

The results show the significant impacts of EDP residual correlation on the regional losses depending on the building types. Similar results for City A (Figure 4.15(a)) and City B (Figure 4.15(b)) indicate that the damping ratios of the buildings do not make a significant difference in the effects of EDP correlations. In contrast, the comparison between City C (Figure 4.15(c)) and City D (Figure 4.15(d)) demonstrates that the higher modes contribute more to the effect of EDP residual correlation than the damping effect, as discussed in Section 4.3. In detail, σ_{ψ} in Eq. (2.10) is significantly lower than $\sigma_{\widehat{S_a}}$ for low-rise buildings with minor higher mode effects, increasing the relative contribution of the IM correlation. This example confirms that ignoring the EDP residual correlation in a region with a high proportion of high-rise buildings can significantly underestimate the loss exceedance probability. On the other hand, EDP correlation effects are not critical in a region where low-rise buildings are predominantly distributed.

4.5.2 Verification of regression-based estimation of EDP residuals

In order to verify the regression equation developed for estimating the variances and correlations of EDP residuals in Section 4.4, the regional loss assessment in Section 4.5.1 is performed using the regression models. The EDP residuals of 44 archetype buildings used in the example were estimated without performing structural analyses. Figure 4.16 compares these new results (shown in black dashed lines) with the loss exceedance probabilities evaluated in Section 4.5.1. The effects of EDP residual correlation can be slightly underestimated or overestimated depending on the building portfolio in the city. This is because, as seen in Figure 4.13, the regression model slightly overestimates the EDP residual of low-rise buildings and slightly

underestimates those of high-rise buildings. However, the proposed regression models provide a high level of accuracy for the 'Both Correlated' cases in all figures. In summary, the proposed regression models may not provide perfectly accurate EDP residual of each building but are accurate enough for the regional loss assessment. If the failure probabilities of buildings in a target region are available, accurate regional seismic loss assessment can be readily performed by substituting the regressed variances and correlations into Eq. (2.10) without performing additional structural analyses.

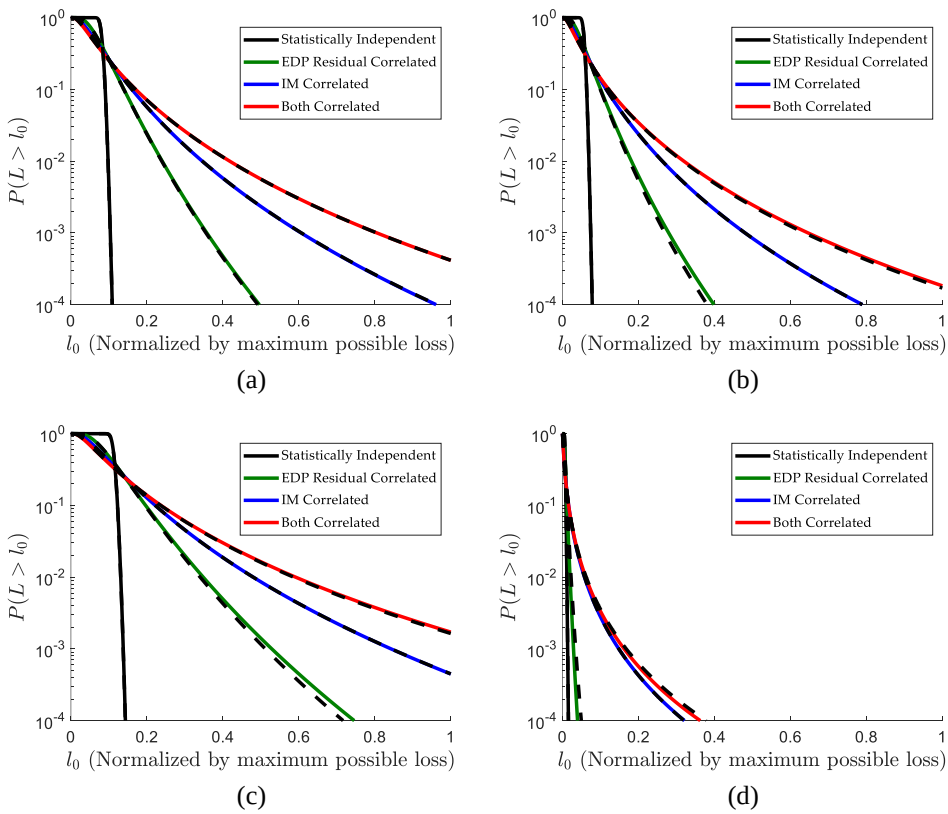

Figure 4.16 Comparison of loss exceedance probability using original EDP residual correlation (solid lines) and regression-based estimates of EDP residual correlation (black dashed lines) : (a) City A, (b) City B, (c) City C, and (d) City D

4.6 Summary

Based on the IDA-based method for evaluating the EDP residual correlation in Chapter 3 (Kang et al., 2021), an IM-invariant method was proposed to estimate the variances and correlation coefficients of EDP residuals of building structures. Taking advantage of the significantly reduced calculation time of the IM-invariant method, a comprehensive investigation was performed using many ground motions to find that the damping and higher mode effects are critical factors in the uncertainties and correlations of EDPs. Furthermore, to facilitate the consideration of EDP residuals in regional loss assessment, nonlinear regression models were developed to accurately predict the variances and correlations of EDP residuals without performing additional structural analysis.

The proposed IM-invariant method and regression models were successfully tested and demonstrated by regional seismic loss assessments of four virtual cities with different building portfolios. It was shown that ignoring the EDP residual correlation underestimates the loss exceedance probability, while the developed regression models can provide sufficient accuracy. Moreover, the effects of damping and higher modes (determined by the material and height of buildings) on EDP correlations and loss exceedance probabilities were investigated through numerical examples covering various building portfolios. The results demonstrated that the effect of EDP residual correlation on regional seismic losses significantly increases when high-rise buildings have dominant contribution to the region's building portfolio. The proposed IM-invariant method, regression models, and guidelines are expected to facilitate accurate and efficient seismic reliability analysis of complex systems.

The proposed regression models can effectively describe the overall trend of EDP residuals in regional loss assessment but may not accurately estimate the EDP residual of specific structures. In particular, the regression model developed for the correlation coefficient between EDP residuals based on the logistic function may not accurately predict the values close to 0 or 1. To overcome this issue, it is desirable to improve the accuracy of regression models using alternative statistical learning approaches.

Chapter 5. Deep Neural Network-based Frameworks for Estimation of EDP residuals of Building Structures

5.1 Introduction

Although the regression models developed in Section 4.4 (Kang et al., 2022) facilitate the efficient evaluation of the EDP residuals of building structures, the accuracy and applicability are still challenging. The regression models can describe the overall trend of EDP residuals of buildings but show a limited level of accuracy for specific structures. In particular, the regression model for the correlation coefficient between EDP residuals based on the logistic function cannot accurately predict the values near 0 or 1. For this reason, many studies have introduced surrogate models instead of the regression model to accurately predict the correlation coefficient between the EDP residuals. In recent researches, machine learning and deep neural network (DNN) model with high accuracy and applicability has been commonly adopted as a surrogate model.

For instance, Stern et al. (2017) constructed machine-learning-based surrogate models for estimating network failure probability for California gas distribution network. Kim et al. (2020a) incorporated a probabilistic DNN model into regional seismic loss assessment to predict the structural responses of buildings in urban areas. Silva-Lopez et al. (2022) evaluated retrofitting policies and seismic risk assessment of road networks using a DNN model with three sampling protocols. These studies demonstrated the great potential of DNN models for accurate and efficient seismic system reliability analysis.

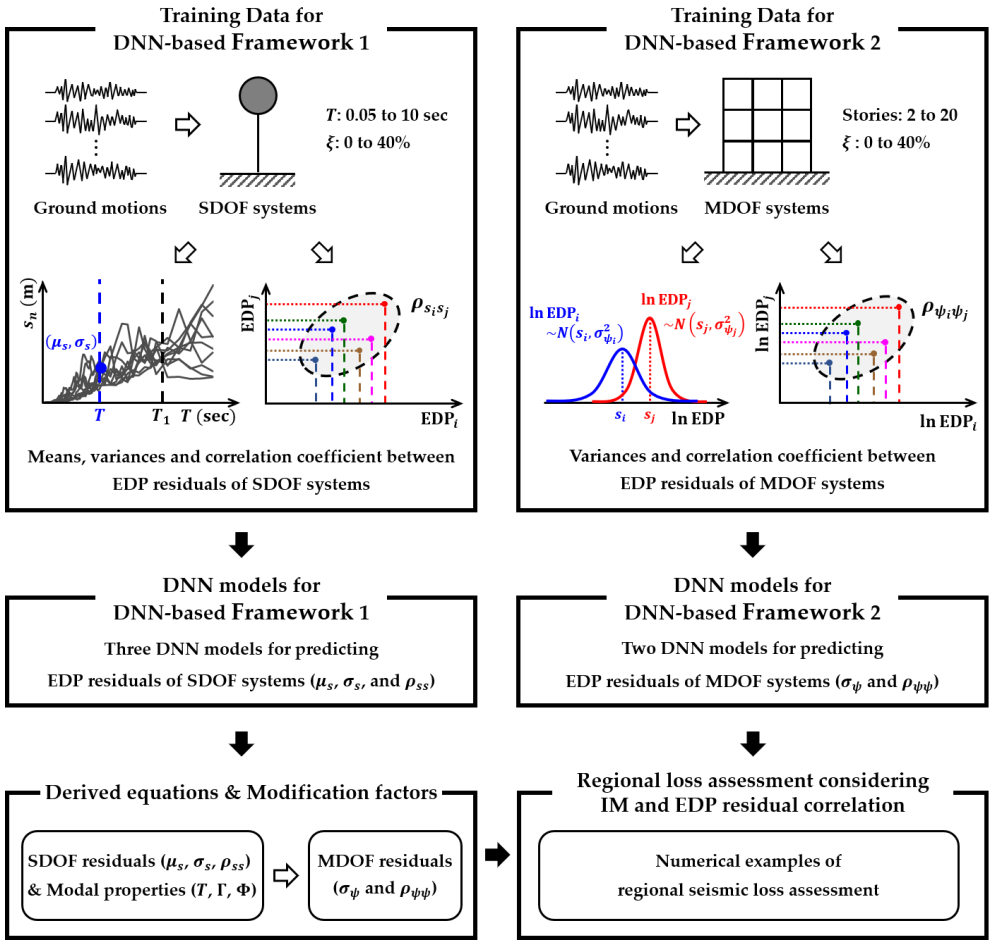

Figure 5.1 Two DNN-based frameworks proposed for estimating EDP residuals of building structures

This study proposes two DNN-based frameworks to utilize these advantages in quantifying the uncertainties of EDP residuals. As illustrated in Figure 5.1, the first framework estimates the standard deviations and correlation coefficients of EDP residuals of multi-degree-of-freedom (MDOF) systems by combining the EDP residuals of single-degree-of-freedom (SDOF) systems through the modal combination. To this end, three DNN models that predict the means, standard deviations, and correlation coefficients of EDP residuals are proposed. On the other hand, the second framework presents two DNN models that directly predict the EDP

residuals of specific types of building structures. A large number of MDOF systems with various first and second modal periods and damping ratios are employed in this regard (Kang et al. – Under review).

5.2 Modal combination-based estimation of EDP residuals

5.2.1 Modal combination rule for EDP residual

An MDOF system subjected to ground acceleration $\ddot{u}_g(t)$ can be described by the equation of motion

$$\mathbf{m\ddot{u}} + \mathbf{c\dot{u}} + \mathbf{ku} = -\mathbf{m}\iota\ddot{u}_g(t) \tag{5.1}$$

where $\mathbf{\ddot{u}}$, $\mathbf{\dot{u}}$, and $\mathbf{u}$ denote the acceleration, velocity, and displacement vectors of the system, respectively; $\mathbf{m}$, $\mathbf{c}$, and $\mathbf{k}$ stand for the mass, damping coefficient, and lateral stiffness matrices, respectively; and ι denotes the influence vector. This study uses Rayleigh damping (Hall, 2006) to calculate the damping coefficient matrix.

When the system behaves in the linear elastic range, the displacement time history of the MDOF system can be described by the superposition of the mode contributions, i.e.,

$$\mathbf{u}(\mathrm{t}) = \sum_{n=1}^{N} \mathbf{u}_n(t) = \sum_{n=1}^{N} \Gamma_n \boldsymbol{\phi}_n D_n(t) \tag{5.2}$$

where $\mathbf{u}_n(t)$ is the contribution of the nth mode to the displacement $\mathbf{u}(t)$; Γ_n and $\boldsymbol{\phi}_n$ respectively denote the modal participation factor and the mode shape vector of the nth mode; and $D_n(t)$ represents the dynamic response of the SDOF system representing the nth mode under the ground motion $\ddot{u}_g(t)$. Using Eq. (5.2),

two of the most widely used EDPs of building structures, roof displacement u_r and dth interstory drift ratio (IDR) IDR_d, can be expressed as

$$u_r(\mathrm{t}) = \sum_{n=1}^{N} \Gamma_n \phi_{r,n} D_n(t) \tag{5.3}$$

$$\mathrm{IDR}_d(\mathrm{t}) = \sum_{n=1}^{N} \Gamma_n \left(\frac{\phi_{d,n} - \phi_{(d-1),n}}{h_d} \right) D_n(t) \tag{5.4}$$

where $\phi_{r,n}$ and $\phi_{d,n}$ denote the nth mode shape value at the roof and the dth story $(d = 1, \dots, r)$, respectively; and h_d is the height of the dth story.

In response spectrum analyses, the peak responses of an MDOF system, which are essential EDPs in designing buildings and evaluating their seismic performances, are calculated by those of SDOF systems representing the modes. Note that the peak value of $D_n(t)$ is readily calculated from each ground motion's response spectrum or design spectrum without a time history analysis. In such a modal combination process, the EDP of an MDOF system is often estimated by the square-root-of-sum-of-squares (SRSS) rule (Rosenblueth, 1951), i.e.,

$$\mathrm{EDP} = \left(\sum_{n=1}^{N} A_n^2 s_n^2 \right)^{1/2} \tag{5.5}$$

where A_n represents the nth mode's effective participation factor for the EDP; and s_n is the peak response of the nth mode. For example, the effective participation factor of the roof displacement is $A_n = \Gamma_n \phi_{rn}$ while that of the dth story's IDR is $A_n = \Gamma_n (\phi_{d,n} - \phi_{(d-1),n})/h_d$.

The standard deviations and correlations of the EDP residuals of MDOF systems can be estimated in terms of those of the modal responses. To this end, the

EDP of the ith MDOF system is first approximated by the first-order Taylor series expansion of Eq. (5.5) at the mean modal peak responses, i.e.,

$$\mathrm{EDP}_i = \left(\sum_{n=1}^{N} A_{n,i}^2 \mu_{s_{n,i}}^2\right)^{1/2} + \sum_{n=1}^{N_i} A_{n,i}^* \left(s_{n,i} - \mu_{s_{n,i}}\right) \tag{5.6}$$

where $\mu_{s_{n,i}}$ is the mean of the nth modal peak response, $n = 1, \ldots, N_i$, and $A_{n,i}^*$ denotes the coefficient of $s_{n,i}$ for the EDP of the ith MDOF system, defined as $A_{n,i}^* = A_{n,i}^2 \mu_{s_{n,i}} / \left(\sum_{m=1}^{N_i} A_{m,i}^2 \mu_{s_{m,i}}^2\right)^{1/2}$. Note that, when the peak value of the dth story's IDR is selected as the EDP, the effective participation factor A_n is calculated based on the assumption that the maximum IDR occurs at the same story for any ground motions applied. In this case, the story d is defined as the story showing the maximum value for the mean of Eq. (5.6), i.e., $\left(\sum_{n=1}^{N_i} A_{n,i}^2 \mu_{s_{n,i}}^2\right)^{1/2}$.

From Eq. (5.6), the first-order approximations of the variances and covariances of EDP are derived, respectively as

$$\sigma_{\mathrm{EDP}_i}^2 = \sum_{k=1}^{N_i} {A_{k,i}^*}^2 \sigma_{s_{k,i}}^2 + 2 \sum_{k=1}^{N_i - 1} \sum_{l=k+1}^{N_i} A_{k,i}^* A_{l,i}^* \sigma_{s_{k,i}} \sigma_{s_{l,i}} \rho_{s_{k,i} s_{l,i}} \tag{5.7}$$

and

$$Cov\left[\mathrm{EDP}_i, \mathrm{EDP}_j\right] = \sum_{k=1}^{N_i} \sum_{l=1}^{N_j} A_{k,i}^* A_{l,j}^* \sigma_{s_{k,i}} \sigma_{s_{l,j}} \rho_{s_{k,i} s_{l,j}} \tag{5.8}$$

in which σ_{EDP_i} and σ_{EDP_j} are the standard deviations of EDP_i and EDP_j, respectively; $Cov\left[\mathrm{EDP}_i, \mathrm{EDP}_j\right]$ denotes the covariance between the EDPs; N_i and N_j are the number of modes of the ith and jth MDOF systems, respectively; $A_{k,i}$ is the kth mode effective participation factor of the ith mode; and $\mu_{s_{k,i}}$ and $\sigma_{s_{k,i}}$

respectively denote the mean and standard deviation of the kth modal peak responses of the ith MDOF system. In other words, $\mu_{s_{k,i}}$ and $\sigma_{s_{k,i}}$ are the mean and standard deviation of structural responses of the SDOF system representing the kth mode when ground motions are scaled to obtain the same IM value S_{a_i} at the first mode period of the ith MDOF system $T_{1,i}$ $\left(\geq T_{k,i}, \text{where } k = 1, \dots, N_i\right)$. $\rho_{s_{k,i}s_{l,j}}$ is the correlation coefficient between peak responses of the kth mode when ground motions are scaled to S_{a_i} at $T_{1,i}$ and of the lth mode when ground motions are scaled to S_{a_j} at $T_{1,j}$. The means, standard deviations, and correlation coefficients of EDP residuals of SDOF systems are estimated through spectral displacements as illustrated in Figure 5.2. Note that the damping ratios of the kth and lth modes vary along with the number of modes and the assumption regarding the damping coefficient.

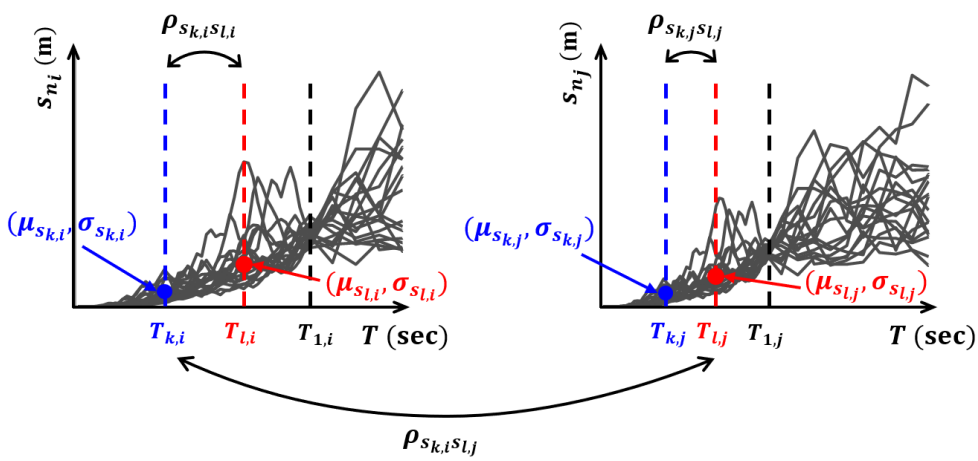

Figure 5.2 Means, standard deviations, and correlation coefficients of EDP residuals of SDOF systems

Finally, using the results in Eqs. (5.8) and (5.9), the correlation coefficient between the EDP residuals is computed as

$$\rho_{\mathrm{EDP}_i\mathrm{EDP}_j} = \frac{Cov\left[\mathrm{EDP}_i, \mathrm{EDP}_j\right]}{\sigma_{\mathrm{EDP}_i}\sigma_{\mathrm{EDP}_j}} \tag{5.9}$$

Similar to the previous studies (Kang et al. 2021, 2022), the EDP residual of the ith MDOF system is assumed to follow a Lognormal distribution with the mean μ_{EDP_i} and standard deviation σ_{EDP_i}. The standard deviation of the natural logarithm of the EDP residual, σ_{ψ_i} and correlation coefficient between the natural logarithm of EDP residuals, $\rho_{\psi_i\psi_j}$ in Eq. (2.10) are respectively derived as

$$\sigma_{\psi_i} = \sqrt{\ln\left(1+\delta_i^2\right)} \tag{5.10}$$

$$\rho_{\psi_i\psi_j} = \frac{1}{\sigma_{\psi_i}\sigma_{\psi_j}} \ln\left(1+\rho_{\mathrm{EDP}_i\mathrm{EDP}_j}\delta_i\delta_j\right) \tag{5.11}$$

where $\delta_i = \sigma_{\mathrm{EDP}_i}/\mu_{\mathrm{EDP}_i}$ denotes the coefficient of variation of the EDP residual of the ith MDOF system. It is noted that, as discussed in Section 2.2 (Kang et al., 2021), the means and standard deviations of the EDP residuals of MDOF systems are estimated based on the assumption that they behave in the linear elastic range.

5.2.2 DNN models for EDP residuals of single-degree-of-freedom systems

A regional seismic loss assessment using the modal combination rule derived in Section 5.2.1 would require evaluations of the three types of parameters – $\mu_{s_{k,i}}$, $\sigma_{s_{k,i}}$, and $\rho_{s_{k,i}s_{l,j}}$. (Note $A_{k,i}$ can be obtained by eigenvalue analysis.) In order to train DNN models that can predict $\mu_{s_{k,i}}$, $\sigma_{s_{k,i}}$, and $\rho_{s_{k,i}s_{l,j}}$ for a practical range of building structures, a large-size dataset is required. Since the seismic demand

database developed by Kim et al. (2019, 2020b) only considers the damping ratio of 5%, a new seismic demand database is developed in this study. By following the criteria provided by Kim et al. (2019, 2020b), we selected 90 steps of the period from 0.05 sec to 10 sec, 20 steps of damping ratio from 0 to 40%, and 1,499 ground motions from the NGA-West database (Power et al., 2008) to cover a wide range of MDOF systems. A total of 2,698,200 ($= 90 \times 20 \times 1{,}499$) time history analyses were performed to construct a (linear elastic) seismic demand database.

Among the three DNN models, the first two DNN models respectively predict $\mu_{s_{k,i}}$ and $\sigma_{s_{k,i}}$ based on the three inputs: the first mode period of the ith MDOF system $T_{1,i}$, the ratio of the period of the kth model to the first mode period of the ith MDOF system $(T_{1,i} - T_{k,i})/T_{1,i} \in [0,1)$, and the damping ratio of the kth mode $\xi_{k,i}$. For the second input, it is found from a comprehensive investigation that the relative ratio of the two periods, $(T_{1,i} - T_{k,i})/T_{1,i}$ is more helpful in extracting the pattern between input and output than T_i. Figures 5.3 and 5.4 show the architectures of the two DNN models. In the figures, ReLU, Lin, and L2(α) represent the rectified linear operator (Nair and Hinton, 2010), linear function, and the L2 regularization having a coefficient value α, respectively. The values of hyperparameters in the network are decided through a grid search. In particular, the hourglass model showed a better performance than other widely-used architectures. In an example, the hourglass model showed ten times better accuracy than a model based on a different architecture that has the same units for each layer.

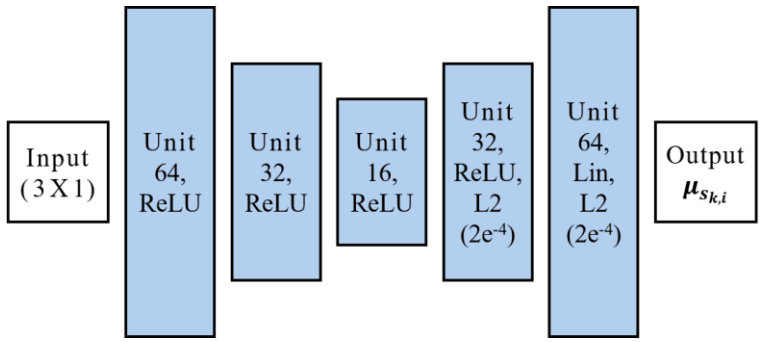

Figure 5.3 Architectures of DNN models to predict mean of EDP residual of SDOF system $\mu_{s_{k,i}}$

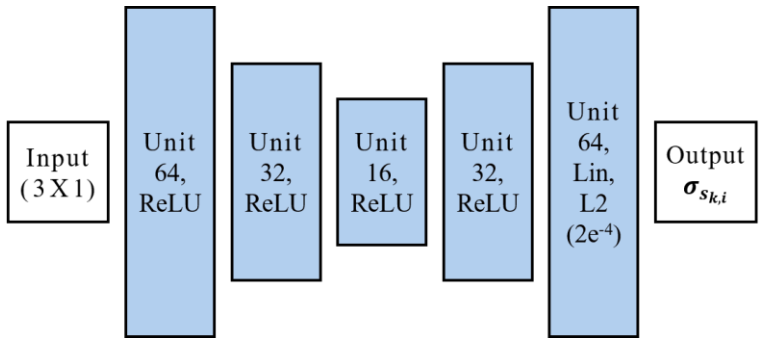

Figure 5.4 Architectures of DNN models to predict standard deviation of EDP residual of SDOF system $\sigma_{s_{k,i}}$

Next, to predict $\rho_{s_{k,i}s_{l,j}}$, i.e., the correlation coefficient between the kth mode of the ith MDOF system and the lth mode of the jth MDOF system, the following six input parameters (three features for each MDOF system) are required: $T_{1,i}$, $(T_{1,i} - T_{k,i})/T_{1,i}$, $\xi_{k,i}$, $T_{1,j}$, $(T_{1,j} - T_{l,j})/T_{1,j}$, and $\xi_{l,j}$. The relationship between two MDOF systems is considered by a one-dimensional (1D) convolutional neural network (CNN) with two different filter sizes. In detail, the two filter sizes (one size of less than three and the other greater than three) are employed to capture features within each MDOF system and those between the two MDOF systems. A hyperbolic

tangent function is used at the final layer of the DNN model because the correlation coefficient always lies between -1 and 1. The detailed architecture of the DNN model is illustrated in Figure 5.5. Similar to the previous DNN models, a grid search is employed to find the hyperparameters of the DNN model.

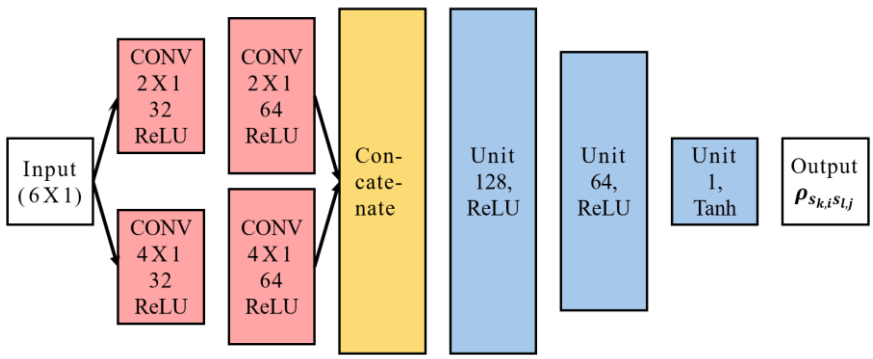

Figure 5.5 Architecture of DNN model to predict correlation coefficient between EDP residuals of SDOF systems $\rho_{s_{k,i}s_{l,j}}$

Among 162,000 cases (= 90 first mode periods × 90 other modes × 20 damping values), only 81,900 data were generated as a train set to utilize the fact that the first mode period is greater than the others. A train set of size 55,692 (68%) and a validation set of size 13,923 (17%) are used to train the DNN models while avoiding over-fitting. The remaining data set of size 12,285 (15%) is employed to test the performance of the trained DNN model. A natural logarithm is applied to the period feature in the input set and the output to resolve the inherent skewness. During the training, we used the Adam optimizer (Kingma and Ba, 2014) to minimize the mean squared error (MSE; $(1/N)\cdot\sum_{i=1}^{N}(\hat{y}_i - y_i)^2$), where $\hat{y}_i$ is the predicted value from the DNN model, and y_i is the data from time history analysis, $i = 1, \dots, N$). The performance of the DNN models is summarized in Tables 5.1 and 5.2 for $\mu_{s_{k,i}}$

and $\sigma_{s_{k,i}}$, respectively in terms of MSE and mean absolute error (MAE; $(1/N) \cdot \sum_{n=1}^{N} |\hat{y}_i - y_i|$) after 1,000 epochs of training. Note that since natural logarithm is applied to the output during training, MSE and MAE of the original scale are also provided in the tables. The DNN models show superior accuracy in predicting the means and standard deviations of EDP residuals.

Table 5.1 Errors of the DNN model that predicts mean of EDP residual of SDOF system

Scale	Dataset	MSE	MAE
Log scale	Train	0.00017	0.00859
	Validation	0.00018	0.00887
	Test	0.00058	0.01698
Original scale	Train	0.00009	0.00231
	Validation	0.00012	0.00241
	Test	0.00015	0.00422

Table 5.2 Errors of the DNN model that predicts standard deviation of EDP residual of SDOF system

Scale	Dataset	MSE	MAE
Log scale	Train	0.00068	0.01941
	Validation	0.00077	0.02048
	Test	0.00059	0.01844
Original scale	Train	0.00011	0.00338
	Validation	0.00014	0.00357
	Test	0.00012	0.00342

While training the DNN model to predict $\rho_{s_{k,i}s_{l,j}}$ based on the information about the relationship between the first and higher mode periods, a computer memory issue was alleviated by reducing the period step from 90 to 40 and generating only 134,488,200 data out of over 1 billion data. 70%, 20%, and 10% of the dataset are randomly selected for train, validation, and test datasets, respectively. Since it is difficult to load all data simultaneously due to the memory issue, 10% of the dataset was randomly selected and loaded for each loop to perform ten epochs of training. Similar to the previous DNN models, MSE was selected as a loss function and minimized by the Adam optimizer. The prediction accuracy of the DNN model after 20 iterations of training is presented in Table 5.3 in terms of MSE and MAE. The results confirm the superior prediction accuracy of the third DNN model.

Table 5.3 Errors of the DNN model that predicts correlation coefficients between EDP residuals of SDOF systems

Dataset	MSE	MAE
Train	0.00026	0.01178
Validation	0.00026	0.01178
Test	0.00026	0.01178

5.2.3 Modification factors for EDP residuals of multi-degree-of-freedom systems estimated by derived equations

The standard deviations and correlations of the EDP residuals of MDOF systems can be estimated by substituting the DNN-based predictions in Section 5.2.2 into Eqs. (5.7)-(5.9) derived in Section 5.2.1. However, the results may not match the predictions based on response history analysis (RHA) using Eqs. (5.3) and (5.4) because of the following assumptions of the approach: (1) the EDP follows a Lognormal distribution, (2) the peak response of an MDOF system is determined by

the combination of peak responses of all modes, (3) the first-order approximation of the SRSS rule is reasonable, and (4) the maximum IDR occurs at the same story for all ground motions. Therefore, modification factors are needed before using the derived EDP residuals for regional seismic loss assessment. It is noted that the modification factors are developed not because of the performance of the DNN models but these assumptions in the proposed approach.

The modification factors are obtained by comparing the EDP residuals of MDOF systems predicted by Eq. (5.10) to those obtained from RHA. To this end, 380 archetype buildings with 19 different heights (from 2 to 20 stories) and 20 damping ratios (0 to 40% damped buildings) are developed based on the 95 archetype buildings in Kang et al. (2022). The modulus of elasticity (E) of the beams and columns of MDOF systems are assumed to be 200 GPa $(29{,}000$ ksi$)$. Based on the 1,499 ground motions used in Section 5.2.2, the EDP residuals of building structures were estimated by RHA and the derived equations. Figure 5.6 shows the standard deviations of EDP residuals of 5-story buildings with 20 different damping ratios. The means, standard deviations, and correlation coefficients in Eqs. (5.7) and (5.8) are estimated from the structural responses in the linear elastic seismic database developed in Section 5.2.2 and plotted in the red square markers. The results show that the derived equations mostly underestimate the standard deviation, especially when the first mode damping ratios are around 5%. As shown in Eq. (2.10), the significant underestimation of the standard deviation substantially affects the overall correlation coefficients between EDP residuals of two buildings, which leads to an inaccurate estimation of the joint failure probability.

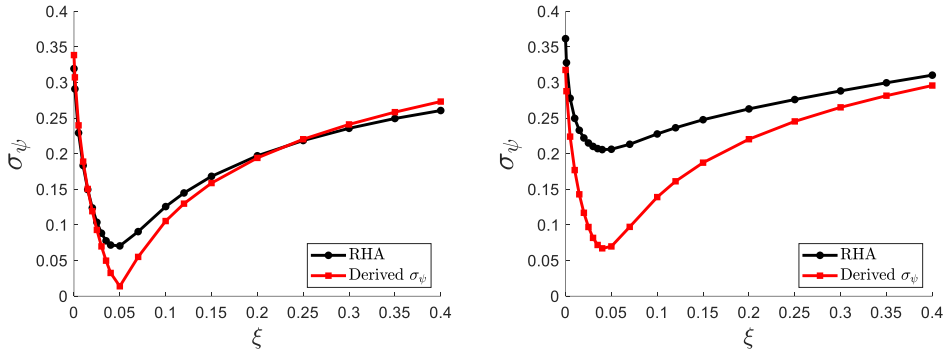

Figure 5.6 Comparison between the standard deviations of EDP residuals of 5-story buildings by the RHA and the predictions by derived equations: (a) roof displacement, and (b) maximum IDR

After an extensive investigation of the results, a modification factor (MF) is introduced for pairs of the first mode period and damping ratio to improve the standard deviation. The standard deviation of EDP residual of the building with the first mode period (T_1) and damping ratio ξ can be estimated by multiplying the derived σ_ψ of the building with T_1 and $\xi = 0$ by the modification factor, i.e., $\sigma_\psi(T_1, \xi) = \sigma_\psi(T_1, \xi = 0) \times MF$. Tables 5.4 and 5.5 show the modification factors proposed for the standard deviations of the EDP residuals. Figure 5.7 compares the standard deviations of EDP residuals of 380 archetype buildings (19 stories with 20 different damping ratios) obtained by Eq. (5.7) and the modification factor with those by RHA. In addition, to demonstrate the prediction accuracy of the three DNN models developed in Section 5.2.2, Figure 5.8 shows the modified standard deviations estimated by derived equations with the three DNN models. The results confirm that the proposed approach has sufficient accuracy even if μ_s, σ_s, and ρ_{ss} in Eqs. (5.7) and (5.8) are replaced with the predictions by the DNN models.

Table 5.4 Modification factors for the standard deviation of roof displacement residual

T_1 (sec)	Damping ratio ξ								
	0	0.005	0.010	0.020	0.030	0.050	0.100	0.200	0.400
0	1.000	1.000	1.000	1.000	1.000	1.000	1.000	1.000	1.000
0.10	0.983	0.872	0.822	0.761	0.719	0.667	0.738	0.815	0.886
0.20	0.966	0.744	0.645	0.521	0.437	0.333	0.475	0.630	0.773
0.30	0.959	0.641	0.500	0.322	0.202	0.055	0.258	0.479	0.682
0.40	1.002	0.681	0.532	0.344	0.215	0.075	0.287	0.517	0.717
0.50	0.985	0.687	0.545	0.363	0.241	0.115	0.291	0.515	0.707
0.75	0.925	0.664	0.534	0.365	0.258	0.174	0.324	0.542	0.731
1.00	0.960	0.704	0.576	0.413	0.313	0.244	0.356	0.564	0.757
1.25	0.913	0.672	0.549	0.396	0.309	0.263	0.409	0.628	0.837
1.50	0.929	0.702	0.585	0.443	0.366	0.329	0.458	0.678	0.900
2.00	1.039	0.812	0.701	0.567	0.499	0.468	0.576	0.781	1.029
3.00	1.104	0.931	0.845	0.749	0.704	0.677	0.723	0.849	1.070
4.00	1.301	1.216	1.199	1.180	1.134	1.063	1.049	1.108	1.321

Table 5.5 Modification factors for the standard deviation of maximum IDR residual

T_1 (sec)	Damping ratio ξ								
	0	0.005	0.010	0.020	0.030	0.050	0.100	0.200	0.400
0	1.000	1.000	1.000	1.000	1.000	1.000	1.000	1.000	1.000
0.10	0.980	0.874	0.829	0.777	0.746	0.725	0.768	0.830	0.892
0.20	0.960	0.747	0.658	0.553	0.492	0.449	0.535	0.661	0.783
0.30	0.952	0.650	0.523	0.373	0.285	0.224	0.345	0.524	0.698
0.40	1.013	0.709	0.581	0.428	0.337	0.276	0.386	0.566	0.736
0.50	1.022	0.735	0.617	0.479	0.400	0.345	0.428	0.588	0.744
0.75	1.042	0.794	0.695	0.591	0.540	0.513	0.582	0.705	0.849
1.00	1.200	0.942	0.859	0.776	0.739	0.724	0.773	0.875	1.039
1.25	1.330	1.094	1.029	0.973	0.947	0.940	0.984	1.096	1.301
1.50	1.406	1.194	1.141	1.097	1.080	1.073	1.108	1.214	1.437
2.00	1.231	1.070	1.041	1.013	1.000	0.993	1.015	1.111	1.293
3.00	0.978	0.861	0.839	0.817	0.804	0.795	0.818	0.905	1.029
4.00	1.046	0.947	0.925	0.904	0.886	0.877	0.926	1.044	1.178

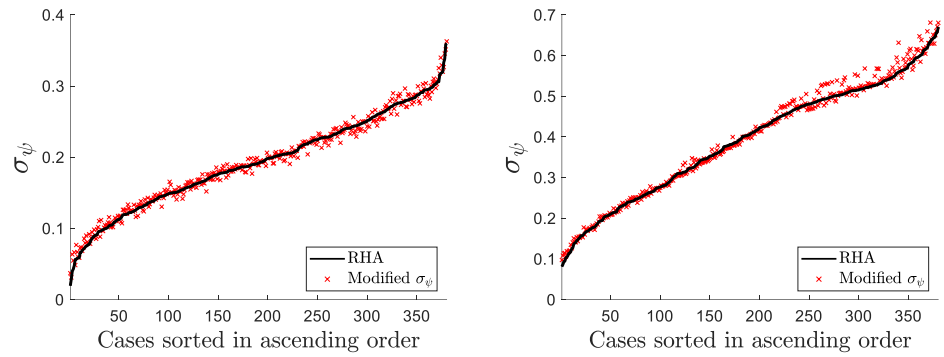

(a) (b)

Figure 5.7 Comparison between the standard deviations of EDP residuals by RHA and the predictions by derived equations with modification factors: (a) roof displacement, and (b) maximum IDR

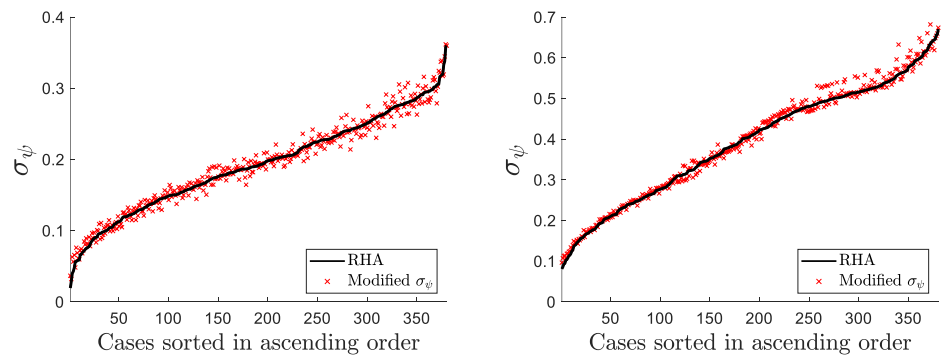

(a) (b)

Figure 5.8 Standard deviations of EDP residuals by RHA and the predictions by derived equations with three DNN models and modification factors: (a) roof displacement, and (b) maximum IDR

Figures 5.9 and 5.10 compare the correlation coefficients between EDP residuals of buildings estimated by RHA, Eq. (5.11) with EDP residuals of SDOF system in the database, and Eq. (5.11) with the three DNN models. In both cases of using the derived correlation coefficient between EDP residuals $\rho_{\psi_i\psi_j}$, there are slight errors for the low-correlated buildings. However, the overall trend is

adequately described by the proposed approaches. Since a regional seismic loss assessment should consider many different characteristics of structural systems simultaneously, a modification factor is not required for the derived correlation coefficients. Furthermore, the similar estimation results by the two approaches using the derived equations confirm that the DNN models can effectively replace the database.

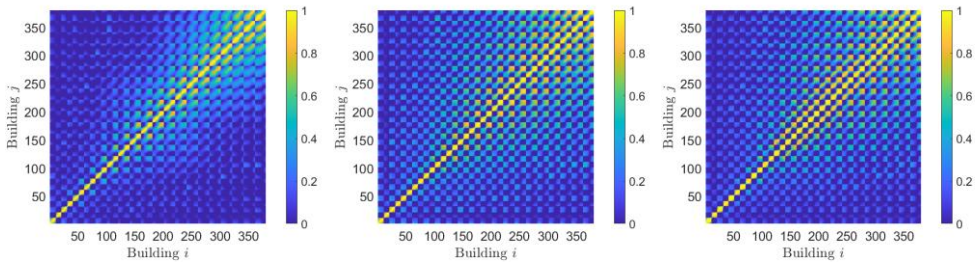

(a) (b) (c)

Figure 5.9 Correlation coefficients between roof displacement residuals estimated by three different method: (a) RHA, (b) derived equation with the database, and (c) derived equations with DNN models

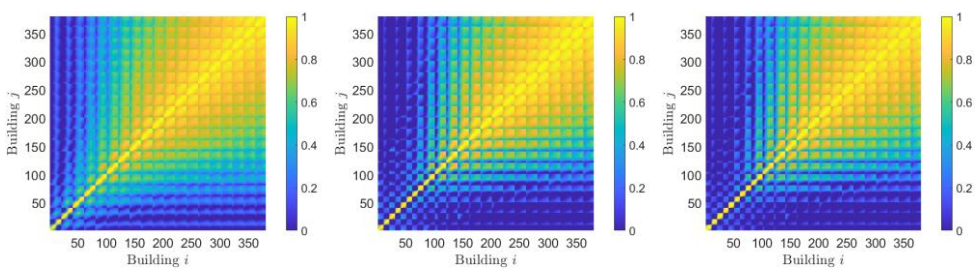

(a) (b) (c)

Figure 5.10 Correlation coefficients between maximum IDR residuals estimated by three different method: (a) RHA, (b) derived equation with the database, and (c) derived equations with DNN models

5.3 Deep neural networks for estimating EDP residuals of building structures

The proposed EDP residual estimation approach based on the equations derived in Section 5.2 applies to buildings with various structural types and damping ratios as long as the periods, participation factors, and shape vectors are available. This study develops DNN models that can directly predict EDP residuals' standard deviations and correlation coefficients to facilitate the EDP residual estimation when such modal properties are not readily available. The model development focuses on buildings whose Rayleigh damping coefficients are determined based on the first and third modal damping ratios to facilitate predictions for generic buildings with limited information – the first and second modal periods and damping ratio.

5.3.1 Developments of DNN models for EDP residuals of building structures

To train DNN models that directly predict standard deviations (σ_{ψ_i} and σ_{ψ_j}) and correlation coefficient ($\rho_{\psi_i\psi_j}$) of two structures, many building structures with various modal periods and damping ratios should be investigated. To this end, 100 randomly generated artificial variations are introduced to the lateral stiffness of the building structures introduced in Section 5.2.3. As a result, we generated 38,000 building structures with 19 building heights (from 2 to 20 stories), 20 damping ratios (from 0 to 40%), and 100 artificial variations. By using 1,499 ground motions, 56,962,000 ($= 38{,}000 \times 1{,}499$) RHAs are performed in the linear range to estimate the EDP residuals of the building structures.

The DNN model for predicting the standard deviation of EDP residual, σ_{ψ_i} has

three input features, the first mode period $T_{1,i}$, the difference between the first two periods normalized by the first one, i.e., $(T_{1,i} - T_{2,i})/T_{1,i}$, and the damping ratio of the ith building, ξ_i. It is noted that the second input was used for the DNN models for SDOF systems in Section 5.2.2. Since the input-output relationship in this case is relatively straightforward compared to the residuals of SDOF systems, the traditional architecture in Figure 5.11 is used instead of the hourglass model. The hyperparameters of the DNN model are determined by a grid search. As before, the natural logarithm is applied to the first input $T_{1,i}$ and the output σ_{ψ_i} to account for inherent skewness. From a total of 38,000 data sets used for developing the DNN model, 25,840 (68%) were assigned as the train set, 6,460 (17%) as the validation set, and 5,700 (15%) as the test set. Tables 5.6 and 5.7 show the error measures for each dataset type after 3,000 epochs of training to reduce MSE using the Adam optimizer.

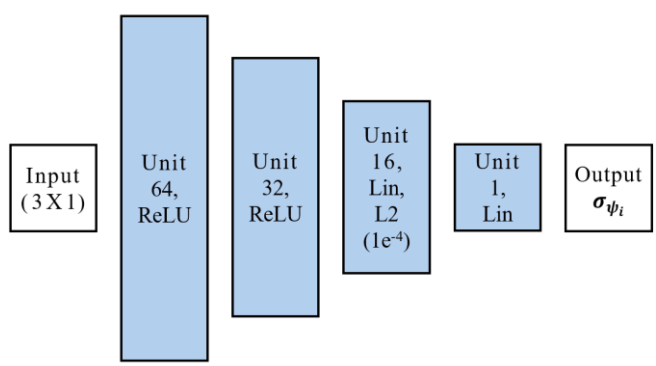

Figure 5.11 Architecture of DNN model that directly predicts the standard deviation of EDP residual σ_{ψ_i}

Table 5.6 Errors of the DNN model that predicts standard deviation of roof displacement residual

Scale	Dataset	MSE	MAE
Log scale	Train	0.00074	0.01651
	Validation	0.00064	0.01349
	Test	0.00067	0.01741
Original scale	Train	0.00001	0.00263
	Validation	0.00001	0.00212
	Test	0.00002	0.00325

Table 5.7 Errors of the DNN model that predicts standard deviation of maximum IDR residual

Scale	Dataset	MSE	MAE
Log scale	Train	0.00039	0.00449
	Validation	0.00029	0.00389
	Test	0.00029	0.00428
Original scale	Train	0.00004	0.00449
	Validation	0.00003	0.00389
	Test	0.00003	0.00428

Next, the DNN model to predict the correlation coefficient between the EDP residuals uses six input parameters: $T_{1,i}$, $(T_{1,i} - T_{2,i})/T_{1,i}$, ξ_i, $T_{1,j}$, $(T_{1,j} - T_{2,j})/T_{1,j}$, and ξ_j. Similar to the DNN model to predict the correlation coefficients of SDOF systems in Section 5.2.2, a one-dimensional CNN with three different sizes is used to effectively capture the relationship between the input and output. A hyperbolic tangent function is introduced at the end process. A grid search was performed to find the hyperparameters of the DNN model in Figure 5.12. In total, 722,019,000 correlation coefficients for the 38,000 buildings (38,000 pairs of

identical buildings and $38{,}000 \times (38{,}000 - 1)/2 = 721{,}981{,}000$ pairs of different buildings) are used for the model development. 70%, 20%, and 10% were randomly assigned to the train, validation, and test sets, respectively. Tables 5.8 and 5.9 show the errors of the DNN models for three datasets after ten iterations to reduce the MSE by the Adam optimizer.

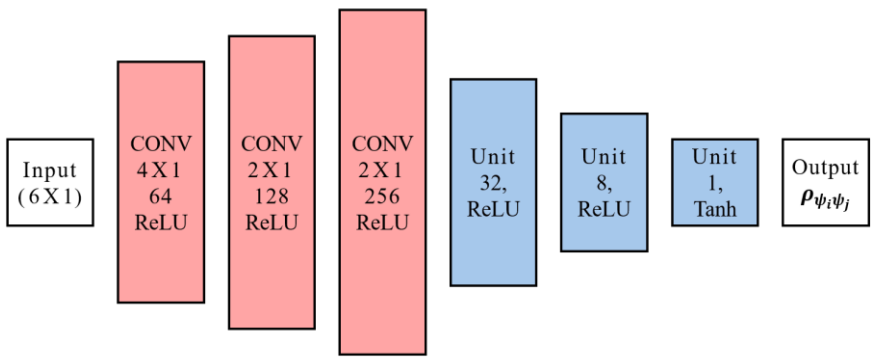

Figure 5.12 Architectures of DNN model to predict the correlation coefficient between EDP residuals $\rho_{\psi_i\psi_j}$

Table 5.8 Errors of the DNN model that predicts correlation coefficient between roof displacement residuals

Dataset	MSE	MAE
Train	0.00007	0.00630
Validation	0.00007	0.00630
Test	0.00007	0.00630

Table 5.9 Errors of the DNN model that predicts correlation coefficient between maximum IDR residuals

Dataset	MSE	MAE
Train	0.00003	0.00367
Validation	0.00003	0.00367
Test	0.00003	0.00367

5.3.2 Performance of DNN models for EDP residuals

Figures 5.13 and 5.14 respectively compare the standard deviations and correlation coefficients of EDP residuals of the 380 archetype buildings estimated by RHA and those by the DNN models described in Section 5.3.1. Figure 5.14 shows 1,000 randomly selected cases out of 72,390 (380 pairs of identical buildings and $380 \times (380-1)/2 = 72{,}010$ pairs of different buildings). In the figure, a scatter plot is shown instead of a two-dimensional surface plot to demonstrate that the model not only captures the overall trend of correlation coefficients of EDP residuals but also has a high level of precision. The results show that the developed DNN models predict the standard deviations and correlation coefficients of EDP residuals of buildings accurately.

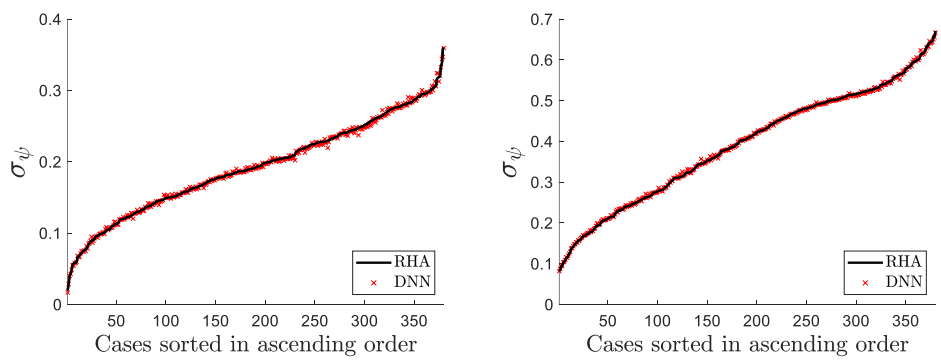

Figure 5.13 Comparison between the standard deviations of EDP residuals by the RHA and those by DNN model: (a) roof displacement, and (b) maximum IDR

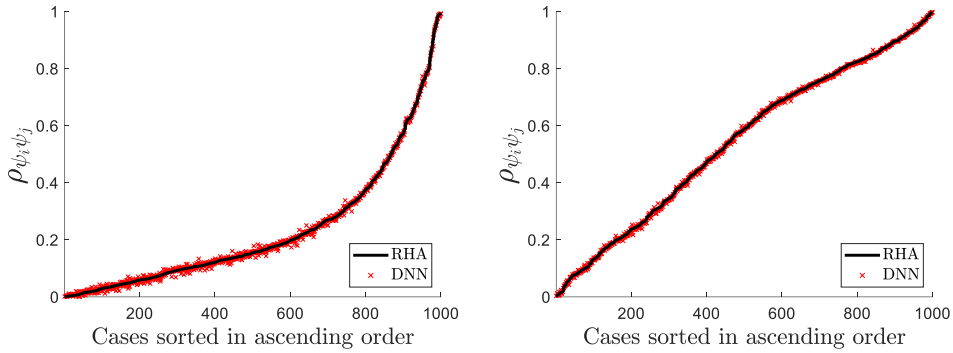

Figure 5.14 Comparison between the correlation coefficients between EDP residuals by the RHA and those by DNN model: (a) roof displacement, and (b) maximum IDR

Furthermore, the performance of the developed DNN models is compared with that of the regression-based models in Section 4.4 (Kang et al., 2022) using 95 example buildings. The regression-based models predict EDP residuals' standard deviation and correlation coefficient using the first mode period and damping ratio as inputs. Figures 5.15, 5.16, and 5.17 compare the EDP residuals of 95 buildings estimated by RHA with those predicted by the regression-based model and the DNN models developed in this study. In Figure 5.15, the regression-based model shows relatively low prediction accuracy when the EDP was the roof displacement. In contrast, the DNN models provided superior prediction accuracy for both EDPs. Figures 5.16 and 5.17 show that the regression-based models only describe the overall trend of the results by RHA, whereas the DNN models accurately predict the correlation coefficient between the EDP residuals in all cases. These results confirm that the developed DNN models have a superior accuracy level to the regression-based models in Section 4.4.

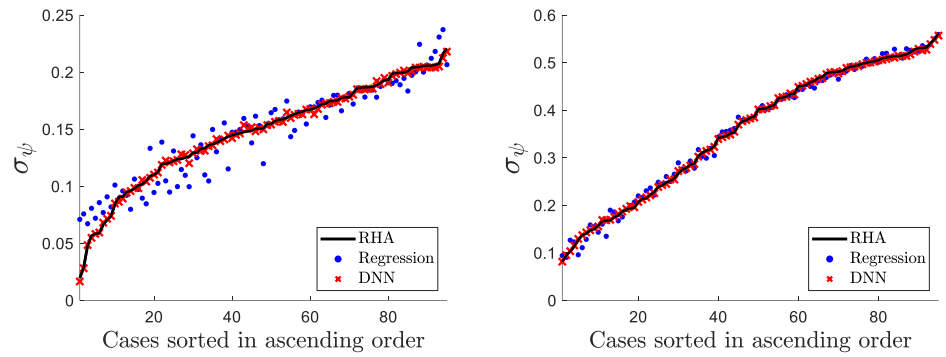

(a) (b)

Figure 5.15 Comparison between the standard deviations of EDP residuals by the RHA, regression-based model, and DNN model: (a) roof displacement, and (b) maximum IDR

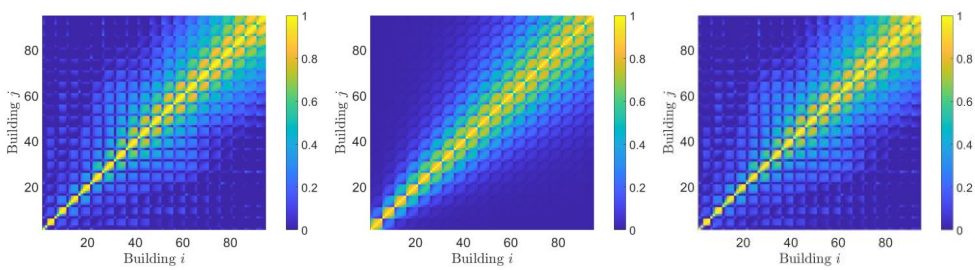

(a) (b) (c)

Figure 5.16 Correlation coefficients between roof displacement residuals estimated by: (a) RHA, (b) regression-based model, and (c) DNN model

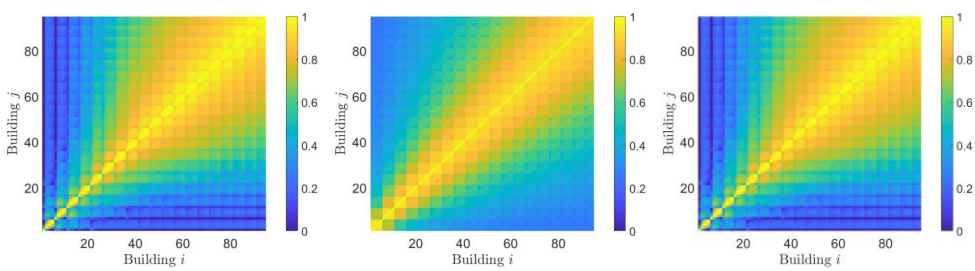

(a) (b) (c)

Figure 5.17 Correlation coefficients between maximum IDR residuals estimated by: (a) RHA, (b) regression-based model, and (c) DNN model

5.4 Numerical example of regional loss assessment

To demonstrate probabilistic regional loss assessment based on the EDP residual estimation by the proposed methods and DNN models, this study consider a virtual city located in California that was created using 44 different archetype buildings in Section 4.5 (Kang et al., 2022). In the city, 500 virtual buildings are randomly generated and distributed over a $2.5\ \text{km} \times 2.5\ \text{km}$ square region with uniform soil conditions, as shown in Figure 5.18. In this example, the seismic damage to each building is described by five states: none, slight, moderate, extensive, and complete, determined by the limit states of the Low-Code seismic design levels in HAZUS (FEMA, 2012a). This example assumes that these damage states are evaluated at each structure's global level in a single type of EDP: maximum IDR. Further details on the structural characteristics, limit states, damage states, and losses of the 44 buildings can be found in Section 4.5.

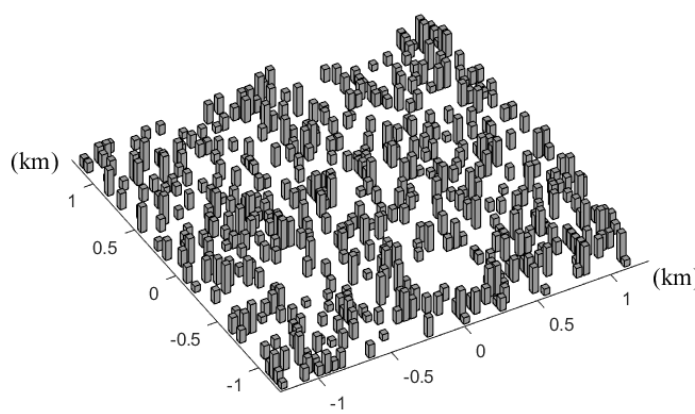

Figure 5.18 A virtual city consisting of 500 randomly generated buildings

An earthquake scenario with a moment magnitude of $M = 7.5$ and an epicentral distance of 35.4 km is considered. The shear wave velocity throughout the region is assumed to be $V_{S30} = 760$ m/s. To predict the ground motion intensities of the building in the region, the GMPE by Boore and Atkinson (2008) is used along with the IM correlation models developed by Baker and Cornell (2006) and Goda and Hong (2008b). The region's seismic loss is evaluated under each of the following four assumptions: (1) 'Statistically Independent' ($\rho_{\widehat{S_{a_i}}\widehat{S_{a_j}}} = \rho_{\psi_i\psi_j} = 0$), (2) 'EDP Residual Correlated' ($\rho_{\widehat{S_{a_i}}\widehat{S_{a_j}}} = 0, \rho_{\psi_i\psi_j} \neq 0$), (3) 'IM Correlated' ($\rho_{\widehat{S_{a_i}}\widehat{S_{a_j}}} \neq 0, \rho_{\psi_i\psi_j} = 0$), and (4) 'Both Correlated' ($\rho_{\widehat{S_{a_i}}\widehat{S_{a_j}}} \neq 0, \rho_{\psi_i\psi_j} \neq 0$). Figure 5.19 compares the total loss exceedance probabilities in Eq. (3.6) computed by the two methods of estimating the EDP residual correlation.

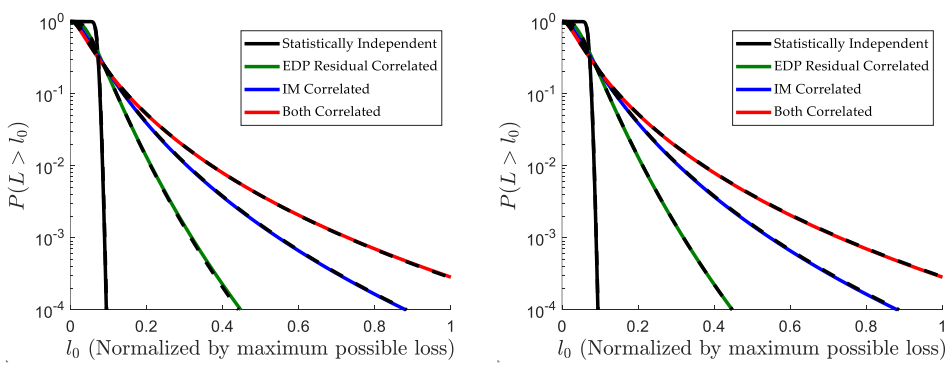

Figure 5.19 Comparison of loss exceedance probability using EDP residual correlation estimated by RHA (solid lines) and those by DNN-based frameworks (black dashed lines): (a) three DNN models combined by derived equations, and (b) two direct DNN models developed for specific types of buildings

The results show that the EDP residual correlation significantly influences the exceedance probability of regional seismic losses. Furthermore, the black dashed lines in the figure confirm that the proposed two DNN-based frameworks can accurately evaluate the loss exceedance probabilities without performing time-consuming RHA. Although the EDP residuals estimated by derived equations with three DNN models have slight differences, as shown in Figures 5.8, 5.9, and 5.10, the approach has enough accuracy from the regional seismic loss assessment viewpoint. In particular, for a city with specific building types, if the failure probabilities of buildings are identified, the regional seismic loss assessment accuracy based on two DNN approaches in Section 5.3 is superior to that based on the regression models in Section 4.4 (Kang et al., 2022). It is also noted that considering the EDP residual correlation by the proposed DNN-based frameworks can prevent a significant underestimation of the regional seismic losses.

5.5 Summary

Based on the previous derivations regarding the EDP residual correlations and estimation methods in Sections 3.2 and 4.2 (Kang et al., 2021 and 2022), two DNN-based estimation frameworks were developed to predict EDP residual's standard deviations and correlation coefficient efficiently and accurately. In the first framework, mathematical equations are derived to utilize DNN-based predictions of EDP residuals of SDOF systems representing the structural modes. In order to improve applicability without compromising accuracy, three DNN models were developed to predict the means, standard deviations, and correlation coefficients of modal responses. On the other hand, the second DNN-based framework directly

predicts the EDP residuals of specific building types by using two DNN models. These two DNN models directly predict the standard deviations and correlation coefficients of the EDP residuals of buildings with superior accuracy for the three inputs: the first and second modal periods and damping ratio. The accuracy of the two DNN-based frameworks was tested and demonstrated by comparing the results to those by RHA and the regression-based models in Section 4.4 (Kang et al., 2022). The numerical example demonstrated the importance of considering EDP residual correlation and the successful performance of the proposed frameworks in regional seismic loss assessment. It is expected that the proposed frameworks will contribute to accurate and efficient loss assessment for general building portfolios.

The first framework can effectively estimate the EDP residuals of various structures based on the modal properties. However, the proposed modification factors are required to alleviate the effects of assumptions in the derivation process. Although the proposed modification factors provide sufficient accuracy for most structures, they may not be suitable for certain types of buildings. To overcome this issue, it is desirable to continuously update the models and modification factors based on the EDP residuals estimated by the structural analysis of a wide range of structures. Moreover, such an effort will improve the applicability and accuracy of the two DNN models in the second framework. The uncertainties and correlations of EDP residuals of buildings located in the same seismic region can be generalized and applied to other types of structures subjected to common source effects from general disasters.

Chapter 6. Conclusions

6.1 Summary and contributions of this dissertation

This dissertation proposed a theoretical framework to evaluate the uncertainties and correlations of engineering demand parameters (EDP) of structures for accurate seismic system reliability analysis. The four main objectives were achieved: (1) safety factor-based correlation formula is derived to incorporate the effects of both IM and EDP residual correlations on the seismic system reliability analysis, (2) two estimation methods that estimate the variances and correlations of EDP residuals of structures, i.e., IDA-based method and IM-invariant method, were proposed, (3) nonlinear regression models and two DNN-based frameworks were developed to predict the EDP residuals of building structures without additional structural analysis, and (4) regional seismic loss assessment of urban areas demonstrated the importance of considering EDP correlation in system reliability analysis and the accuracy and efficiency of the developed estimation methods, regression models and two DNN-based frameworks. The major developments and contributions of this dissertation are summarized as follows:

- Theoretical framework was proposed to incorporate the effect of correlation between EDPs of structures on seismic system reliability analysis. To this end, the EDP of a structure was defined as the sum of a regression function of the selected IM, and EDP residual. This framework considered both correlations between intensity measures ("IM correlation") and EDP residuals ("EDP

residual correlation"). The proposed framework formulated the correlation between the safety factors of two structures as a linear combination of the IM correlation and EDP residual correlation.

- Based on the derived formula, the contribution of IM correlation and EDP residual correlation to the correlation coefficient between safety factors were quantified. The contributions of two correlations were affected by the power-law regression parameters of structures and the standard deviations of IMs and EDP residuals. After investigation of these parameters, it was found that the ratio of uncertainties of IM and EDP residual was relatively dominant to power-law regression parameter. In the case where the uncertainty of EDP residual was relatively large than that of IM, the proposed theoretical framework can correct the significant bias in estimating the correlation between the safety factors of structures.
- IDA-based method was developed to accurately estimate the variances and correlation coefficients of EDP residuals of structures. Using this method, the relationship between IM and EDP can be described in structural performance level. In order to minimize the subjectivity of the estimated EDP residuals by selected ground motion set applied to the IDA-based method, a far-field ground motion set with 44 ground motions was adopted. The application to the fifteen steel moment frame buildings with five different heights and three SCWB ratios successfully demonstrated the performance and contribution of the developed method.
- To demonstrate the theoretical framework and the effect of considering EDP correlation, a probabilistic regional seismic loss assessment was performed for

a virtual urban area and a strong earthquake scenario. Total loss excess probabilities were evaluated for considered correlations by four different assumptions. The comparison of the results confirmed that ignoring the EDP residual correlation significantly underestimated the high level of total loss exceedance probability.

- IM-invariant method was proposed to estimate the EDP residuals of building structures using the elastic-range responses. This method dramatically reduced the computational cost compared to the IDA-based method, and handled much more ground motion in the estimation of EDP residual. Using a set of 1,499 ground motions in the NGA database, a more general expression for the EDP residuals of various types of building structures and their correlations is obtained.
- Taking advantage of the IM-invariant method, a comprehensive investigation was performed to find that the damping and higher mode effects are critical factors in the uncertainties and correlations of EDPs of building structures. It was found that the uncertainty of EDP residual increased as the damping ratio of building deviates from 5%. On the other hand, as the height of a building increased, the relative contribution of higher mode effects was dominant compared to the effect of damping ratio.
- The effects of structural characteristics on the EDP correlations and total regional loss were investigated through numerical examples of four virtual urban areas with different building portfolios. The contribution of the EDP residual correlation to probabilistic regional seismic loss assessment and the effects of the spatial distribution of buildings were identified. In addition,

guidelines were provided on whether the EDP residual correlation needs to be considered.

- To facilitate the consideration of EDP residual correlation, regression models were developed to predict the standard deviations and correlation coefficients of EDP residuals without performing additional structural analysis. The proposed regression models effectively described the overall trend of EDP residuals of building structures in regional seismic loss assessment. The accuracy and efficiency of the proposed regression models were confirmed by repeating the same numerical examples of regional seismic loss assessment.
- Two DNN-based frameworks were proposed to further improve the prediction accuracy and efficiency of EDP residuals. In the first framework, EDP residuals of MDOF systems were mathematically derived to utilize DNN-based predictions of EDP residuals of SDOF systems representing the structural modes. In order to improve applicability three DNN models that predict the means, standard deviations, and correlation coefficients of modal responses were developed but without compromising accuracy. On the other hand, the second DNN-based framework directly predicts the EDP residuals of specific building types by using two DNN models. These two DNN models predict the standard deviations and correlation coefficients of the EDP residuals of buildings with superior accuracy by setting the inputs as three primary structural characteristics: the first and second modal periods, and damping ratio.
- The accuracy of two DNN-based frameworks was tested and demonstrated through the comparison of estimates by RHA and the previously developed regression models. The merits and performance of the proposed DNN-based

frameworks for regional seismic loss assessment were demonstrated through numerical examples.

6.2 Recommendations for further studies

In order to promote and improve the evaluation of uncertainties and correlations of EDPs of structures for seismic system reliability analysis, the following topics are recommended for future studies:

- Although this dissertation focuses on the regional seismic loss assessment, the theoretical framework can be applied to other seismic system reliability analyses in which structures in the system are closely related to each other, e.g., complex structural systems with a large number of components, lifeline networks for transportation, gas, water, and electricity. Moreover, it is expected that the concept of considering correlations between residuals of structural responses subjected to other disasters and risks can be adopted in various engineering fields.
- The IM-invariant method solved the computational challenges in IDA-based method by using elastic-range-responses. By adopting 1,499 ground motions in estimating the EDP residuals, the IDA-based method's main limitation – the estimation results may vary depending on the selected ground motion set – can be minimized. However, some selected ground motions may not be adequate to represent the earthquake scenario that can occur in a given area. Therefore, it is desirable to develop a method for selecting a set of ground motions that can properly describe the earthquake hazard of a given area through a further study.

- In this study, the roof displacement and maximum IDR were considered as the EDP of building structure. However, the IDA-based method and the IM-invariant method can be applied to various types of EDP depending on the structural failure of interest.
- The two DNN-based frameworks can predict the EDP residuals of most building structures with superior accuracy. However, the modification factors in the first DNN-based framework may not be suitable for certain types of buildings and the second DNN-based framework focuses on generic buildings whose Rayleigh damping coefficients are determined based on the first and third modal damping ratios. In order to cover a wider range of archetype buildings, it is desirable to continuously perform structural analysis for various types of buildings and update the modification factors and seismic database through the estimated EDP residuals.
- In the probabilistic regional seismic loss assessment, additional losses (other than structural damage) such as non-structural damage and demolition cost were not considered. Taking these into account further, the effect of the EDP residual correlation on the regional seismic loss assessment can be tested and demonstrated for a practical region. Furthermore, these efforts can establish an emergency response plan in the event of an earthquake and reduce casualties and socioeconomic losses in an urban community.
- The theoretical framework dealt with the uncertainties and correlations of the IM and EDP residual. However, uncertainties structural modeling were not considered. As these can significantly affect the EDPs of structures, further studies are needed to handle the modeling uncertainties in structural analysis.

- To properly consider the higher mode effects of structures, ASCE 7 (ASCE, 2010) recommends that the selected ground motions be scaled over the period range of $0.2T_1$ to $1.5T_1$, where T_1 is the first mode period of a structure. The lower bound is adopted to adequately excite the higher modes, whereas the upper bound is to account for the period lengthening by nonlinearity. In future studies, more reliable estimates can be obtained by scaling the selected ground motions according to this criterion.

References

Abrahamson, N. A., and Youngs, R. R. (1992). A stable algorithm for regression analysis using the random effects model. *Bulletin of the Seismological Society of America*, 82, 505–510.

Abrahamson, N. A., Gregor, N., and Addo, K. (2016). BC Hydro Ground Motion Prediction Equations for Subduction Earthquakes. *Earthquake Spectra*, 32(1), 23–44.

Adachi, T., and Ellingwood, B. R. (2009). Serviceability Assessment of a Municipal Water System Under Spatially Correlated Seismic Intensities. *Computer-Aided Civil and Infrastructure Engineering*, 24, 237-248.

AISC (2010a). Seismic Provisions for Structural Steel Buildings, ANSI/AISC 341-10. American Institute for Steel Construction, Chicago, IL.

AISC (2010b). Prequalified Connections for Special and Intermediate Steel Moment Frames for Seismic Applications, ANSI/AISC 358-10. American Institute for Steel Construction, Chicago, IL.

ASCE (2010). Minimum Design Loads for Buildings and Other Structures, ASCE/SEI 7-10. American Society of Civil Engineers, Reston, VA.

Bakalis, K., and Vamvatsikos, D. (2018). Seismic Fragility Functions via Nonlinear Response History Analysis. *Journal of Structural Engineering*, 144(10), 04018181.

Baker, J. W., and Cornell, C. A. (2006). Correlation of response spectral values for multicomponent ground motions. *Bulletin of the Seismological Society of America*, 96, 215–227.

Baker, J. W., and Cornell, C. A. (2008). Uncertainty propagation in probabilistic seismic loss estimation. *Structural Safety*, 30(3), 236-252.

Boore, D. M., and Atkinson, G. M. (2008). Ground-motion prediction equations for the average horizontal component of PGA, PGV and 5% damped SA at spectral periods between 0.1 s and 10s. *Earthquake Spectra*, 24(1), 99–138.

Boore, D. M., Gibbs, J. F., Joyner, W. B., Tinsley, J. C., and Ponti, D. J. (2003). Estimated ground motion from the 1994 Northridge, California, earthquake at the site of the Interstate 10 and La Cienega Boulevard bridge collapse, west Los Angeles, California. *Bulletin of the Seismological Society of America*, 93, 2737–2751.

Billah, A. H. M. M., Alam, M. S., and Bhuiyan, A. R. (2013). Fragility Analysis of Retrofitted Multicolumn Bridge Bent Subjected to Near-Fault and Far-Field Ground Motion. *Journal of Bridge Engineering*, 18(10), 992-1004.

Bradley, B. A. (2013). A critical examination of seismic response uncertainty analysis in earthquake engineering. *Earthquake Engineering and Structural Dynamics*, 42(11), 1717-1729.

Bradley, B. A., and Lee, D. S. (2010). Component correlations in structure-specific seismic loss estimation. *Earthquake Engineering and Structural Dynamics*, 39(3), 237-258.

Campbell, K., and Bozorgnia, Y. (2008). NGA ground motion model for the geometric mean horizontal component of PGA, PGV, PGD and 5% damped linear elastic response spectra for periods ranging from 0.01 to 10 s. *Earthquake Spectra*, 24(1), 139-171.

Cornell, C. A., Jalayer, F., Hamburger, R. O., and Foutch, D. A. (2002). The probabilistic basis for the 2000 SAC/FEMA steel moment frame guidelines. *Journal of Structural Engineering*, 128(4), 526–533.

Deniz, D., Song, J., and Hajjar, F. (2018). Energy-based sidesway collapse fragilities for ductile structural frames under earthquake loadings. *Engineering Structures*, 174, 282-294.

De Risi, R., De Luca, F., Kwon, O., and Sextos, A. (2018). Scenario-based seismic risk assessment for buried transmission gas pipelines at regional scale. *Journal of Pipeline Systems Engineering and Practice,* 9(4), 04018018.

Ditlevsen, O., and Madsen, H. O. (1996). *Structural Reliability Methods.* New York, USA: J. Wiley & Sons.

Dong, Y., and Frangopol, D. M. (2017). Probabilistic assessment of an interdependent healthcare–bridge network system under seismic hazard. *Structure and Infrastructure Engineering*, 13(1), 160-170.

Elkady, A., and Lignos, D. G. (2015). Effect of gravity framing on the overstrength and collapse capacity of steel frame buildings with perimeter special moment frames. *Earthquake Engineering and Structural Dynamics*, 44(8), 1289–1307.

Elkady, A. (2016). Collapse risk assessment of steel moment resisting frames designed with deep wide-flange columns in seismic regions. Ph.D. Thesis, McGill University.

Ellingwood, B. R., Celik, O. C., and Kinali, K. (2007). Fragility assessment of building structural systems in Mid-America. *Earthquake Engineering and Structural Dynamics*, 36(13), 1935–1952.

FEMA (2000). Prestandard and Commentary for the Seismic Rehabilitation of Buildings, Report FEMA-356, SAC Joint Venture, Federal Emergency Management Agency, Washington, DC.

FEMA (2009). Quantification of Building Seismic Performance Factors. Report FEMA-P695. Federal Emergency Management Agency, Washington, DC.

FEMA (2012a). Multi-Hazard Loss Estimation Methodology. Earthquake model – HAZUS MH 2.1 Technical Manual, Washington, DC.

FEMA (2012b). Seismic Performance Assessment of Buildings. Report FEMA P58-1. Federal Emergency Management Agency, Washington, DC.

Gardoni, P., van de Lindt, J. W., Ellingwood, B., Lee, J. S., Cutler, H., Peacock, W., and Cox, D. (2018). The interdependent networked community resilience modeling environment (IN-CORE). *16th European Conference on Earthquake Engineering*, Thessaloniki, Greece.

Goda, K., and Hong, H. P. (2008a). Estimation of Seismic Loss for Spatially Distributed Buildings. *Earthquake Spectra*, 24(4), 889–910.

Goda, K., and Hong, H. P. (2008b). Spatial correlation of peak ground motions and response spectra. *Bulletin of the Seismological Society of America*, 98(1), 354–365.

Goda, K., and Ren, J. (2010). Assessment of Seismic loss Dependence Using Copula. *Risk Analysis*, 30(7), 1076-1091.

Gupta, A., and Krawinkler, H. (1999). Seismic Demands for the Performance Evaluation of Steel Moment Resisting Frame Structures. Report No. 132. The John A. Blume Earthquake Engineering Center, Stanford University.

Hall, J. F. (2006). Problems encountered from the use (or misuse) of Rayleigh damping. *Earthquake Engineering and Structural Dynamics*, 35(5), 525-545.

Ibarra, L. F., Medina, R. A., and Krawinkler, H. (2005). Hysteretic Models that Incorporate Strength and Stiffness Deterioration. *Earthquake Engineering and Structural Dynamics*, 34(12), 1489-1511.

Jalayer, F., and Cornell, C.A. (2009). Alternative non-linear demand estimation methods for probability-based seismic assessments. *Earthquake Engineering and Structural Dynamics*, 38(8), 951-972.

Jalayer, F., Ebrahimian, H., Miano, A., and Sezen, H. (2017). Analytical fragility assessment using unscaled ground motion records. *Earthquake Engineering and Structural Dynamics*, 46(15), 2639-2663.

Jayaram, N., and Baker, J. W. (2009). Correlation model for spatially distributed ground-motion intensities. *Earthquake Engineering and Structural Dynamics*, 38(15), 1687-1708.

Kang, C., Kwon, O.-S., and Song, J. (2021). Evaluation of Correlation between Engineering Demand Parameters of Structures for Seismic System Reliability Analysis. *Structural Safety*, 93, 102133.

Kang, C., Kwon, O.-S., and Song, J. (2022). Quantifying Uncertainties and Correlations of Engineering Demand Parameters of Building Structures for Regional Seismic Loss Assessment. *Earthquake Engineering and Structural Dynamics*, 51(7), 1751-1769.

Kang, C., Kim, T., Kwon, O.-S., and Song, J. Deep Neural Network-based Regional Seismic Loss Assessment Considering Correlation Between EDP Residuals of Building Structures. (Under review).

Kazantzi, A. K., and Vamvatsikos, D. (2015). Intensity measure selection for vulnerability studies of building. *Earthquake Engineering and Structural Dynamics*, 44(15), 2677-2694.

Kiani, J., and Khanmohammadi, M. (2015). New Approach for Selection of Real Input Ground Motion Records for Incremental Dynamic Analysis (IDA). *Journal of Earthquake Engineering*, 19(4), 592-623.

Kim, T., Kwon, O-S., and Song, J. (2019). Response prediction of nonlinear hysteretic systems by deep neural networks. *Neural Networks*, 111, 1-10.

Kim, T., Song, J., and Kwon, O-S. (2020a). Pre- and post-earthquake regional loss assessment using deep learning. *Earthquake Engineering and Structural Dynamics*, 49, 657-678.

Kim, T., Song, J., and Kwon, O-S. (2020b). Probabilistic evaluation of seismic responses using deep learning method. *Structural Safety*, 84, 101913.

Kim, T., O.-S. Kwon, and J. Song (2021). Clustering-based adaptive ground motion selection algorithm for efficient estimation of structural fragilities. *Earthquake Engineering and Structural Dynamics*, 50(6), 1755-1776.

Kingma, D. P., and Ba, J. (2014). Adam: A Method for Stochastic Optimization. ArXiv:14126980 Cs.

Kohrangi, M., Vamvatsikos, D., and BazzurroSite, P. (2017). Site dependence and record selection schemes for building fragility and regional loss assessment. *Earthquake Engineering and Structural Dynamics*, 46(10), 1625–1643.

Kurtz, N., Song, J., and Gardoni, P. (2016). Seismic Reliability Analysis of Deteriorating Representative U.S. West Coast Bridge Transportation

Networks. *Journal of Structural Engineering*, 142(8), C4015010.

Lee, R., and Kiremidjian, A. S. (2007). Uncertainty and Correlation for Loss Assessment of Spatially Distributed Systems. *Earthquake Spectra*, 23(4), 753-770.

Lignos, D. G., and Krawinkler, H. (2011). Deterioration Modeling of Steel Components in Support of Collapse Prediction of Steel Moment Frames under Earthquake Loading. *Journal of Structural Engineering*, 137(11), 1291-1302.

Lim, H.-W., and Song, J. (2012). Efficient risk assessment of lifeline networks under spatially correlated ground motions using selective recursive decomposition algorithm. *Earthquake Engineering and Structural Dynamics*, 41(13), 1861-1882.

Lim, S., Kim, T., and Song, J. (2022). System-reliability-based disaster resilience analysis: framework and applications to structural systems. *Structural Safety*, 96, 102202.

Loth, C., and Baker, J. W. (2013). A spatial cross-correlation model of spectral accelerations at multiple periods. *Earthquake Engineering and Structural Dynamics*, 42, 397-417.

Maniatakis, C. A., Psycharis, I. N., Spyrakos, C. C. (2013). Effect of higher modes on the seismic response and design of moment-resisting RC frame structures. *Engineering Structures*, 56, 417-430.

Mazzoni, S., Mckenna, F., Scott, M. H., and Fenves, G. L. (2006). The Open System for Earthquake Engineering Simulation (OpenSEES) User Command-Language Manual.

Miano, A., Jalayer, F., Ebrahimian H., and Prota, A. (2017). Cloud to IDA: Efficient fragility assessment with limited scaling. *Earthquake Engineering and Structural Dynamics*, 47(5), 1124-1147.

Nair, V., and Hinton, G. E. (2010). Rectified Linear Units Improve Restricted Boltzmann Machines 8.

PEER (2013). The PEER Ground-Motion Selection Web Application. Pacific Earthquake Engineering Research Center. http://ngawest2.berkeley.edu/.

Power M, Chiou B, Abrahamson N, Bozorgnia Y, Shantz T, Roblee C. (2008). An Overview of the NGA Project. Earthquake Spectra, 24(1), 3-21.

Rosenblueth, E. (1951). A Basis for Aseismic Design. Ph.D. thesis, University of Illinois, Urbana, Illinois.

Rossetto, T., Gehl, P., Minas, S., Galasso, C., Duffour, P., Douglas, J., and Cook, O. (2016). FRACAS: A capacity spectrum approach for seismic fragility assessment including record-to-record variability. *Engineering Structures*, 125, 337-348.

Shinozuka, M., Feng, M. Q., Member, A., Kim, H., and Kim, S. (2000). Nonlinear Static Procedure for Fragility Curve Development. *Journal of Engineering Mechanics*, 126, 1287–1295.

Silva-Lopez, R., Baker, J. W., and Poulos, A. (2022). Deep Learning-Based Retrofitting and Seismic Risk Assessment of Road Networks. Journal of Computing in Civil Engineering; 36(2), 04021038.

Sokolov, V., Wenzel, F., Jean, W. Y., and Wen, K. L. (2010). Uncertainty and Spatial Correlation of Earthquake Ground Motion in Taiwan. *Terrestrial Atmospheric and Oceanic Sciences*, 21(6), 905-921.

Sokolov, V., and Wenzel, F. (2011). Influence of ground-motion correlation on probabilistic assessments of seismic hazard and loss: sensitivity analysis. *Bulletin of Earthquake Engineering*, 9, 1339-1360.

Song, J., and Ok, S.-Y. (2010). Multi-scale system reliability analysis of lifeline networks under earthquake hazards. *Earthquake Engineering and Structural Dynamics*, 39(3), 259-279.

Steelman, J., Song, J., and Hajjar, J. (2007). Integrated data flow and risk aggregation for consequence-based risk management of seismic regional loss. Report of the Mid-America Earthquake Center. University of Illinois at Urbana-Champaign.

Stern, R. E., Song, J., and Work, D. B. (2017). Accelerated Monte Carlo system reliability analysis through machine-learning-based surrogate models of network connectivity. *Reliability Engineering and System Safety*, 164, 1-9.

Vamvatsikos, D., and Cornell, C. A. (2002). Incremental Dynamic Analysis. *Earthquake Engineering and Structural Dynamics*, 31(3), 491-514.

Vamvatsikos. D., and Fragiadakis, M. (2010). Incremental dynamic analysis for estimating seismic performance sensitivity and uncertainty. *Earthquake Engineering and Structural Dynamics*, 39, 141-163.

Wang, C., Feng, K., Zhang, H., and Li, Q. (2019). Seismic performance assessment of electric power systems subjected to spatially correlated earthquake excitations. *Structure and Infrastructure Engineering*, 15(3), 351-361.

Wang, M., and Takada, T. (2005). Macrospatial correlation model of seismic ground motions. *Earthquake Spectra*, 21, 1137–1156.

Appendix

Appendix A. Derivation of the safety factor correlation coefficient between safety factors (Eq. (2.10))

Substituting Eq. (2.5) into the safety factor $F_i = \ln d_i - \ln D_i = \hat{d}_i - \widehat{D}_i$, we obtain

$$F_i = \hat{d}_i - \ln a_i - b_i \widehat{S_{a_i}} - \psi_i \tag{A.1}$$

where ψ_i stands for $\psi_i(\widehat{S_{a_i}})$ for simplicity. The correlation coefficient between safety factors F_i and F_j is defined as

$$\rho_{F_i F_j} = \frac{Cov[F_i, F_j]}{\sigma_{F_i}\sigma_{F_j}} \tag{A.2}$$

where $Cov[F_i, F_j]$ denotes the covariance between the safety factors; and σ_{F_i} and σ_{F_j} are the standard deviations of F_i and F_j respectively. From Eq. (A.1), the variance of F_i and covariance are derived as

$$\sigma_{F_i}^2 = b_i^2 \sigma_{\widehat{S_{a_i}}}^2 + \sigma_{\psi_i}^2 + 2 b_i \sigma_{\widehat{S_{a_i}}} \sigma_{\psi_i} \rho_{\widehat{S_{a_i}}\psi_i} \tag{A.3}$$

$$\begin{aligned} Cov[F_i, F_j] &= b_i b_j Cov\left[\widehat{S_{a_i}}, \widehat{S_{a_j}}\right] + Cov[\psi_i, \psi_j] \\ &\quad + b_i Cov[\widehat{S_{a_i}}, \psi_j] + b_j Cov\left[\widehat{S_{a_j}}, \psi_i\right] \end{aligned} \tag{A.4}$$

If the spectral acceleration and EDP residual are assumed to be uncorrelated, the variance and covariance in Eqs. (A.3) and (A.4) are simplified as

$$\sigma_{F_i}^2 = b_i^2 \sigma_{\widehat{S_{a_i}}}^2 + \sigma_{\psi_i}^2 \tag{A.5}$$

$$Cov[F_i, F_j] = b_i b_j \sigma_{\widehat{S_{a_i}}} \sigma_{\widehat{S_{a_j}}} \rho_{\widehat{S_{a_i}}\widehat{S_{a_j}}} + \sigma_{\psi_i}\sigma_{\psi_j}\rho_{\psi_i\psi_j} \tag{A.6}$$

Substituting Eqs. (A.5) and (A.6) into Eq. (A.2), the correlation coefficient between safety factors is finally derived as Eq. (2.10).

Appendix B. Far-field ground motion set records

For each ground motion record, Tables A.1 and A.2 summarize the earthquake event and characteristics of site and source, respectively.

Table A.1 Summary of earthquake event and recording station data

No.	Earthquake			Recording Station
	M	Year	Name	
1	6.7	1994	Northridge	Beverly Hills - Mulhol
2	6.7	1994	Northridge	Canyon Country-WLC
3	7.1	1999	Duzce, Turkey	Bolu
4	7.1	1999	Hector Mine	Hector
5	6.5	1979	Imperial Valley	Delta
6	6.5	1979	Imperial Valley	El Centro Array #11
7	6.9	1995	Kobe, Japan	Nishi-Akashi
8	6.9	1995	Kobe, Japan	Shin-Osaka
9	7.5	1999	Kocaeli, Turkey	Duzce
10	7.5	1999	Kocaeli, Turkey	Arcelik
11	7.3	1992	Landers	Yermo Fire Station
12	7.3	1992	Landers	Coolwater
13	6.9	1989	Loma Prieta	Capitola
14	6.9	1989	Loma Prieta	Gilroy Array #3
15	7.4	1990	Manjil, Iran	Abbar
16	6.5	1987	Superstition Hills	El Centro Imp. Co.
17	6.5	1987	Superstition Hills	Poe Road (temp)
18	7.0	1992	Cape, Mendocino	Rio Dell Overpass
19	7.6	1999	Chi-Chi, Taiwan	CHY101
20	7.6	1999	Chi-Chi, Taiwan	TCU045
21	6.6	1971	San Fernando	LA - Hollywood Stor
22	6.5	1976	Friuli, Italy	Tolmezzo

Table A.2 Summary of site and source data

No.	Site Data		Fault Type	Site-Source Distance (km)			
	Class	V_{S30} (m/s)		Epicentral	Closet to Plane	Campbell	Joyner-Boore
1	D	356	Thrust	13.3	17.2	17.2	9.4
2	D	309	Thrust	26.5	12.4	12.4	11.4
3	D	326	Strike-slip	41.3	12.0	12.4	12.0
4	C	685	Strike-slip	26.5	11.7	12.0	10.4
5	D	275	Strike-slip	33.7	22.0	22.5	22.0
6	D	196	Strike-slip	29.4	12.5	13.5	12.5
7	C	609	Strike-slip	8.7	7.1	25.2	7.1
8	D	256	Strike-slip	46.0	19.2	28.5	19.1
9	D	276	Strike-slip	98.2	15.4	15.4	13.6
10	C	523	Strike-slip	53.7	13.5	13.5	10.6
11	D	354	Strike-slip	86.0	23.6	23.8	23.6
12	D	271	Strike-slip	82.1	19.7	20.0	19.7
13	D	289	Strike-slip	9.8	15.2	35.5	8.7
14	D	350	Strike-slip	31.4	12.8	12.8	12.2
15	C	724	Strike-slip	40.4	12.6	13.0	12.6
16	D	192	Strike-slip	35.8	18.2	18.5	18.2
17	D	208	Strike-slip	11.2	11.2	11.7	11.2
18	D	312	Thrust	22.7	14.3	14.3	7.9
19	D	259	Thrust	32.0	10.0	15.5	10.0
20	C	705	Thrust	77.5	26.0	26.8	26.0
21	D	316	Thrust	39.5	22.8	25.9	22.8
22	C	425	Thrust	20.2	15.8	15.8	15.0

초 록

강철영

건설환경공학부

서울대학교 대학원

도시 인프라 시스템이 정교해지고 복잡해짐에 따라 많은 사상자와 심각한 사회 경제적 손실을 유발할 수 있는 지진 재해에 대한 사회적 기반 시스템의 복원력을 증대하는 것이 점점 더 중요해지고 있다. 이를 위해서는 지진동과 구조물 지진응답의 불확실성 및 상관관계를 적절히 고려한 시스템의 지진 신뢰성 해석이 필수적이다. 정확한 지진 신뢰성 해석에는 지진응답변수(Engineering Demand Parameter, EDP)의 불확실성과 상관관계를 정확히 추정하는 것이 우선적으로 요구된다. 지진응답변수는 선택한 지진강도(Intensity Measure, IM)에 대한 구조물의 지진응답을 나타내는 회귀 함수와 지진응답 잔차(EDP residual)의 합으로 설명된다. 따라서 지진응답변수 간의 상관관계를 정확하게 평가하기 위해서는 지진강도 상관관계(IM 상관관계) 뿐만 아니라 지진응답 잔차 상관관계(EDP residual 상관관계)의 영향 또한 적절히 고려되어야 한다. 그러나 대부분의 기존 연구들에서는 지진 시스템 신뢰성 해석에 지진강도 상관관계만 고려되었을 뿐 지진응답 잔차의 상관관계는 정확하게 고려되지 않았다. 따라서 본 논문에서는 두 가지 상관관계를 모두 고려하여 서로 다른 구조물의 지진응답변수 간의 상관관계를 평가하는 이론적인 프레임워크를 제안할 뿐만 아니라 다양한 지진동을 이용한 구조해석, 비선형 회귀모델 및 심층신경망(deep neural network, DNN)을 기반으로 지진응답변수의 잔차를 추정하는 다양한 방법을 개발한다.

먼저 지진 신뢰성 해석에서 지진응답변수 상관관계를 정확하게 고려하기 위해 서로 다른 두 구조물의 안전계수 간의 상관관계를 지진강도 상관관계와 지진응답 잔차 상관관계로 공식화하였다. 이러한 공식에 기반하여 구조물의 결합파괴확률(joint failure probability)을

계산하고 각각의 상관관계가 지진응답변수 상관관계에 미치는 영향을 파악하였다. 또한 지진응답 잔차의 분산 및 상관계수를 추정하기 위한 IDA(Incremental Dynamic Analysis) 기반 방법을 개발하였다. 다양한 선행 연구에서 제안된 지반운동예측방정식(ground motion prediction equation, GMPE)과 본 연구에서 개발한 IDA 기반 통계적 분석을 통합하여 두 가지 상관관계가 모두 고려된 지진응답변수의 상관관계를 추정하였다. 또한 가상의 도시지역에 대한 지진 손실 평가 예제를 통해 개발된 상관관계 통합 공식과 IDA 기반 추정방법을 검증하였다. 특히 기존 방법과 같이 지진강도 상관계수만 고려하고 지진응답 잔차의 상관관계를 고려하지 않을 경우 지역의 총 손실이 상당히 저평가 될 수 있음을 확인하였다.

두번째로 IDA 기반 방법의 대안으로 구조물의 탄성응답을 이용하여 지진응답 잔차를 추정하는 IM−invariant 방법을 제안하였다. 해석 시간을 크게 단축시키는 IM−invariant 방법의 장점을 활용하여 더욱 일반적인 표현의 지진응답 잔차의 분산과 상관관계를 추정하였다. 또한 많은 지진동을 활용하여 다양한 건축구조물에 대한 해석을 수행하고 추정된 결과를 바탕으로 포괄적인 조사를 수행함으로써 지진응답변수의 불확실성과 상관관계에 영향을 주는 주된 구조적 특성을 파악하였다. 다양한 유형의 건축구조물이 분포된 도시 지역들에 대한 지역 손실 평가 예제들을 통해 IM−invariant 방법을 검증하였으며, 구조적 특성들이 지진응답 잔차와 지역의 총 손실에 미치는 영향을 입증하였다. 나아가 본 연구는 수치 예제 결과를 바탕으로 지역에 분포된 건물의 유형에 따른 지진응답 잔차 상관관계 고려에 대한 지침을 제공하였다. 실제 지역에 대한 적용을 더욱 용이하게 하기 위해 주된 구조적 특성만으로 지진응답변수의 잔차를 예측하는 비선형 회귀모델들을 개발하였으며, 정확도 또한 수치 예제를 통해 입증하였다.

앞서 개발된 비선형 회귀모델들은 지역 지진 손실 평가에 적용하기 위한 지진응답변수 잔차의 분산과 상관관계를 효율적으로 예측할 수 있음을 확인하였으나 정확도과 활용가능성을 향상시키는 것이 문제로

남아있었다. 이를 해결하기 위하여 두 가지 심층신경망에 기반한 새로운 프레임워크가 개발되었다. 첫 번째 프레임워크는 모드조합법(modal combination)을 사용하여 단자유도(single degree of freedom, SDOF) 시스템의 지진응답 잔차를 결합하여 다양한 모드 특성을 가진 다자유도(multi degree of freedom, MDOF) 시스템의 지진응답 잔차를 추정하였다. 이 프레임워크에서 요구되는 단자유도 시스템의 세가지 지진응답 잔차를 예측하기 위해 심층신경망 모델들을 개발하여 프레임워크의 적용 가능성을 향상시켰다. 두 번째 프레임워크는 특정 유형의 건축구조물에 대한 지진응답변수의 잔차를 직접 예측하는 두 가지 심층신경망 모델들을 제시하였다. 이와 관련하여 다양한 1차 및 2차 모드 주기와 감쇠비를 갖는 다양한 건축구조물들을 도입하였다. 수치 예제를 통해 IM-invariant 방법과 앞서 개발된 회귀 모델들을 이용하여 추정된 건축구조물의 지진응답 잔차를 제안된 프레임워크들과 비교함으로써 심층신경망 기반 프레임워크들의 높은 정확도, 적용 가능성 및 예측 효율성을 검증하였다.

본 학위논문에서 개발된 방법을 통해 지진응답변수 상관관계의 불확실성 및 상관관계를 효율적이고 정확하게 평가한다면 지진 재해에 의한 도시 인프라 시스템의 사회경제적 피해 예측 및 복원력 증대에 크게 기여할 수 있을 것으로 기대된다.

주요어: 지진 공학, 지진응답변수, 상관관계, 지진 신뢰성 해석, 지역 지진 손실 평가, 비선형 회귀, 심층신경망, 취약도 분석, 불확실성 정량화, 모드해석, 시간 이력 해석.

학번: 2016-22796